DESIGN AND CONSTRUCTION OF AN ULTRASONIC PROBE FOR USE IN A CRYO-MAGNET NMR SPECTROMETER

Anna Louise Weekes

Doctor of Philosophy

Aston University

June 1998

ACKNOWLEDGEMENTS

I would like to thank my supervisor Professor John Homer for all his expert advice and assistance.

I would also like to thank the support staff in the CEAC department, especially Dr Mike Perry for the loan of books and equipment. Also Ian Murkett and Roger Wheeler receive my thanks for the production of specialist items from the workshop and their assistance and advice concerning the practical engineering aspects of this thesis

I would like to thank Dr. Detlef Muller of Bruker Analytische Messtechnik GMBH for the sponsorship of my PhD and his hospitality during my stay in Karlsruhe. My thanks also go to all at Bruker Spectrospin Ltd, and in particular to Ian Francis for his technical expertise.

My thanks would not be complete without mentioning my friends as well as colleagues in the NMR Research Group: Dr. Mark Howard, Dr. Stuart Palfreyman, Dr. Steven Reynolds, Dr. John Robson, Spencer Davies and more recently Claire Burrows and Mohammed Rahmen.

I would like to thank Dr. John Robson for his help in the writing of this thesis and his collaborative input into the development of modifications to the transducer holder. Also my thanks to Dr. Steven Reynolds for his collaborative input on the design and manufacture of all transducer holders.

Finally my thanks to Beth Coulthard for proof reading this thesis and to Robert Hague for his help in the production of this thesis.

Aston University

THE DESIGN AND CONSTRUCTION OF AN ULTRASONIC PROBE FOR USE IN A CRYO-MAGNET NMR SPECTROMETER.

ANNA LOUISE WEEKES

Doctor of Philosophy

1998

SINNMR (Sonically Induced Narrowing of the Nuclear Magnetic Resonance spectra of solids), is a novel technique that is being developed to enable the routine study of solids by nuclear magnetic resonance spectroscopy. SINNMR aims to narrow the broad resonances that are characteristic of solid state NMR by inducing rapid incoherent motion of solid particles suspended in a support medium, using high frequency ultrasound in the range 2-10 MHz.

The width of the normal broad resonances from solids are due to incomplete averaging of several components of the total spin Hamiltonian caused by restrictions placed on molecular motion within a solid. At present Magic Angle Spinning (MAS) NMR is the classical solid state technique used to reduce line broadening, but this has associated problems, not least of which is the appearance of many spinning side bands which confuse the spectra. It is hoped that SINNMR will offer a simple alternative, particularly as it does not reveal spinning sidebands

The fundamental question concerning whether the use of ultrasound within a cryo-magnet will cause quenching has been investigated with success, as even under the most extreme conditions of power, frequency and irradiator time, the magnet does not quench.

The objective of this work is to design and construct a SINNMR probe for use in a super conducting cryo-magnet NMR spectrometer. A cell for such a probe has been constructed and incorporated into an adapted high resolution broadband probe. It has been proved that the cell is capable of causing cavitation, up to 10 MHz, by running a series of ultrasonic reactions within it and observing the reaction products. It was found that the ultrasound was causing the sample to be heated to unacceptable temperatures and this necessitated the incorporation of temperature stabilisation devices. Work has been performed on the investigation of the narrowing of the solid state ^{23}Na spectrum of tri-sodium phosphate using high frequency ultrasound. Work has also been completed on the signal enhancement and T_1 reduction of a liquid mixture and a pure compound using ultrasound.

Some preliminary "bench" experiments have been completed on a novel ultrasonic device designed to help minimise sample heating. The concept involves passing the ultrasound through a temperature stabilised, liquid filled funnel that has a drum skin on the end that will enable the passage of ultrasound into the sample. Bench experiments have proved that acoustic attenuation is low and that cavitation in the liquid beyond the device is still possible.

Key Words: SINNMR, Line Narrowing, Ultrasound, Enhanced Signals, T_1 Reduction

TABLE OF CONTENTS

LIST OF FIGURES

APPENDICES

LIST OF TABLES

APPENDICES

CHAPTER 1 INTRODUCTION

1. INTRODUCTION

Nuclear magnetic resonance (NMR) is one of the most important analytical techniques for the elucidation of the structure, conformation and dynamics of molecules. The idea that certain atomic nuclei possess magnetic moments was first outlined by Pauli in 1924 (1). It was then, (not until) 1945, that Purcell, Torrey and Pound (2), and also Bloch, Hansen and Packard (3) detected nuclear resonance effects in bulk matter. The main application of NMR in science is based on the fundamental observation that the measured NMR transition frequency for an atomic nucleus is a highly sensitive probe of the chemical and structural environment of that nucleus. The distinct "chemically shifted" transitions of nuclei of the same element in different environments can be resolved by NMR spectroscopy, allowing the spectroscopist unique information on the structure, conformation and dynamics of the system. The ability of NMR to distinguish between individual resonance lines of chemically shifted transitions of nuclei, in structurally distinct nuclei locations, defines the use of the phrase "high resolution" NMR spectroscopy.

During the early development of the NMR technique; NMR was used to study the liquid state due to the fact that line broadening interactions are either averaged to zero or averaged to an isotropic value by the rapid molecular motion in liquids. Until the 1970's the continuous wave method of measurement was used: this requires slowly sweeping the radio frequency field applied to a sample in a static magnetic field, or the magnetic field applied to a sample in a static radio frequency field. A major breakthrough in NMR came with the discovery by Onnes of superconductivity, and subsequently the superconducting magnet, and also the development of pulse and Fourier transform NMR

spectroscopy (FT-NMR) (4). These discoveries permitted the routine observation of low abundance and/or low sensitivity nuclei such as ^{29}Si and ^{13}C (5).

Solid state NMR started coming into focus when higher magnetic fields, more powerful computers and a variety of decoupling methods and other sophisticated techniques became available. The main problem with the analysis of solid samples is the inherent lack of resolution due to incomplete averaging of the total spin Hamiltonian, which leads to the inherent information becoming obscured by line broadening effects. Therefore, it is a major technical goal in NMR to develop techniques that can reduce or remove these broadening interactions to achieve high resolution solid state spectra. The most popular techniques to be developed have been coherent averaging techniques. Magic angle spinning developed by Andrew (6) and Lowe (7) enables the reduction of the dipolar and chemical shift broadening interactions. High power dipolar decoupling removes the dipolar interaction: combined with this technique has been the development of the cross polarisation (CP) experiment by Hartman and Hahn (8) to enhance relaxation while simultaneously reducing the strong dipolar broadening. The use of appropriate multiple pulse techniques, such as WAHUHA (9) or MREV-8 (10) (11) can be used for the removal of strong homonuclear dipolar interactions. These techniques can be used alone but are often used in tandem with each other to maximise resolution. For example CP MAS (12) (13) and CRAMPS (Combined Rotation and Multiple Pulse Spectroscopy) (14) (15) are common place in solid state NMR. More recently, techniques such as Double Rotation Spectroscopy (DOR) (16) (17), CPDOR (18) and Dynamic Angle Spinning (DAS) (19) have been developed to remove higher order interactions.

SINNMR (the Sonically Induced Narrowing of Nuclear Magnetic Resonance spectra of solids) (20) (21) (22) (23), has been developed to facilitate the incoherent particle motion of solid particles suspended in a support medium. It is hoped that the application of the ultrasound will modulate the motional behaviour of these particles such that they will possess enhanced rotational and translational motions, generally mimicking liquid behaviour. This incoherent averaging will offer advantages over coherent averaging techniques as all angular dependent interactions should be reduced by its application and facilitate line narrowing for solids. One area of this work is concerned with developing and optimising the SINNMR technique.

Ultrasound can also be applied to liquid samples to modulate their motional characteristics and so reduce their T_1 and enhance the NMR signals they generate (24)(25). This is especially important for nuclei situated within a liquid sample such that they are not well connected to the lattice environment and have a long T_1 relaxation time. A common example of such a nucleus is a quaternary ^{13}C nucleus. Pulse FT NMR requires that a time delay of 5.3 T_1 should be left between pulsing to ensure that the nuclei has relaxed completely before it is pulsed again. Consequently the spectrometer time required to achieve spectra for such compounds is long. Thus an area of the work in this thesis is concerned with acoustically reducing the T_1 and thus enhancing the signals from ^{13}C nuclei.

There follows discussions of those aspects of NMR and acoustic theory that are essential to the work discussed herein. Reference to any other familiar aspects of both subjects have been deliberately minimised.

CHAPTER 2 INTRODUCTION TO NMR

2.1 SPIN ANGULAR MOMENTUM

The atomic nuclei of certain elements can produce an NMR signal for reasons dependent on the fact that they possess both charge and spin. A nucleus with spin (angular momentum), I, will have an associated magnetic moment, μ, which can interact with an applied magnetic field to generate different nuclear energy states. The values of I may be zero, integer or half integer, depending on the composition of the nucleus. For example:

- If the numbers of protons and neutrons are both even numbers then I is zero (e.g. ^{12}C and ^{16}O)
- If the number of protons plus the number of neutrons is an odd number, then I is a half integer (e.g. ^{13}C, ^{23}Na)
- If the number of protons and the number of neutrons are odd numbers then I is an integer (e.g. ^{2}H, ^{14}N)

Thus, nuclei with I =0 have no spin angular momentum and therefore no magnetic moment, so no NMR signal can be observed.

In the absence of an external magnetic field the spin states of I >1/2 are degenerate, but when placed in a magnetic field can take up one of a number of quantised orientations with respect to that field. Each nuclear orientation corresponds to an energy level, the lowest energy level being when the nuclear magnetic moment is aligned "parallel" to the field.

The magnetic field $\mathbf{B_0}$ creates a torque on the spinning, charged nucleus causing its magnetic moment to precess. Figure 2.1 shows a nucleus precessing around the direction of the magnetic field like a gyroscope.

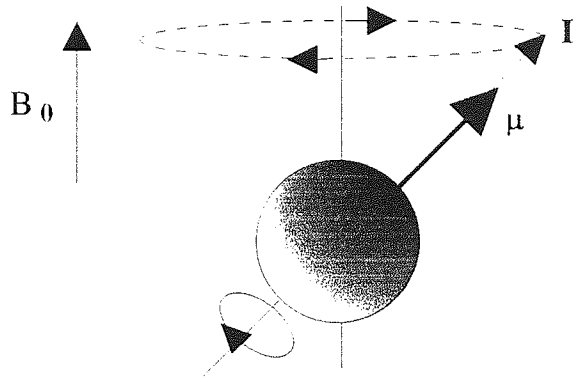

Figure 2.1: A precessing nucleus

The total magnitude of the spin angular momentum is defined by $\hbar\left[I(I+1)\right]^{1/2}$ where $\hbar$ is the reduced Plank constant, equal to h/2π, and **I** is the spin quantum number. The magnetic spin quantum number m, is an expression of the observable magnitudes of **I**, where m can assume the values I, I-1, I-2 ···· – I, so that there will be 2I +1 equally spaced spin states. Quantum mechanical selection rules dictate that only Δm ± 1 transitions are observable in NMR spectra, Forbidden transitions, Δm ≠1, although not directly observable are important in relaxation processes and multiple quantum coherence spectroscopy. The energy levels for a spin 3/2 nucleus are shown in Figure 2.2

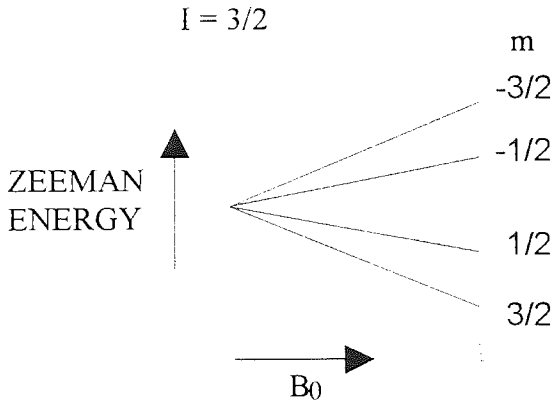

Figure 2.2: Energy level separations for a spin 3/2 nucleus

The constant of proportionality that exists between the total observable angular momentum, $I\hbar$, and the magnetic moment, μ, (which are both vector quantities) is known as the magnetogyric ratio, γ.

$$\mu = \gamma I\hbar \qquad \text{Equation 2.1}$$

The magnetogyric ratio is constant for a particular nucleus and determines the resonant frequency of the nucleus. The angular frequency of nuclear precession is known as the Larmor frequency, ω_0, ($\nu_0 = \omega_0/2\pi$) of the nucleus and is simply its NMR absorption angular frequency. Equation 2.2 shows that this frequency is dependent on the applied field as well as on the intrinsic properties of the nucleus (reflected in the magnetogyric ratio).

$$\omega_0 = -\gamma B_0 \qquad \text{Equation 2.2}$$

Application of a radio frequency magnetic field, $\mathbf{B}_1$, rotating perpendicular to, and at the Larmor frequency of a nucleus will cause a transition between adjacent energy states. The separation of energy levels, ΔE, of a nucleus is obtained from the Bohr relationship

where $\Delta E = h\nu$ and is shown by equation 2.3 to be proportional to $\mathbf{B_0}$ and the magnetogyric ratio, γ, for the nucleus.

$$\Delta E = -\gamma h B_0 \qquad \text{Equation 2.3}$$

2.1.1 Shielding and chemical shift

NMR absorption frequencies are dependent on the chemical environment of the nucleus; the differences in resonance conditions are known as chemical shifts (26) (27) (28). The chemical shift phenomena arises because the electrons surrounding a nucleus shield the nucleus from the external magnetic field, $\mathbf{B_0}$. Shielding occurs because the electrons surrounding a nucleus are induced to circle the nucleus about the direction of $\mathbf{B_0}$, this circulation of electronic charge has an associated induced magnetic moment which opposes the applied field $\mathbf{B_0}$. Thus the effective magnetic field at a nucleus is given by equation 2.4

$$B = B_0(1-\sigma) \qquad \text{Equation 2.4}$$

where σ is the shielding constant

Since the shielding effect is dependent on the electronic environment, values of σ will vary with the position of a nucleus within a molecule. The resonance condition for a nucleus j can be given by equation 2.5

$$\nu_j = \frac{\gamma}{2\pi} B_0\left(1-\sigma_j\right) \qquad \text{Equation 2.5}$$

where σ_j is the shielding constant for the nucleus, j.

A more detailed account of chemical shift can be found in an article by Musher (29) and a text by Slichter (30)

2.2 THE POPULATION OF ENERGY LEVELS

In the presence of a magnetic field, $\mathbf{B_0}$, the nuclei will distribute themselves into either the lower, N_α or upper state, N_β (in the case of a spin ½ system) according to the Boltzmann distribution, given by equation 2.6:

$$\frac{N_\beta}{N_\alpha} = e^{-\Delta E/kT} \qquad \text{Equation 2.6}$$

where k is a constant and T is the equilibrium temperature. This difference between the ratio of populations can be described in thermodynamic terms by a spin temperature T_s: by replacing T with T_s in equation 2.6. The concept of spin temperature can be used to explain the heat flow, created by the population difference, between the spin system and the lattice or vice versa. The lower energy level, N_α, is thermodynamically favourable and therefore the largest number of spins exists in the lower level.

As the probabilities of experimentally inducing absorption or emission transitions are equal, a net absorption of energy by the sample arises because there exists the Boltzmann excess of nuclei in the lower energy level: a small excess of α nuclei flipping into the upper energy level compared to β-nuclei flipping down. It is this slight excess absorption that gives rise to NMR signals. Inducing transitions, by application of an appropriate B_1 field, will eventually even out this population difference and saturate the sample, so that an NMR signal is no longer observed. The system is then in a non-equilibrium situation,

and because thermodynamics dictates that the probability of natural emission transitions is greater than the corresponding absorption, the system will relax to equilibrium in a characteristic time T_1. Thus an understanding of the time required for the complete relaxation of different nuclei in different environments is essential. Equation 2.7 shows that the size of the excess low energy population is proportional to $\mathbf{B_0}$, and so signal intensity will increase with increasing $\mathbf{B_0}$.

$$\frac{N_\beta}{N_\alpha} = e^{-2\mu B_0/kT}$$

Equation 2.7

2.3 BULK MAGNETISATION

The total magnetic moment or magnetisation, M, of a sample is the resultant of an ensemble of nuclear moments, μ, according to equation 2.8.

$$M = \sum_i \mu_i$$

Equation 2.8

At equilibrium there are more spins in the lower than the upper energy state. Therefore an overall magnetisation, $\mathbf{M_0}$, will exist, which by convention is aligned along the z axis with respect to $\mathbf{B_0}$, and is often termed the longitudinal magnetisation, $\mathbf{M_z}$. Bulk magnetisation is established when a sample is placed in a magnetic field. NMR is a quantitative technique in that the intensity of an absorption is proportional to the number of nuclei giving rise to it.

2.4 THE PULSE FT-NMR EXPERIMENT

In pulse Fourier transform NMR spectroscopy, the entire spectrum of resonant frequencies is stimulated by the application of a single monochromatic radio frequency pulse, ω, of duration t_p. The frequency, ω, usually termed the carrier frequency, is chosen to be close to the resonance of the nuclei of interest. Heisenberg's uncertainty principle (31) implies that a pulse of length t_p will contain a bandwidth of frequencies, $1/t_p$ centred about ω. Increasing the pulse length reduces the uncertainty in the frequency thereby reducing the bandwidth of frequencies.

At equilibrium the bulk magnetisation is aligned along $\mathbf{B_0}$. Application of a $\mathbf{B_1}$ pulse along the x-axis, at frequency ω_0 and duration t_p causes $\mathbf{M_0}$ to be rotated through an angle, θ, into the z-y plane. The angle of rotation, θ, can be calculated using equation 2.7

$$\theta = \gamma B_1 t_p \qquad \text{Equation 2.7}$$

The essential advantage of the pulse FT NMR experiment over the continuous wave (CW) method is that since all resonant frequencies of interest are sampled simultaneously, the time spent sampling is very much reduced. (A typical acquisition that may take 1s on an FT NMR would take about 100s on a CW instrument). Also the 1s, in a FT-NMR experiment is time spent sampling the frequency/frequencies of interest, compared to a CW experiment when the majority of instrument time is spent scanning the baseline. This has permitted the routine practice of taking multiple acquisitions to improve signal to noise (32). Signal averaging improves the signal to noise ratio of the spectra being acquired by recording the NMR spectra a number of times. Noise is generated incoherently, whereas a true signal will accumulate coherently, building up

over a number of scans. Over a number of repetitions the NMR signal can be said to build up by n, (where n is the number of repetitions in the pulse experiment), whereas the noise will build up at $\sqrt{n}$. Thus signal to noise will be proportional to $\sqrt{n}$.

2.4.1 Free induction decay

In FT-NMR spectroscopy the response of the spin system to a given perturbation is measured by the induction of an electromotive force in the receiver coils of the spectrometer by the precessing transverse magnetisation. A plot of signal intensity against time is referred to as a free induction decay (FID). If the sample being monitored contains many different spins each with its own resonance frequency, the FID will be a complex interferogram, as shown in Figure 2.3.

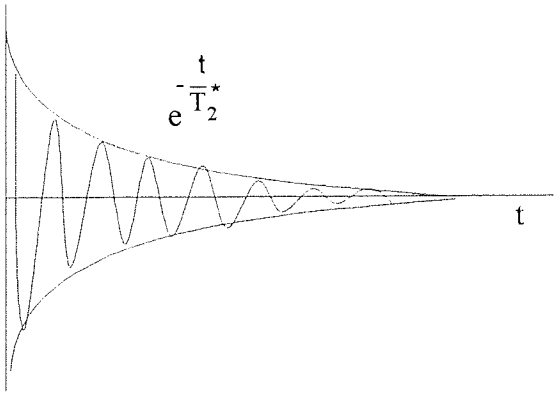

Figure 2.3: Free induction decay

If all spins being monitored are equivalent and the magnetisation is exactly on resonance then a single exponential decay will be observed.

2.4.2 Signal detection and acquisition

A receiver coil detects the decaying magnetisation, $\mathbf{M}_x$ and $\mathbf{M}_y$. The intensity of the FID is amplified and sent on through a phase sensitive detector, which subtracts the carrier frequency, ω, from the NMR signal, leaving only the lower frequency chemical shift components. These electrical signals, (voltages), are converted into binary form based on the size of the voltage by an analogue to digital converter (ADC). The dynamic range of the ADC is characterised by the ratio of the weakest to the strongest signal. If the dynamic range is exceeded the weakest signals will not be digitised.

The next consideration is how long and how often to sample the signal, characterised by sampling theorem and digital resolution respectively.

2.4.2.1 Signal sampling

The signal that enters the ADC is sampled for a particular time, A_t, known as the acquisition time. In order to distinguish between spectral features separated by $\Delta\nu$ Hz, the signal must be sampled at least $1/\Delta\nu$. This supposes that the NMR signal lasts for that long; if it does not, then it is not possible to resolve such close spectral features. The duration of sampling depends on the minimum separation of the frequencies being detected, whereas the rate of sampling depends on the total spectral range that is present in the sample. The Nyquist frequency defines the highest frequency or spectral width which can be sampled by the ADC. This frequency is denoted by N; if frequencies up to N Hz are present then sampling must be carried out every 1/2Ns.

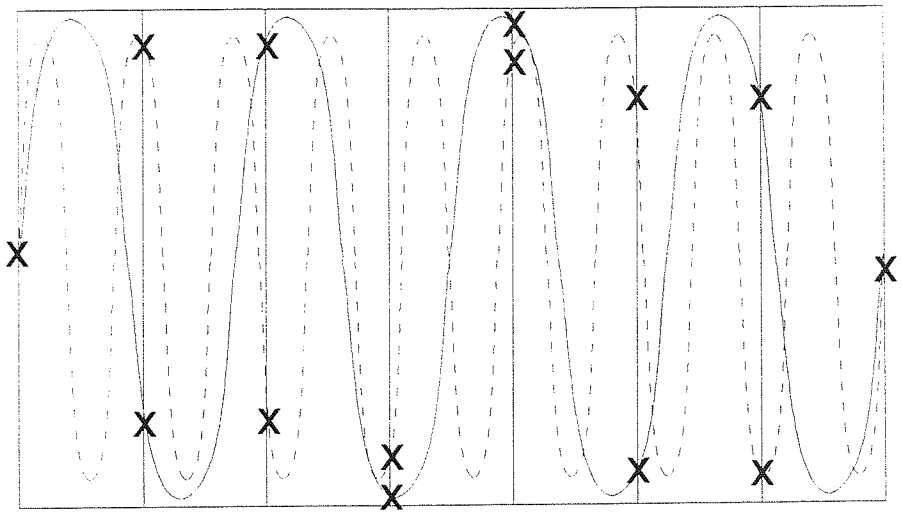

Figure 2.4: Digitising a sample with insufficient data points.

Figure 2.4 shows what can happen if a waveform is digitised with a frequency greater than the Nyquist. Each frequency is digitised at points defined by X: the solid line is correctly sampled, but the dashed line is incorrectly sampled and will appear on the transformed spectra as a peak at low frequency. Signals occurring in the wrong place are known as aliased or folded peaks. Folded peaks can be recognised as they show an unusual phase compared to the rest of the peaks in the spectrum. A folded peak can be determined by moving the carrier frequency, a real peak will move by that same amount in the opposite direction. A folded peak will move in the wrong direction by the wrong amount.

The gain in sensitivity produced by signal averaging can potentially be destroyed by electrical noise, (which is essentially white noise containing all frequency components) folding unwanted frequencies into the spectrum. To avoid this, adjustable bandpass filters can be placed before the ADC to limit the electrical bandwidth of the spectrometer.

2.4.2.2 Spectral range and digital resolution

The sweep width, also known as the spectral width or window, is chosen so that all the frequencies to be detected lie within its range. Digital resolution depends on the number of data points which span a given sweep width. To adequately resolve peaks they must be characterised by a sufficient number of data points. The digital resolution can then be defined by equation 2.8 and again by equation 2.9.

$$R_d = \frac{1}{A_t} \qquad \text{Equation 2.8}$$

$$R_d = \frac{2SW}{n} \qquad \text{Equation 2.9}$$

where SW is the sweep width and n is the size of the data set

Inadequate digital resolution can distort the intensities of the lineshapes. Digital resolution can be improved by zero filling, as long as the FID has decayed close to zero by the end of A_t. The acquisition is stopped and the computer is used to fill in FID data at the tail end of an acquisition with zero points. Zero filling adds no information to the frequency spectrum produced and is used simply to reduce the time for acquiring the spectra, while increasing the digital resolution.

2.4.3 The Fourier transform

Fourier transformation (33) allows inter conversion of time domain (amplitude as a function of time) and frequency domain (i.e. amplitude as a function of frequency) data. The two data sets are related through the Fourier relationship, defined by equation 2.10.

$$f(\omega) = \int_{-\infty}^{\infty} f(t) e^{i\omega t} dt$$ Equation 2.10

as $e^{i\omega t} = \cos(\omega t) - i \sin(\omega t)$, This equation can be written as

$$f(\omega) = \int_{-\infty}^{\infty} f(t)[\cos(\omega t) - i \sin(\omega t)]dt$$ Equation 2.11

Equation 2.11 shows that the Fourier transform output data consists of two components, referred to as the real and imaginary parts of the transform. The real component is known as the absorption mode whereas the corresponding sine transform of an exponential is known as the dispersive mode. Both modes are Lorentzian in form and have the same frequency and wave amplitude. They differ due to each component having a different phase, shifted by 90°. The NMR spectrum is normally plotted as the absorption lineshape, where the peak amplitude is determined by the intensity of the first data point in the FID, and the width of a peak in the transformed frequency spectrum is inversely proportional to the duration of the sine wave and has a full width at half height of $2/\pi T_2^*$ (see page 40). This is true because the longer a sine wave exists the more precisely its frequency can be determined.

The inverse transform to convert the frequency spectrum back to the time domain is given by equation 2.12

$$f(t) = \frac{1}{2\pi} \int_{-\infty}^{\infty} f(\omega) e^{i\omega t} d\omega$$ Equation 2.12

where F(t) is the time domain data and f(ω) the frequency domain data.

2.4.3.1 The lock signal

A dispersive mode signal has zero intensity at the centre of resonance. Therefore, any shift in the magnetic field strength on frequency can be detected by the dispersive signal becoming positive or negative in value. A feedback system detects this change and applies an appropriate field strength correction to return the signal intensity to zero. For this reason a deuterated "lock" compound is usually added to the sample being observed: deuterium is generally used for frequency locking because its resonant frequency is very different from common nuclei of interest, specifically ^{1}H and ^{13}C.

2.4.4 Truncation

Truncation occurs when the acquisition time, A_t, is not sufficiently long enough to acquire the whole FID. In such cases the FID acquired has a partial step character and a partial exponential character. The Fourier transform of a step is the function (sin x)/x ≡sinc x, and when this is mixed with a Lorentzian line (which is the Fourier transform of an exponential): the resulting spectrum shows a peak that has "wiggles" at its base, as shown in Figure 2.5.

There are two approaches to curing this problem: to increase the acquisition time or to smooth the step function out by multiplying the FID by a function which begins at 1 then decays smoothly to zero by the end of the acquisition time. A second potential cause of "wiggles" at the base of a peak on a transformed spectrum is electronic saturation of the ADC. This occurs if the receiver gain has been set too high, as this overloads the ADC. The ADC simply registers maximum binary numbers, which has the effect of clipping the top and bottom of the FID.

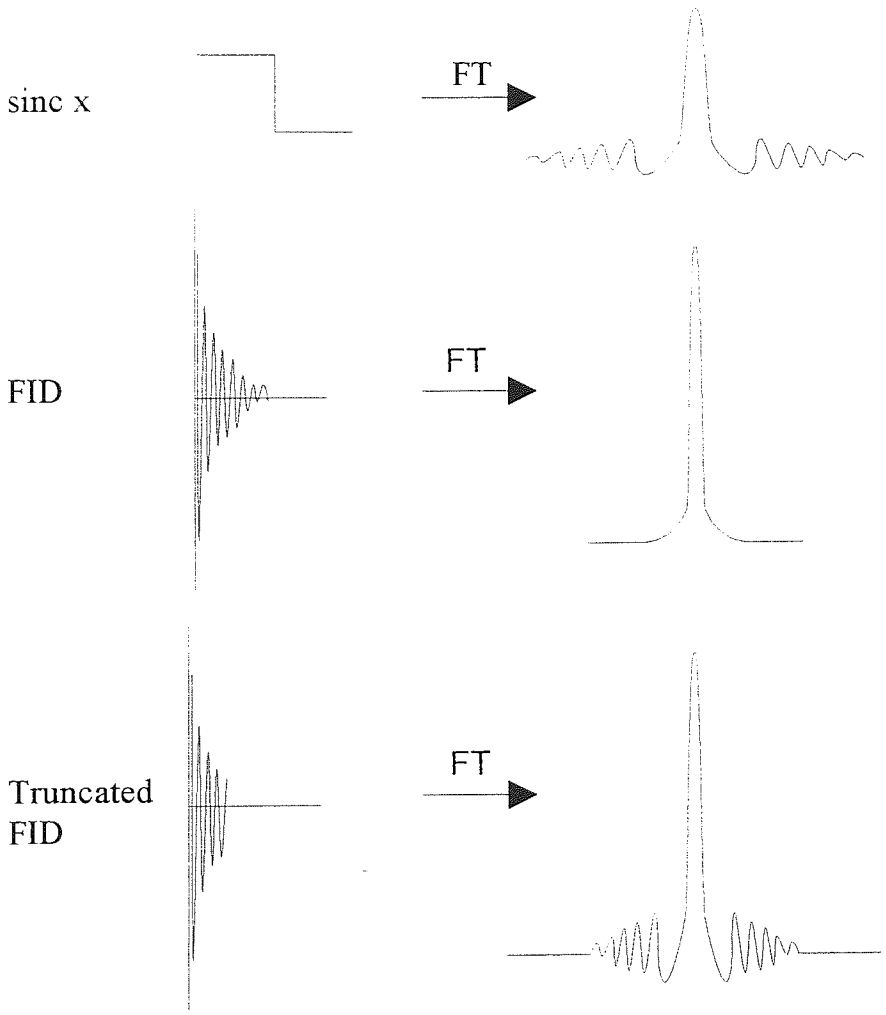

Figure 2.5: Transforming FID's

2.4.5 Window functions

Windows functions are used to manipulate time domain information prior to Fourier transformation. They are often used to optimise sensitivity or to increase resolution of a transformed spectrum. This is achieved by multiplication of the data in the time domain by an exponential function. This function essentially speeds the apparent decay of the signal, causing a visual reduction in the tail end of the FID data. This results in a broadening of the lines in a frequency spectrum. Thus multiplication of the FID by a decreasing exponential function enhances S/N at the expense of resolution.

CHAPTER 3 RELAXATION

3.1 RELAXATION

In 1946 Felix Bloch (34) derived a set of equations predicting that the population difference between two spin states will decay exponentially to equilibrium with a time constant T_1, known as spin-lattice relaxation.

The bulk magnetisation, at equilibrium, can be described by three orthogonal components $\mathbf{M}_x$, $\mathbf{M}_y$ and $\mathbf{M}_z$, in the laboratory frame.

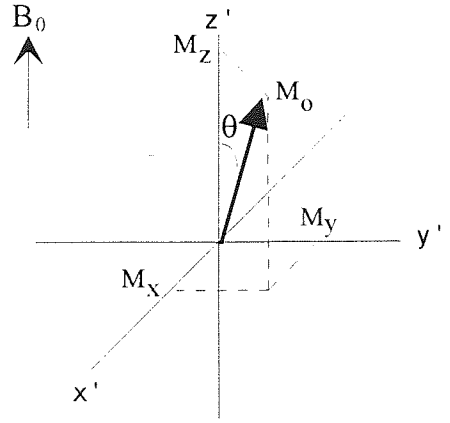

Figure 3.1: Magnetisation in the laboratory frame

Spin lattice relaxation involves the exponential decay of the population dependent magnetisation $\mathbf{M}_z$ to an equilibrium value of magnetisation, $\mathbf{M}_0$, in the presence of a static magnetic field $\mathbf{B}_0$. The decay of this longitudinal component, $\mathbf{M}_z$, is accompanied by an energy flow between the nuclear spin system to the lattice degrees of freedom: according to equation 3.1

$$\frac{dM_z}{dt} = \frac{-\left(M_z - M_0\right)}{T_1}$$ Equation 3.1

The loss of magnetisation from the x-y plane has a decay time T_2, and is known as spin-spin relaxation. T_2 involves the mutual exchange of spin energy and unlike T_1 processes does not involve the exchange of Zeeman energy with the lattice. The net effect of the energy exchange is to cause loss of phase coherence in the x-y plane: in thermodynamic terms it is an entropic process. This relaxation of $\mathbf{M}_x$ and $\mathbf{M}_y$ back to zero can be described by equation 3.2.

$$\frac{dM_x}{dt} = \frac{-M_x}{T_2} \text{ and } \frac{dM_y}{dt} = \frac{-M_y}{T_2}$$ Equation 3.2

The magnetic field is not perfectly homogenous and different nuclei will experience slightly different values of $\mathbf{B}_0$, and consequently they will precess at differing frequencies to the rotating frame. In practise, the experimental value of T_2 is shortened by this inhomogeneity and T_2 is represented by a new time constant T_2^*. The efficiency of spin-spin relaxation increases as molecular motion slows down, because each nuclear spin finds it easier to encounter another nuclear spin with which to interact: accordingly, T_2 is small in solids. The lineshape of an NMR spectrum is an indication of this field inhomogeneity over the sample. Thus the experimental linewidth at half maximum is given by equation 3.3

$$\Delta \nu_{1/2} = (\pi T_2^*)^{-1}$$ Equation 3.3

T_1 relaxation processes require an oscillating magnetic field of the correct frequency, occurring at the nucleus. A magnetic field of the order of the transition frequency for the spin, as required to induce relaxation, can be produced by the random molecular motion

of molecules. This random molecular motion is characterised by the molecular correlation time, τ_c, which can be defined as the average time that a molecule remains in a state of motion before a collision occurs. τ_c can be further defined as a combination of τ_c(rot), which is the time for motion over 4π and τ_c(trans) which is the time for the molecule to move through one molecular diameter These quantities are a function of molecular weight, solution viscosity, temperature, hydrogen bonding and even solution pH. A molecule in a typical non viscous liquid will remain in state of motion for on average of 10^{-12} s after which time it will undergo a collision. The motion of these molecules with their associated nuclear magnetic moments moving about in space generates fluctuating magnetic fields. Relaxation will be most efficient if the value of τ_c is such that there are large Fourier components of the molecular motion at the resonance frequency, ω_0. If τ_c is too large (solids) or too short (liquids), there will be small Fourier components at ω_0 and consequently much longer values of T_1 and T_2.

The quantity J, is the spectral density function of these fluctuating magnetic fields, which is a measure of their power at frequency, ω. Thus the spectral density term, $J(\omega)$, allows the motional characteristics of the system, (described by τ_c), to be defined in terms of power at frequency, ω, is given by equation 3.4

$$J(\omega) = \frac{2\tau_c}{1+\omega^2\tau_c^2} \qquad \text{Equation 3.4}$$

Figure 3.4 shows the spectral density function for three values of τ_c. The flat region of the function occurs when $\omega\tau_c << 1$, and is known as the extreme narrowing condition. This suggests that the amount of molecular power available for molecular motions is fixed and that changing τ_c only changes the way the power is distributed. From this graph

it can be seen that as τ_c increases the area under the function must be kept constant and the magnitude of $J(\omega)$ increases for the extreme narrowing region

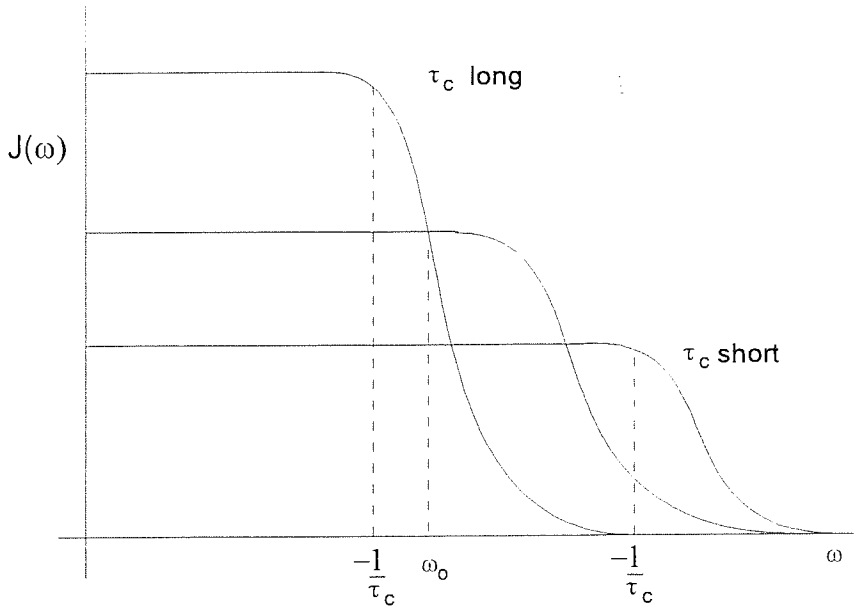

Figure 3.2: Spectral density function

If τ_c is long then low motional frequencies have a high probability of occurring whereas higher frequencies are almost absent. Similarly, if τ_c is short the molecular motions are distributed over a wider frequency range and have a smaller but equal probability of being found in a given molecule. The T_1 minimum occurs when the sudden drop in $J(\omega)$ as a function of ω corresponds to the resonance frequency for the nucleus.

Figure 3.2 shows the effect of τ_c on the relaxation times T_1 and T_2. Increasing τ_c will cause T_1 and T_2 to decrease because the nucleus will experience a larger spectral density. At $\omega\tau_c = 1$, T_1 is minimised because the resonance condition for the spin is met.

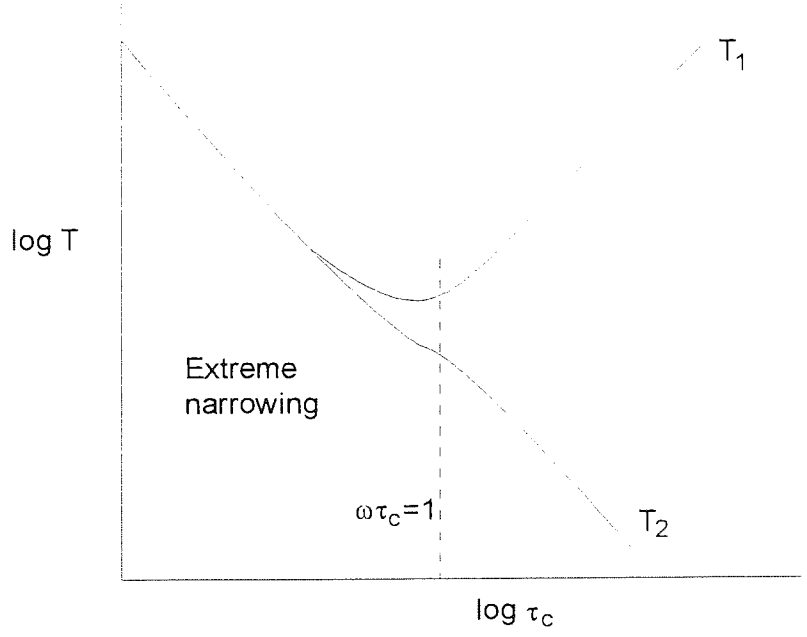

Figure 3.3: Relaxation time versus correlation time for a fixed field

The theory for calculating T_1 is usually complicated by the differing relaxation pathways available and for this reason the T_1 is usually determined experimentally (3.1.2)

3.1.1 Important mechanisms to facilitate T_1 relaxation

There are a number of different physical interactions responsible for coupling the nuclei to the lattice and providing the link through which energy can be exchanged.

3.1.1.1 The dipole -dipole mechanism for relaxation

A spinning nucleus generates a local magnetic field, B_{loc}, which can be experienced by other nuclei. The strength of the dipolar interaction between two magnetic nuclei

depends on their magnetic moments, their separation and their relative orientation to each other. The tumbling motion of the magnetic nuclei modulates the strength of the dipolar interaction by varying the angle, θ, between the magnetic field and the dipolar vector.

The dipolar contribution to spin lattice relaxation is found generally to increase with increasing temperature.

3.1.1.2 Quadrupolar relaxation mechanisms

Nuclei with I>½ possess a nuclear quadrupole moment that arises because their nuclear charge distribution is non spherical . Electric field gradients exist at atomic nuclei due to asymmetries in the spatial arrangement of the bonding electrons. The Brownian motion of molecules causes resultant rotating electric torque components to vary randomly around the nucleus. Some of these components will exist at the nuclear resonant frequency, ω_0, of the nucleus which will allow interchange of energy between the nucleus and the system. This interaction is usually the dominant relaxation mechanism for nuclei of spin I>1/2.

3.1.1.3 Paramagnetic relaxation

For paramagnetic nuclei the magnetic moment of an electron provides an efficient means for relaxation. The magnetic moment of an electron is much greater than that of the proton and consequently the presence of paramagnetic impurities has a profound effect on relaxation times. Modulation of relaxation occurs either by the spin-lattice relaxation of the electron itself or by the electron being transferred between different molecules.

Paramagnetic species include oxygen and many transition metals ions such as, Fe^{3+}, Mn^{2+}, Cr^{3+}.

3.1.1.4 Relaxation by chemical shift anisotropy

The chemical shift of a nucleus depends on the orientation of the molecule in the magnetic field. For molecules in the liquid state, the rapid molecular motion means that these values average to an isotropic value given by equation 3.5

$$\sigma = \tfrac{1}{3}\left(\sigma_{xx} + \sigma_{yy} + \sigma_{zz}\right) \qquad \text{Equation 3.5}$$

where σ is the shielding constant, σ_{xx} is shielding in the x direction, σ_{yy} is shielding in the y direction and σ_{zz} is the shielding in the z direction.

Although the nucleus on average sees a chemical shift value, σ, it can still see fluctuations in the local magnetic field, and this can also contribute to relaxation. This mechanism is generally not very efficient and only substantial for nuclei with high screening anisotropy and high chemical shift ranges (at high field).

3.1.1.5 Spin rotation relaxation

Spin rotation relaxation is caused by fluctuating magnetic fields generated at a nucleus by the motion of a molecular magnetic moment which arises from the electron distribution within the molecule. Spin rotation relaxation times depend on two correlation times τ_2 and τ_J. The correlation time, τ_J is the angular momentum correlation time, which is a measure of the time between changes in angular momentum. The orientation correlation

time, τ_2, describes the time in-between changes in orientation. The two quantities are dependent on each other and related as shown by equation 2.19

$$\tau_2 \tau_J = A/T \qquad \text{Equation 2.19}$$

where A is a constant and T is temperature. As the molecule rotates the electrons rotate about the nucleus: this gives rise to a small magnetic moment which is proportional to τ_J. This relaxation mechanism is unique in that increasing the temperature causes τ_J to become longer and τ_2 to become smaller: thus T_1 decreases.

3.1.1.6 Scalar coupling relaxation

Scalar coupling occurs if a fast relaxing nucleus is coupled to a slow relaxing nucleus, as in the case of a nucleus coupled to a quadrupolar nucleus. Scalar coupling can happen in one of two ways: if relaxation at one nucleus is short, then the relaxation of that nucleus will alter the field experienced by the coupled spin, causing fluctuations at a rate of $1/T_1$. Secondly, the scalar coupling experienced by two nuclei can be interrupted by chemical exchange. If the rate of chemical exchange is faster than J or $1/T_1$ then the nuclei will experience a fluctuating field which can contribute to relaxation

3.1.2 T_1 measurement

Pulse sequences for measuring T_1 either work by initialising the spin system and monitoring its consequent evolution or they operate on the system to achieve a steady state condition in which the intensity of the signal depends on T_1. The work in this thesis uses the DESPOT sequence, developed by Homer et al (35) (36) (37) rather than other

popular techniques such as inversion or saturation recovery. The reason for this is to reduce experimental time and thus minimise the heating effect caused by the application of ultrasound to the sample. This technique is faster than other techniques such as inversion recovery because it is not necessary to wait 5.3 T_1 between pulses.

3.1.2.1 DESPOT

DESPOT (Driven Equilibrium Single Pulse Observation of Spin Lattice Relaxation Times) can be used for the rapid measurement of T_1. For the relaxation of $\mathbf{M}_{zi}$ back towards $\mathbf{M}_0$, the transient magnetisation $\mathbf{M}_z$ can be described by equation 3.6

$$M_z = M_0 - (M_0 - M_{zi})e^{-t_i/T_1} \qquad \text{Equation 3.6}$$

where t_i is the total relaxation time to include the acquisition time, A_t, and the relaxation delay, (RD), used.

The DESPOT technique involves driving the magnetisation to an equilibrium value, $\mathbf{M}_{zeq}$, with a series of dummy pulses corresponding to the rapid multi-pulsing sequence $(\theta\text{-FS-t})_n$.

where FS is a field spoil pulse, applied to eliminate T_2 magnetisation and θ is the nutation angle.

The acquisition (A) of $\mathbf{M}_{zeq}$ is achieved using the pulse sequence $(\theta\text{-A-FS-t}^*)$m

The equilibrium magnetisation achieved by the DESPOT sequence can be described by equation 3.7

$$M_{zeq} = M_{zeq}\cos\theta e^{-t_i/T_1} + M_0\left(1 - e^{-t_i/T_1}\right) \qquad \text{Equation 3.7}$$

where $M_{zeq} \alpha I\sin\theta$, (I is signal intensity and θ the nutation angle) and as as $I_{eq} = KM_{zeq}\sin\theta$, it follows that

$$\frac{I_{eq}}{\sin\theta} = \frac{I_{eq}\cos\theta e^{-t/T_1}}{\sin\theta} + M_0\left(1 - e^{-t/T_1}\right) \qquad \text{Equation 3.8}$$

A straight line graph of $I/\sin\theta$ verses $I\cos\theta/\sin\theta$ will have a gradient equal to $e^{-ti/T1}$ and from this T_1 can be calculated.

CHAPTER 4 SOLID STATE NMR

4.1 INTRODUCTION

Solid state NMR spectra usually consist of a number of relatively broad lines. These broad lines are due to incomplete averaging of certain nuclear interactions which are orientation dependent. This anisotropic broadening often conceals structural and dynamical information that is present in the solid state. Conversely in liquid state NMR, the orientation dependent interactions can be represented by isotropic chemical shift and scalar spin-spin interactions, as all anisotropic interactions are reduced to zero due to rapid incoherent molecular motion.

4.1.1 The Hamiltonians of NMR

A Hamiltonian is an energy operator: the Hamiltonian that describes the NMR experiment can be written briefly as given by equation 4.1

$$\mathcal{H}_{NMR} = \mathcal{H}_{INT} + \mathcal{H}_{EXT} \qquad \text{Equation 4.1}$$

where $\mathcal{H}_{INT} = \mathcal{H}_{CSA} + \mathcal{H}_{SR} + \mathcal{H}_{D} + \mathcal{H}_{J} + \mathcal{H}_{Q}$ and

$$\mathcal{H}_{EXT} = \mathcal{H}_{Z} + \mathcal{H}_{RF}$$

where $\mathcal{H}_{z}$ is the Zeeman interaction, $\mathcal{H}_{RF}$ is the spin interaction with the external magnetic field, $\mathcal{H}_{CS}$ is the chemical shift interaction, $\mathcal{H}_{Q}$ is the quadrupolar interaction, $\mathcal{H}_{D}$ is the is the dipolar interaction $\mathcal{H}_{J}$ is the J-coupling interaction and $\mathcal{H}_{SR}$ is the spin rotation interaction.

The major operators in solid state NMR that are responsible for line broadening are the dipolar, the quadrupolar and the chemical shift Hamiltonians. $\mathcal{H}_{J}$, the indirect nuclear spin-spin or J coupling interaction is negligible in comparison with other interactions in

solids due to its small orientation dependence. Likewise, $\mathcal{H}_{SR}$, the spin rotation interaction which is the coupling interaction between the angular momentum and the nuclear spin caused by the rapid rotation in molecules is also negligible.

Hamiltonians are discussed more fully in two review papers by Smith et al (38)(39).

4.1.2 Dipole-dipole interactions and the dipolar Hamiltonian, $\mathcal{H}_D$

The dipolar interaction occurs due to dipole-dipole interactions between two or more nuclear dipoles. Figure 4.1 shows how the orientation of the internuclear vector for two dipoles with respect to the magnetic field is characterised by polar co-ordinates.

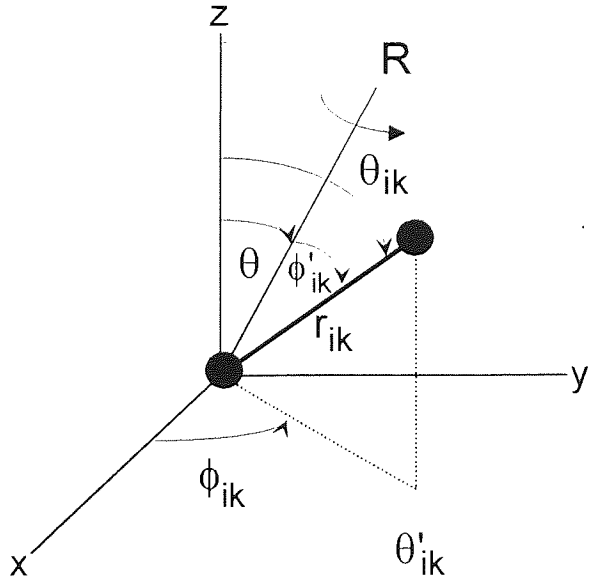

Figure 4.1: The anisotropic internal rotation of the spin vector r_{ik} between two dipoles about an axis of rotation, R.

Dipolar couplings are often the dominant line broadening mechanism in solid samples. Such line broadening can obscure other information present and this often calls for their

removal; though their presence can be an important source of structural information as their magnitudes are dependent upon the distance between nuclear spins.

Referring to figure 4.1, the magnetic dipole-dipole interaction Hamiltonian for a dipole-dipole interaction between magnetic moments $\gamma_i \hbar I^i$ and $\gamma_k \hbar I^k$ is defined by equation 4.2.

$$\hbar \mathcal{H}_D = \frac{\gamma_i \gamma_k \hbar^2}{r_{ik}^3}\left[I^i I^k - 3\left(I^i r_{ik}\right)\left(I^k r_{ik}\right)\right] \qquad \text{Equation 4.2}$$

where r is the distance between spins, i and k. As the dipolar Hamiltonian is proportional to r^{-3}, then the closer together the nuclei are, the stronger the interaction will be. The dipolar interaction will be the largest for nuclei with high magnetogyric ratios and thus is most important for nuclei of spin ½ that have large magnetic moments.

The energy of interaction, E, between two magnets i.e. dipoles , μ_1 and μ_2, separated by r, can be expressed by equation 4.3.

$$E = \left\{\frac{\mu_1 - \mu_2}{r^3} - \frac{3(\mu_1 . r)(\mu_2 . r)}{r^5}\right\}\frac{\mu_0}{4\pi} \qquad \text{Equation 4.3}$$

where μ_0 is the permeability constant and r is a vector quantity joining two magnetic dipole moments. Given that $\mu_1 = \gamma_1 \hbar I_1$ and $\mu_2 = \gamma_2 \hbar I_2$ this equation can be expressed in terms of polar co-ordinates. The result, given that $Ir = I_xX + I_yY + I_zZ$, is known as the dipolar alphabet (40), equation 4.4.

$$\mathcal{H}_D = r^{-3}\gamma_1\gamma_2\hbar^2[A+B+C+D+E+F]\mu_0 / 4\pi \qquad \text{Equation 4.4}$$

where:

$$A = I_{1z}I_{2z}(1-3\cos^2\theta)$$

$$B = -\tfrac{1}{2}[I_{1+}I_{2-} + I_{1-}I_{2+}](1-3\cos^2\theta)$$

$$C = -\tfrac{3}{2}[I_{1Z}I_{2+} + I_{1+}I_{2Z}]\sin\theta\cos\theta\exp(-i\phi)$$

$$D = -\tfrac{3}{2}[I_{1Z}I_{2-} + I_{1-}I_{2Z}]\sin\theta\cos\theta\exp(i\phi)$$

$$E = -\tfrac{3}{4}I_{1+}I_{2+}\sin^2\theta\exp(-2i\phi)$$

$$F = -\tfrac{3}{4}I_{1-}I_{2-}\sin^2\theta\exp(2i\phi)$$

where θ and ϕ are the polar angles of r, (as defined in Figure 4.1).

For a heteronuclear AX system, where $\mathcal{H}_Z >> \mathcal{H}_D$, the A term in the alphabet expansion is the only secular expression, that contributes to the total energy and therefore to the transition intensities and frequencies. Energy levels joined by non-secular terms have a low probability of induced transitions due to the low amplitude of internal thermal motions. Thus the contribution of the terms B to F in the calculation of energy levels is negligible. Thus, a reduced dipolar Hamiltonian is given by equation 4.5

$$\mathcal{H}_D = -h\left(\nu_A I_{Az} + \nu_x I_{xz}\right) + DI_{Az} I_{xz}\left(1 - 3\cos^2\theta\right) \qquad \text{Equation 4.5}$$

where ν is the resonant frequency of the spin and D is the dipolar coupling constant (not to be confused with the D term of the alphabet expansion), and D is equal to

$$\gamma_A \gamma_X (\hbar / 2\pi) r_{AX}^{-3} \mu_0 / 4\pi \qquad \text{Equation 4.6}$$

For a pair of isolated spins in a single crystal the spectrum of A (or X) will consist of two lines for a given orientation, each having a frequency given by equation 4.7

$$\nu = \nu_A \pm \tfrac{1}{2} D\left(1 - 3\cos^2\theta\right) \qquad \text{Equation 4.7}$$

The doublet, $D(1-3\cos^2\theta)$, will vary with crystal orientation with respect to the direction of the external field and is zero if θ is 54°44'. For a microcrystalline or powdered sample, all orientations are possible, the resultant spectrum, shown in Figure 4.2, is a Pake doublet (41), with the maxima 'horns' separated by D.

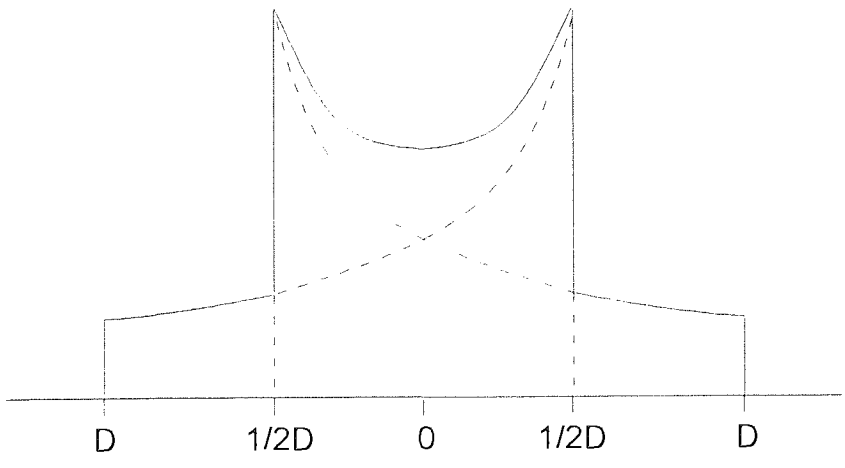

Figure 4.2: Pake powder pattern for a heteronuclear two spin system

For the homonuclear case, $\mathscr{H}_Z >> \mathscr{H}_D$ the B term in the alphabet expansion becomes secular. The total secular contribution is given by equation 4.8.

$$\mathscr{H}_D = -\nu_L(I_{1z} + I_{2z}) + D(1-3\cos^2\theta)\left[I_{1z}I_{2z} - \tfrac{1}{4}(I_{1+}I_{2-} + I_{1-}I_{2+})\right] \qquad \text{Equation 4.8}$$

where ν_L is the Larmor frequency and D is now

$$\gamma^2(\hbar/2\pi)r^{-3}\mu_0/4\pi \qquad \text{Equation 4.9}$$

Thus for a homonuclear two spin system, spin transitions will occur at

$$\nu = \nu_0 \pm \tfrac{3}{4}D(1-3\cos^2\theta) \qquad \text{Equation 4.10}$$

This corresponds to a doublet separation of 3/2D.

4.1.3 Chemical shift anisotropy (CSA) and the CSA Hamiltonian, $\mathscr{H}_{cs}$.

Chemical shift anisotropy occurs due to the screening effect of electrons surrounding a nucleus. Generally the electrons are not evenly distributed around a given nucleus, causing the shielding to be anisotropic. The additional internal magnetic field created by these circulating electrons opposes the external magnetic field B_0, its effect increasing with increasing B_0. This interaction is highly specific to orientation, and gives rise to a number of characteristic powder patterns, depending on the orientation of the molecule with respect to B_0.

The chemical shift interaction can be described by equation 4.11.

$$\hbar\,\mathscr{H}_{CS} = -\gamma\hbar I\sigma B_0 \qquad \text{Equation 4.11}$$

where σ is the screening or chemical shift tensor

From equation 4.12 it can be seen that the CSA interaction is dependant upon the field B_0, thus CSA lineshapes will become more prominent and broader when using high field spectrometers. The full shielding Hamiltonian is a tensor quantity that can also be defined by the principal axis system, as shown by equation 4.12.

$$\hat{\sigma} = \begin{pmatrix} \sigma_{xx} & 0 & 0 \\ 0 & \sigma_{yy} & 0 \\ 0 & 0 & \sigma_{zz} \end{pmatrix} \qquad \text{Equation 4.12}$$

Equation 4.13, shows the shielding constant σ_{iso} ,derived from the time averaging of the full shielding tensor due to rapid molecular interactions that occurs in the liquid state experiment

$$\sigma_{iso} = \frac{1}{3}\left(\sigma_{xx} + \sigma_{yy} + \sigma_{zz}\right) \qquad \text{Equation 4.13}$$

For a single crystal of axial symmetry the NMR transition frequency is given by equation 4.14:

$$\nu = \left(\gamma / 2\pi\right) B_0 \left(1 - \sigma_{zz}\right) \qquad \text{Equation 4.14}$$

In this situation the shielding contribution, σ, only has a single value, determined by the diagonal values in the shielding tensor and the orientation of the crystal with respect to B_0. For a microcrystalline sample, all values of θ are possible and a chemical shift anisotropy powder pattern is formed. A molecule of axial symmetry ($\sigma_{xx} = \sigma_{yy} \neq \sigma_{zz}$) will have a powder pattern as shown in Figure 4.3. The zero position in this diagram corresponds to the isotropic shift.

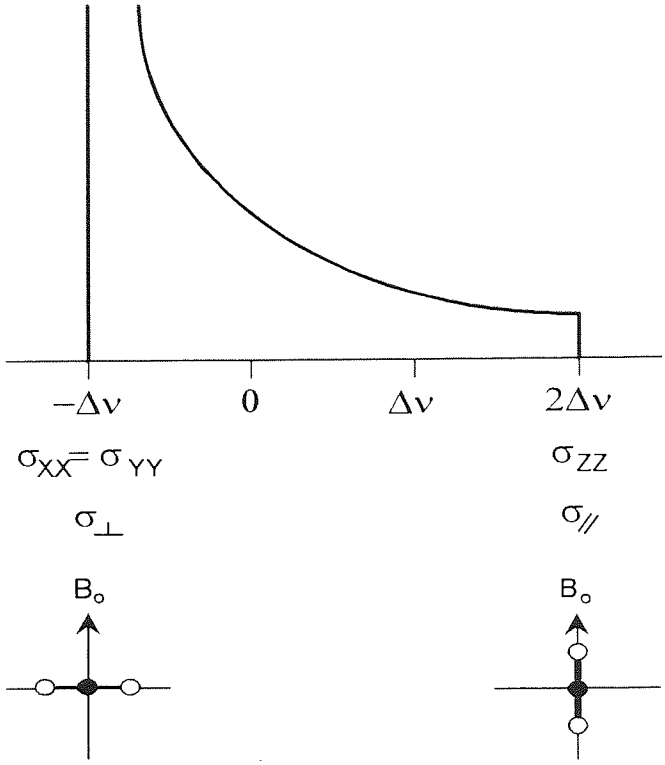

Figure 4.3: CSA powder pattern showing axial symmetry

The effective shielding in the z direction is given by equation 4.15

$$\sigma_{zz} = \tfrac{1}{3}\left(\sigma_{//} + 2\sigma_{\perp}\right) + \tfrac{1}{3}\left(3\cos^2\theta - 1\right)\left(\sigma_{//} - \sigma_{\perp}\right) \qquad \text{Equation 4.15}$$

The characteristic shape of the axially symmetry CSA powder pattern is because it is statistically more likely for the molecular symmetry axis of the molecule to be perpendicular than to be parallel to B_0. However, the more intense edge can be at either $\sigma_{\perp}$ or $\sigma_{//}$, and will depend on the preferred orientation of the molecule and whether $\sigma_{\perp} < \sigma_{//}$ or $\sigma_{\perp} > \sigma_{//}$. For a less than axial symmetry, the shielding in the z direction is given by equation 4.16.

$$\sigma_{ZZ} = \sigma_{iso} + \tfrac{1}{3}\sum_{j=x,y,z}\left(3\cos^2\theta - 1\right)\sigma_{jj} \qquad \text{Equation 4.16}$$

Such non-symmetric molecules have a powder pattern as shown in Figure 4.4

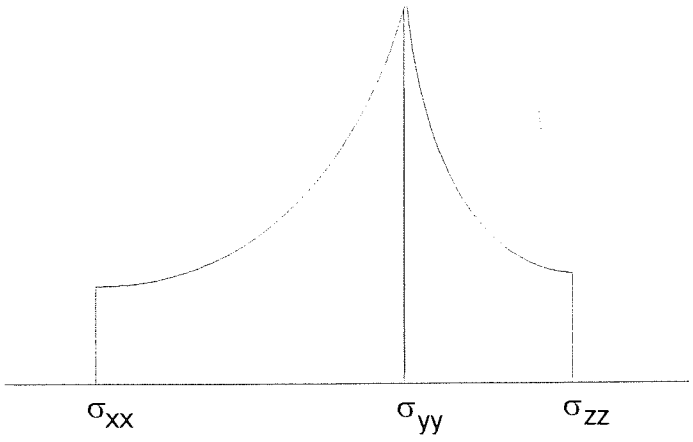

Figure 4.4: CSA powder pattern showing less than axial symmetry

The maximum intensity at σ_{yy} is not the isotropic shift value, this value can be calculated using equation 4.13.

Finally if the nucleus under observation is at a site of cubic symmetry, shielding will be independent of orientation and the powder or single crystal spectrum will give a single broadened line, as shown in Figure 4.5.

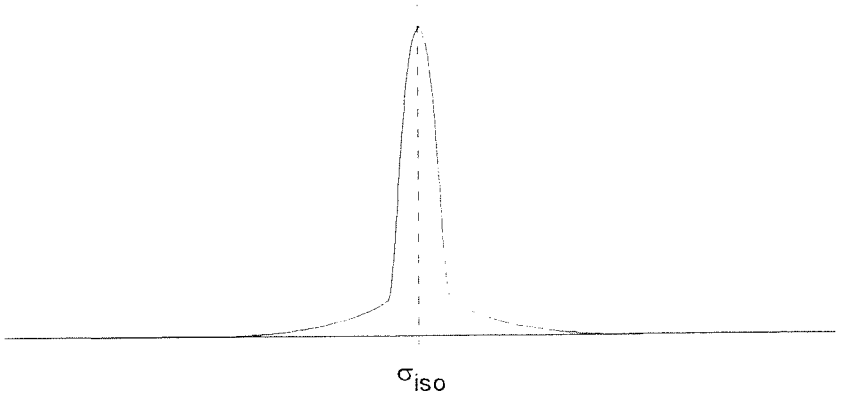

Figure 4.5: CSA powder pattern showing cubic symmetry

4.1.4 Quadrupolar coupling and the quadrupolar Hamiltonian, $\mathscr{H}_Q$.

The quadrupolar interaction (42) occurs for nuclei with I>½. It arises from the interaction between a the nuclear electric quadrupole moment, Q, with an asymmetrical electric field gradient (EFG) around the nucleus. The nature of the interaction is dependent upon whether the nucleus has a half integral or integral spin. Both first and second order quadrupolar interactions are produced which broaden the shift resonance from its isotropic value. If the EFG is zero, as in the case of cubic symmetry, then the energy gaps between the spin states and the transition energies possible for a 3/2 nucleus are all equal, resulting in a single resonance.

The quadrupole interaction Hamiltonian for a spin I may be described by equation 4.17

$$\mathscr{H}_Q = I_{\alpha\beta}Q_{\beta\alpha}I_{\alpha\beta} \qquad \text{Equation 4.17}$$

where $I_{\alpha\beta}$ is the nuclear spin and $Q_{\beta\alpha}$ is the nuclear quadrupole coupling tensor given by equation 4.18.

$$Q_{\beta\alpha} = \frac{eQ}{2I(2I-1)h}.V \qquad \text{Equation 4.18}$$

where eQ is the quadrupole moment and V is the electric field gradient tensor.

V itself is a tensor quantity, where the three principal elements V_{xx}, V_{yy} and V_{zz} describe the orientation and magnitude of the field gradient, which in turn can be described in terms of the asymmetry parameter, η, described by equation 4.19.

$$\eta = \frac{V_{xx} - V_{yy}}{V_{zz}}$$ Equation 4.19

For an axially symmetric interaction the electric field gradient will be symmetric around the principal axis and $V_{xx} = V_{yy}$ and $\eta=0$. Only V_{zz} will be unique, which means that the molecule will be orientated such that the EFG is characterised by the z component of the electric potential, V_{zz}.

The quadrupolar energy of this interaction, when $\mathcal{H}_Z >> \mathcal{H}_Q$ is defined by equation 4.20

$$h^{-1}U_Q = \left[\frac{3m_I^2 - I(I+1)}{8I(2I-1)}\right](3\cos^2\theta - 1)\frac{e^2 Q q_{zz}}{h}$$ Equation 4.20

For a first order interaction, when $\mathcal{H}_Z >> \mathcal{H}_Q$, the EFG will perturb the energy levels from their Zeeman splitting, ν_0, to give a shift in frequency for the m↔m-1 transition, defined by equation 4.21

$$\nu_Q = \frac{3(2m-1)}{8I(2I+1)}(3\cos^2\theta - 1)\frac{e^2 Q q_{zz}}{h}$$ Equation 4.21

where θ is the angle of the V_{zz} component of the EFG tensor with respect to B_0. And e^2Qq_{zz}/h is the quadrupole coupling constant, χ.

The first order quadrupole effect is the way these spin transitions alter as the orientation of the crystal is altered. The EFG perturbs the energy levels away from their Zeeman positions to give a displacement of the satellites (e.g. 3/2 ↔ 1/2 and -1/2↔-3/2) that is proportional to the magnitude of the quadrupole coupling constant and $3\cos^2\theta$-1, where

θ is the angle between the EFG tensor axis, V_{zz}, and the direction of the magnetic field, B_0. Figure 4.6 shows how this alters the energy levels: the 1/2 $\leftrightarrow$ -1/2 transition frequency is unchanged, whereas the -3/2 $\leftrightarrow$ -1/2 is increased whilst the 1/2 $\leftrightarrow$ 3/2 is decreased. If a single orientation is considered a spectrum will contain three lines as shown in Figure 4.7, spaced by $\chi(3\cos^2\theta\text{-}1)/4$. An amorphous powder where all orientations are possible will show an intense central transition, with the satellite lines being lower in intensity, often becoming obscured in the baseline.

Second order quadrupole effects become important when $\mathscr{H}_Z \approx \mathscr{H}_Q$. This situation causes the 1/2 $\leftrightarrow$-1/2 transition to be perturbed from the Larmor frequency, ν_0, as shown in Figure 4.6 and given by equation 4.22.

$$\nu_2 = \left(\frac{-\nu_Q^2}{16\nu_0}\right)\left[I(I+1) - 3/4\right]\left(1-\cos^2\theta\right)\left(9\cos^2\theta - 1\right) \qquad \text{Equation 4.22}$$

If χ, the quadrupole coupling constant is large, then the satellite transitions (3/2$\leftrightarrow$1/2 and $-1/2\leftrightarrow$-3/2) will be too weak to be observed in the NMR spectrum due to the influence of $(3\cos^2\theta\text{-}1)$.

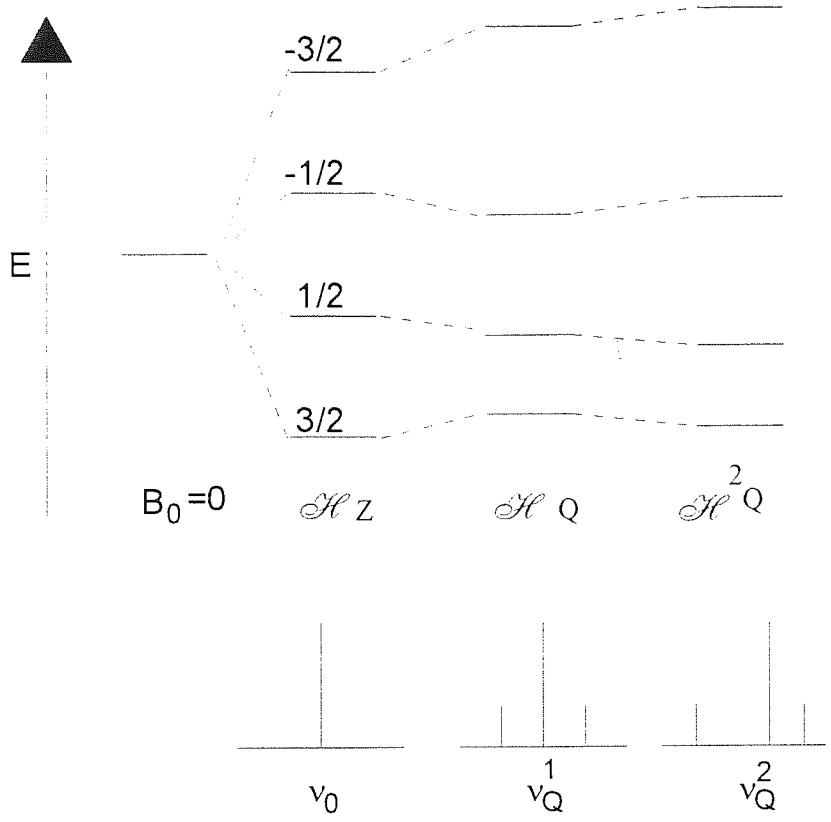

Figure 4.6: Energy level diagram showing the quadrupolar influence for a spin 3/2 nucleus

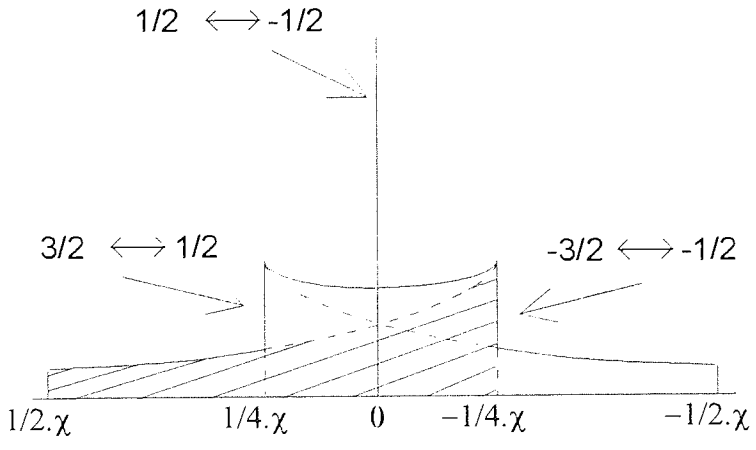

Figure 4.7: Quadrupolar powder pattern for an axially symmetric spin 3/2 nucleus, under first order conditions

4.2 METHODS OF LINE NARROWING

There is a variety of ways of narrowing the broad lines typical of solid state nuclear magnetic resonance spectra.

4.2.1 Magic angle spinning

MAS NMR developed by Andrew et al (6) and Lowe (7) involves rapidly rotating a sample around the so called magic angle (54°44') to the magnetic field B_0. Any interaction that can be described by the term $3\cos^2\theta-1$ will reduce to zero. In solids, dipolar interactions and chemical shift anisotropy have an angular dependence of the form $3\cos^2\theta-1$, and their broadening effects can consequently be eliminated by this technique. Quadrupolar interactions are only reduced if they are first order interactions, as these also have an angular dependency on $3\cos^2\theta-1$. The second order term which has an angular dependency on $(9\cos^2\theta-1)$ is not eliminated by spinning at the magic angle, although it is reduced by a factor of about four.

In practice a real sample will typically be a powder sample where the internuclear vectors take all possible angles, θ. Figure 4.8 shows the internuclear vector being spun about the magic angle. It can be seen that by rotating at high speed, the average direction of the vector r_{jk} becomes magic.

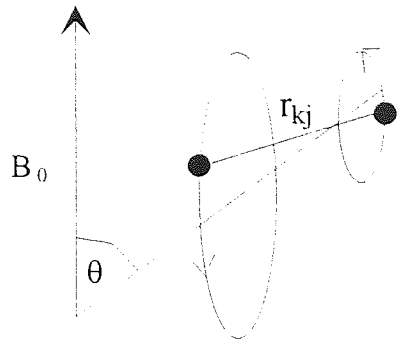

Figure 4.8: Magic angle spinning NMR: internuclear vectors rotating about the magic angle

In practice, the sample is mounted within in a rotor whose axis is inclined to 54°44' with respect to the magnetic field B_0. The turbine, which is air driven, rotates the sample at the magic angle at high speed. The rate of rotation has to at least equal the CSA linewidth (in Hz) of the sample being observed. If the spinning speed is less than this the spectrum will contain a series of spinning sidebands which will occur at multiples of the spinning speed.

Magic angle spinning is discussed more fully in review articles by Schaefer, J & Stejskal, E (43) and Andrew E.R. (44)

4.2.2 Double angle rotation techniques

Double angle rotation techniques represent an important advancement in the solid state NMR study of quadrupolar nuclei.

4.2.2.1 Double rotation (DOR NMR)

Double rotation NMR (17) involves the simultaneous rotation of the sample about two different angles, 54.74° and 30.6°, corresponding to the zeros in both the second and fourth order Legendre polynomials respectively, defined by equations 4.23 and 4.24.

$P2 = 1/2(3\cos^2\theta-1)$ Equation 4.23

$P4 = 1/8\ (35\cos^4\theta-30\cos^2\theta+3)$ Equation 4.24

DOR uses a double rotor assembly as shown in Figure 4.9, the outer rotor being set to θ_1 =54.74° (with respect to B_0). to remove dipolar interactions, and the inner to θ_2 = 30.6°(with respect to B_0),. to remove quadrupolar interactions. Other solutions to DOR are possible, and have been calculated (45). The rotors can be spun at individual rotation frequencies, ω_1 and ω_2.

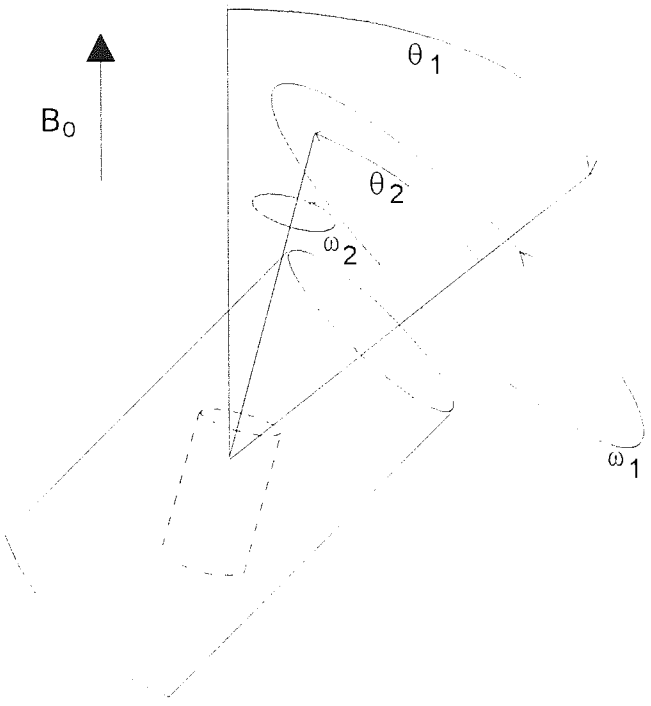

Figure 4.9: Double angle rotation

One problem with this technique is that the speed of the external rotor is limited and this can lead to problems of overlapping sidebands destroying resolution. One way of overcoming this problem is by only exciting the sample when the rotor phase is at 0° and 180°; the resulting spectrum will consequently contain only odd numbered spinning sidebands.

4.2.2.2 Dynamic angle spinning (DAS NMR)

Dynamic angle spinning (DAS) (19) involves spinning the sample about an angle of θ_1=37.38°, and then rapidly flipping the sample to an angle of θ_2=79.18°. These angles are chosen as they are the simplest of an infinite number of solutions of equation 4.25 that have been calculated (46)

$$\sum_i^N P_2(\cos\theta)k_i = \sum_i^N P_4(\cos\theta)k_i = 0 \qquad \text{Equation 4.25}$$

Figure 4.10 shows the pulse sequence used in this technique. Firstly the magnetisation vector is tipped over into the xy plane; the Hamiltonians develop at this angle θ_1 for τ_1 seconds. A flipping process then takes the magnetisation to the new angle θ_2 and the magnetisation is again allowed to develop. This flipping process takes about 35ms; during this time the magnetisation is stored along the Zeeman field, to prevent the Hamiltonians developing during the switching process. A FID is acquired during the two evolution times.

The DAS spectrum is a combination of the two FID's obtained for each angle, where the two superimposed spectra cross is the isotropic shift position.

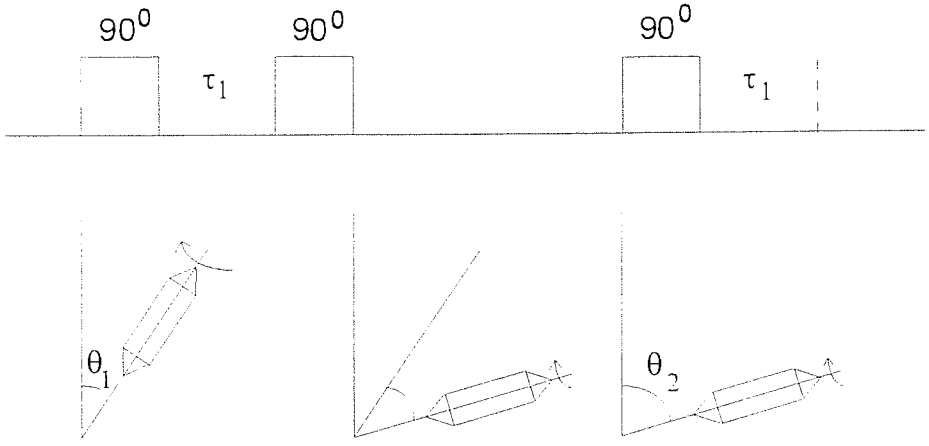

Figure 4.10:Dynamic angle spinning

CHAPTER 5 THEORY OF ULTRASOUND

5.1 INTRODUCTION TO ULTRASOUND

Acoustic waves refer to mechanical perturbations (displacement, pressure, density) of the equilibrium state of the medium through which they are travelling. The perturbations are periodic and classified according to their frequency, f (in Hz): 20Hz-20 kHz is known as the sound range (for hearing), while 20kHz-10^9 Hz, is known as the ultrasound range.

Conventionally ultrasound is divided into two areas: power (low frequency) ultrasound (20-100kHz) and diagnostic (high frequency) ultrasound (2-10MHz).

5.1.1 Sound waves

Ultrasound can be regarded as a pressure wave, transmitting its disturbance through an intervening medium. Practically any material that has elasticity can support ultrasonic waves. The medium through which a sound wave travels can be regarded as a large number of layers or particles; a particle being the fundamental unit of the displaced propagating medium. The passage of ultrasound through a medium can be regarded as a time dependant disturbance of these particles from their equilibrium positions. Ultrasound can originate from a plane surface vibrating with simple harmonic motion. Vibrations are characterised by their frequencies, the number of complete periodic cycles undergone in a unit time. Thus frequencies are denoted by the number of cycles per second, hertz (Hz). When the plane surface vibrates longitudinally, in the direction of the wave motion, a longitudinal wave is generated, (see Figure 5.1). This consists of a series of compressions and rarefactions. A region of compression within a material means that the density of the material is increased within that area, conversely a region of rarefaction has a decreased "particle" density. Conversely, when the generating plane surface is at

right angles to the direction of wave motion a transverse, or shear wave, is generated, in which there are no localised density fluctuations. Shear waves can generally only be propagated in solids or some highly viscous liquids as gases and liquids are unable to support shear stresses.

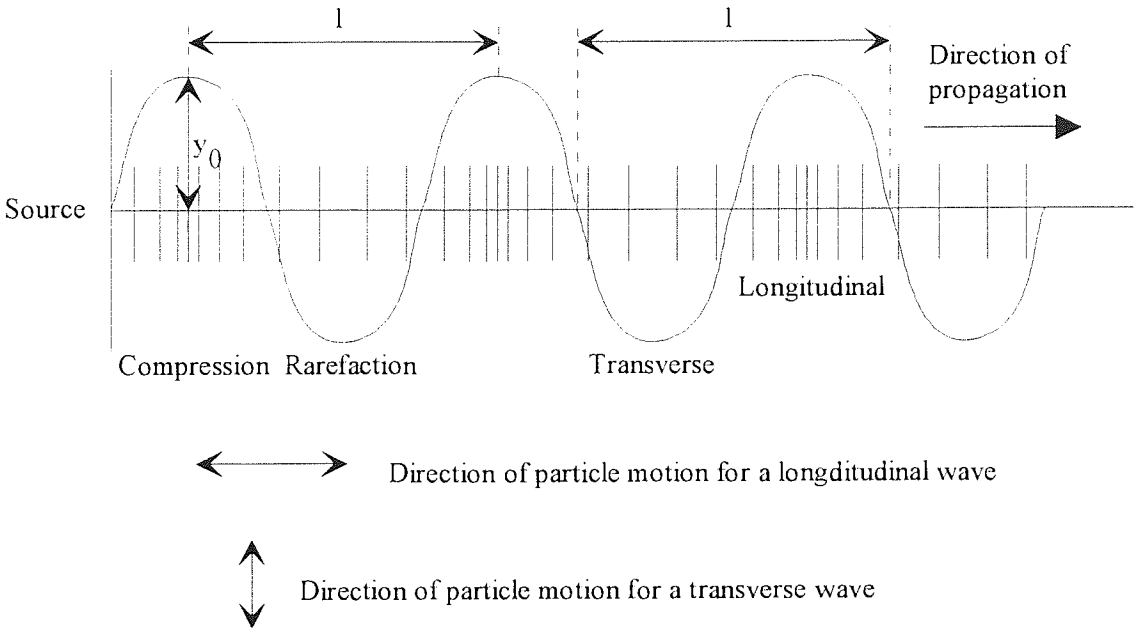

Figure 5.1: Diagram showing longitudinal and transverse wave motion

Energy transfer continues through the medium until a boundary is reached. The phase of the wave will change as it passes through the material due to each layer in the wave path moving a little later than its neighbour.

Figure 5.1 shows that sound can be represented by a sinusoidally varying pressure wave. The shape of the sine wave can be expressed in terms of the displacement of the layer, y, during a time, t according to equation 5.1

$$y = y_0 \sin \omega t$$ Equation 5.1

where ω is the angular frequency, which can itself be expressed by $\omega=2\pi f$ and y_0 is the maximum displacement amplitude. This particle displacement can also be expressed in terms of the velocity of the vibrating particles in the medium, u, shown by equation 5.2.

$$u = u_0 \sin \omega t$$ Equation 5.2

where u_0 is the particle velocity amplitude. Alternatively particle displacement can be expressed in terms of the excess acoustic pressure of the medium, as defined by equation 5.3.

$$p = p_0 \sin \omega t$$ Equation 5.3

where p_0 is the maximum acoustic pressure amplitude

All wave trains are rich in harmonics; the analysis of such a train by the Fourier method reveals a great number of frequency components. The lowest frequency is the fundamental frequency, all higher frequencies are known as harmonics of the fundamental.

5.1.2 Acoustic impedance

Acoustic impedance (47) can be regarded as the resistance imposed by the medium on the progression of an ultrasonic wave. It can be defined by equation 5.4 as the ratio of

acoustic pressure to particle velocity. Thus, if the acoustic impedance is high the particle velocity will be low.

$$Z_a = \frac{p}{u}$$ Equation 5.4

Acoustic impedance is usually highly complex, but can be approximated if a plane progressive wave and conditions of infinite boundary are considered. In other words the plane wave is not reflected to form a stationary wave (discussed in 5.4.5), which would contain an imaginary as well as real component. The real quantity, R_a, defined by equation 5.5 is known as the characteristic impedance.

$$R_a = \rho c$$ Equation 5.5

where ρ is the density and c is the velocity of sound for the medium.

5.1.3 Attenuation

Plane waves propagating through a medium will be subject to processes that cause attenuation. One cause of attenuation is by absorption, whereby internal friction causes mechanical energy to be turned to heat; this can occur by a hysteric or relaxational process. Attenuation of a plane wave can also arise from reflection, diffraction, refraction or scattering producing a deviation of energy from the parallel beam.

5.1.3.1 The coefficient of absorption

The intensity of an ultrasonic wave, (assuming attenuation to be uniform), will decrease exponentially with distance from source according to equation 5.6,

$$A = A_0 \exp^{-2\alpha x}$$ Equation 5.6

where A_0 is the amplitude at x =0, A is the reduced amplitude of the wave after it has travelled a distance x and α is the intensity absorption coefficient, usually expressed in nepers per second. This type of attenuation can also be defined by δ, the logarithmic amplitude loss per cycle, according to the equation 5.7:

$$\frac{1}{Qm} = \frac{\delta}{\pi}$$ Equation 5.7

where Q_m is the quality factor (see 5.2.2.3)

5.1.3.2 Absorption

Absorption can occur by relaxation processes. As an acoustic wave passes sinusoidally through a medium, energy is absorbed by the medium during the positive half of the stress cycle and emitted during the negative half. If this event causes sinusoidal variations of the translational energy of a molecule then this event takes place instantaneously. However, if these sinusoidal variations of applied stress couple with other vibrational energy modes occurring in that layer, this results in a time lag, t, before energy exchanges re-establish equilibrium conditions. This culminates in a phase lag of that sinusoid and a resultant lowering of peak height and subsequent attenuation of the ultrasonic wave. At low frequencies, the time lag, t << T (T being the time period of the compressional wave), is small and thus the amount of absorption is small. At increasing frequencies, the ratio t/T increases, increasing both the phase lag and the attenuation of

the ultrasonic wave. At very high megahertz frequencies attenuation is once again reduced as the wave cycle occurs too quickly for coupling to happen.

Absorption can also occur by a hysteretic process, due to the finite time required for the energy from the wave to be transferred to the medium. Thus the stress applied to the medium by the wave front will not vary linearly with the resultant strain. The stress/ strain curve then takes the form of a hysteresis loop.

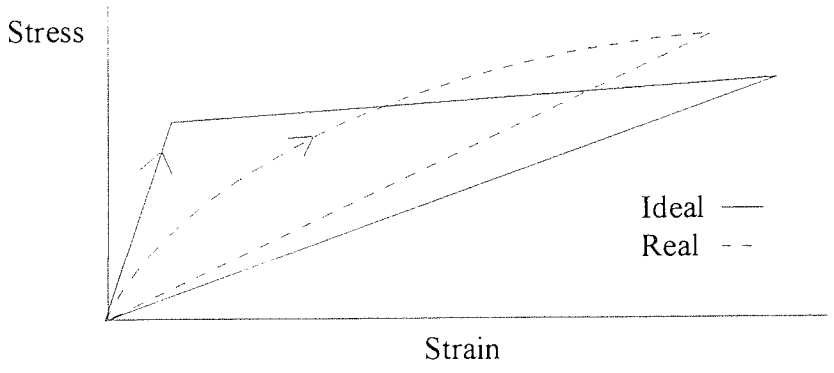

Figure 5.2: Stress- strain hysteresis curve

The area within such a loop, as shown in Figure 5.2, denotes the amount of energy lost per cycle.

5.1.3.3 Ultrasound transmission at a plane boundary.

As an ultrasonic wave is transmitted through a boundary, some of the energy is transmitted while some is reflected. The reflection coefficient, Rc, is equal to the intensity of waves reflected at the boundary divided by the intensity of those incident at it, according to equation 5.8.

$$Rc = \left(\frac{R_2 - R_1}{R_1 + R_2} \right)^2$$

Equation 5.8

The transmission coefficient, Tc, is the intensity of transmitted waves at the boundary divided by the intensity of those incident to it according to equation 5.9.

$$Tc = \frac{4R_1R_2}{(R_1 + R_2)^2}$$

Equation 5.9

where R_1 and R_2 are the characteristic impedances of the two media.

Thus it is possible to match the characteristic impedances so that the transmission coefficient can be maximised, minimising the reflection coefficient. This is achieved when R_1 and R_2 are equal, as the above equations show that in this situation Tc will be increased while Rc is reduced to zero.

5.1.3.4 Reflection and refraction at a plane boundary

Reflection and refraction at a plane boundary occurs when an acoustic wave travelling through a medium with a given specific acoustic impedance meets a boundary to another medium which differs in acoustic impedance. The amount of energy that is either reflected or refracted is dependant on the angle of incidence of the incoming wave as well as on the acoustic impedances of the two media.

Figure 5.3 shows that an incoming longitudinal wave, XY, will be reflected along, YW, or refracted along, YZ.

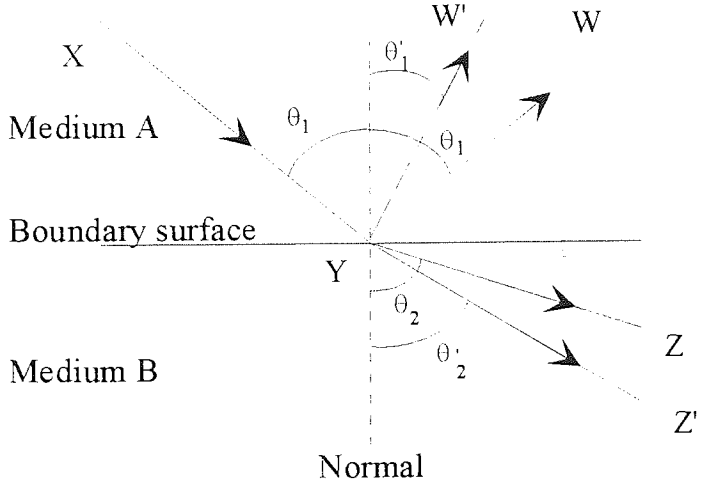

Figure 5.3: Reflection and refraction at a plane boundary

This situation is more complicated than this in practice due to the fact that an incident wave may itself be a shear wave, or it is possible for an incident longitudinal wave to be resolved into parallel and perpendicular components as it meets with the boundary by a process known as mode conversion. This occurs because the pressure of the incoming wave causes the boundary to oscillate and generate both transverse as well as longitudinal waves.

Calculating reflection and transmission parameters for this scenario is again complex, owing to the diversity of situations that can arise. Although in the general case of a longitudinal wave being incident to a plane surface and in the absence of mode conversion, these parameters can be calculated using equations 5.10 and 5.11

$$Rc = \left(\frac{R_2 \cos\theta_1 - R_1 \cos\theta_2}{R_2 \cos\theta_1 + R_1 \cos\theta_2} \right)^2 \qquad \text{Equation 5.10}$$

$$Tc = \frac{4R_1R_2\cos\theta_1\cos\theta_2}{(R_2\cos\theta_1 + R_1\cos\theta_2)^2}$$ Equation 5.11

5.1.3.5 Diffraction

A beam of progressive plane waves generated from a circular source will remain parallel for a distance dependant on the diameter of the source: and after this it will diverge. This phenomena is known as diffraction (48) and it occurs when the parallel rays propagated from the source diverge so as to appear as though they have been emitted from the centre of the source. As shown by figure 5.4 the region where the rays are parallel with the source axis is known as the Fresnel zone, while the region further away where the rays diverge is known as the Fraunhofer region.

Attenuation by diffraction can be reduced by ensuring that the sound field does not extend beyond the Fresnel zone: in practical terms for a source of diameter a, this is a distance a^2/λ from source. Where a is the diameter of the source.

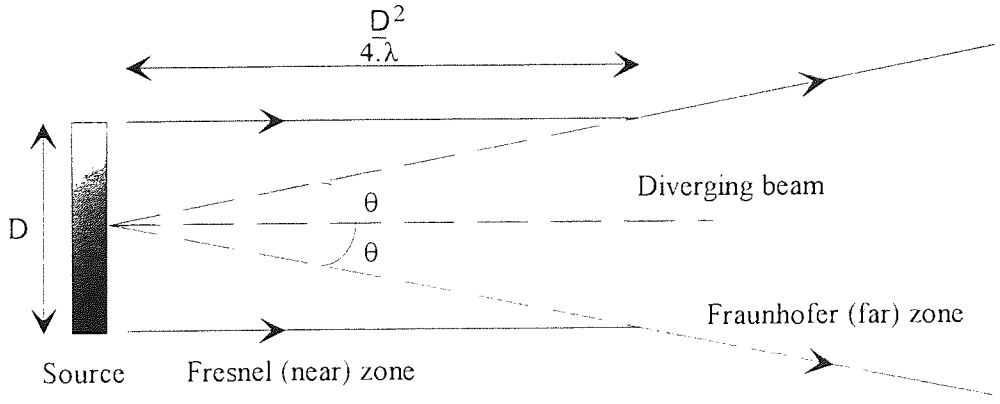

Figure 5.4: Diffraction

5.1.3.6 Scattering

Scattering (49) (50) of energy in liquids occurs through inhomogeneities such as suspended particles, turbulence or small bubbles. A body in the path of an acoustic wave will modify the pressure distribution of the wave, according to the dimensions of the disturbance (51). If the body size is very much larger than the wavelength of the incident radiation, then almost total reflection from its surface will occur, resulting in an acoustic shadow behind the body. When the body dimensions are of the same order of magnitude as the wavelength, the resultant scattered wave becomes highly complex and dependant on the dimensions of the body. The third scenario is that the body is very much smaller than the wavelength of incident radiation. In this situation scattering is minimal as the radiation tends to diffract around the disturbance.

5.2 CRYSTALS FOR ULTRASONIC PRODUCTION

An acoustic transducer is a device that either generates sound waves by the transformation of electrical energy into mechanical oscillation, or receives sound waves by the opposite process. There are many types of transducer, the choice of which will depend on the application required.

5.2.1 Piezoelectric oscillators

Piezoelectricity was discovered in 1880 by the Curie brothers (52). It was found to be exhibited in crystals that lack a centre of symmetry and have one or more polar axes. If a plate is cut from such a crystal with its parallel surfaces lying normal to a polar axis and an alternating electric field applied, the plate will expand and contract with the same frequency as the field. Conversely, if the plate is subjected to a mechanical stress a

voltage will be formed across the plate. A trigonal system such as quartz can be cut along its X,Y or Z axes, see Figure 5.5. The Z-axis is non polar, and will not exhibit the piezoelectric effect. The polar X and Y axis lie perpendicular to the z axis.

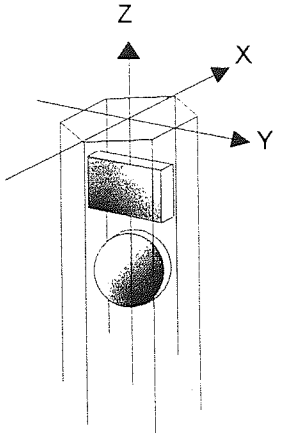

Figure 5.5: X-cut rectangular and circular transducers from a quartz crystal

Crystals are said to be X-cut when they are to be used for the generation of longitudinal, compression waves. Crystals are said to be Y-cut when they are to be used for the generation of shear waves, shown in figure 5.6.

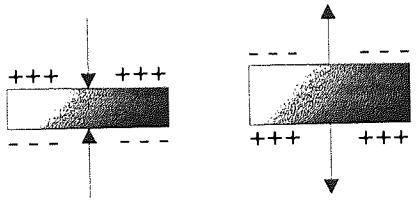

Compressional Wave Transducer

Shear Wave Transducer

Figure 5.6: X and Y-cut crystals

When an alternating current is applied across an X-cut quartz crystal, the X –axis will compress while the Y axis will expand and vice versa as the electric current reverses direction: there will be no strain on the Z axis. If the transducer surfaces normal to the X and Y-axis are coated with a layer of conducting metal paint, an alternating current applied across these electrodes will cause the transducer to oscillate in the same direction as the applied field. The amplitude of these oscillations is at a maximum when the voltage frequency coincides with the natural resonant frequency of the crystal.

5.2.1.1 Running at upper harmonics

Maximum acoustic energies are obtained when the transducer is being operated at its natural frequency. A crystal can be made to operate at upper harmonics of its natural frequency (53). As the piezoelectric effect can only occur when opposite charges appear on its electrodes (see Figure 5.7) only odd harmonics can be generated. Another way of looking at this is by considering that you need to have a potential difference across the faces of the plate to carry the current which requires an opposite charge on either electrode.

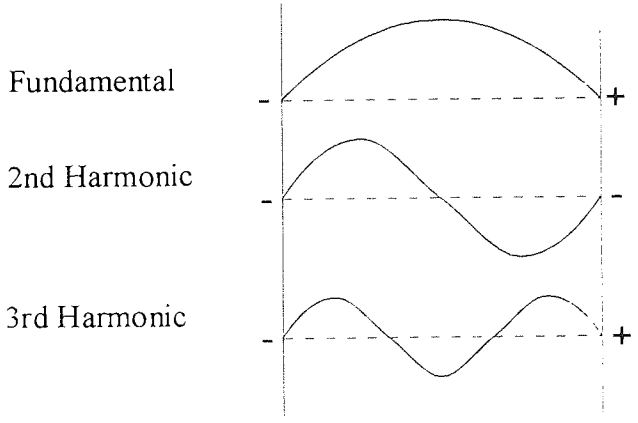

Figure 5.7: Fundamental and upper harmonics

5.2.1.2 Ceramic transducers

Ceramic transducers are formed by bonding together small crystallites of ferromagnetic material. The advantages of using this type of transducer over a naturally occurring crystal such as quartz is that it is possible to bond them in such a way as to produce a concave transducer suitable for focusing the ultrasonic radiation. Also they possess a higher efficiency for the conversion of electrical energy to mechanical energy, so they can be operated at much lower voltages.

The Curie temperature of an acoustic transducer is the temperature at which the piezoelectric effect disappears. The piezoelectric strain constant, d, of a transducer can be defined as the charge density output per unit of applied stress, or, in other words, the mechanical strain produced per applied voltage, V. It can be defined mathematically by equation 5.12

$$d = \frac{q}{F}$$ Equation 5.12

where q is the amount of charge which flows for a given mechanical stress, F. Table 5.1 outlines some of the properties of a selection of the many different ceramics available.

Table 5.1: Piezoelectric properties of some common transducer materials (54)

Ceramic	d/ coulomb Newton^{-1} *10^{12}	Dielectric constant	Upper Curie Temperature °C
Quartz (X-Cut)	2.3	4.5	550
Barium titanate	60-190	400- 1700	120-140
Lead zirconate titanate	80-320	900 - 1500	350-450
Lead meta-niobate	85	225	550

Varying the composition of the transducer material can provide the properties that are required for a particular acoustic application (55), (56).

5.2.2 Efficiency

Transducer efficiency, η, can, in general, be described by equation 5.13

$$\eta = \frac{\text{Power radiated in the load}}{\text{Total power input}}$$

Equation 5.13

Efficiency is determined by two factors, the efficiency of conversion of electrical to mechanical energy, followed by the conversion efficiency of mechanical into acoustic energy. Losses due to energy conversion between mechanical to acoustic are relatively constant over a range of frequencies while energy conversion from electrical to mechanical is frequency dependent, resulting in larger losses for higher frequencies.

5.2.2.1 Motional impedance

Vibration created by a transducer causes a back electromotive force (emf) on the circuit. This back emf will oppose the forward impressed one. This consequently results in a change of the circuit impedance. This change is referred to as the motional impedance and its influence impinges on how efficiently the transducer will operate.

5.2.2.2 Acoustic intensity

Acoustic intensity can be described as the average rate of energy flow through a unit area normal to the direction of wave propagation as a result of sound pressure acting on that

area. The energy density will vary throughout the wave cycle, but it is possible to calculate an average acoustic intensity, according to equation 5.14

$$I = \frac{\rho c \omega^2 \xi_{max}^2}{2}$$ Equation 5.14

where ρ is the medium density, c is the velocity of sound in the medium, ω is the angular frequency of the sound wave, ξ_{max} is the maximum amplitude of vibration of the medium. The power of the sound wave can be calculated by multiplying the acoustic intensity by the area through which the energy flows. By calculating this power and knowing the power supplied to the transducer it is possible to determine the efficiency of the transducer (5.2.2).

5.2.2.3 The Q factor

The quality of the resonance of a transducer can be described in terms of either its electrical quality factor, Q, or its mechanical quality factor, Q_m. This quantity is a measure of the ability of a transducer to operate over a range of frequencies. By reference to figure 5.6, it can be seen that a high quality factor will provide a narrow frequency range at a high velocity amplitude, as required by high power applications. Conversely a low quality factor provides a greater spread of frequencies at lower velocity amplitude, as required for sensing applications.

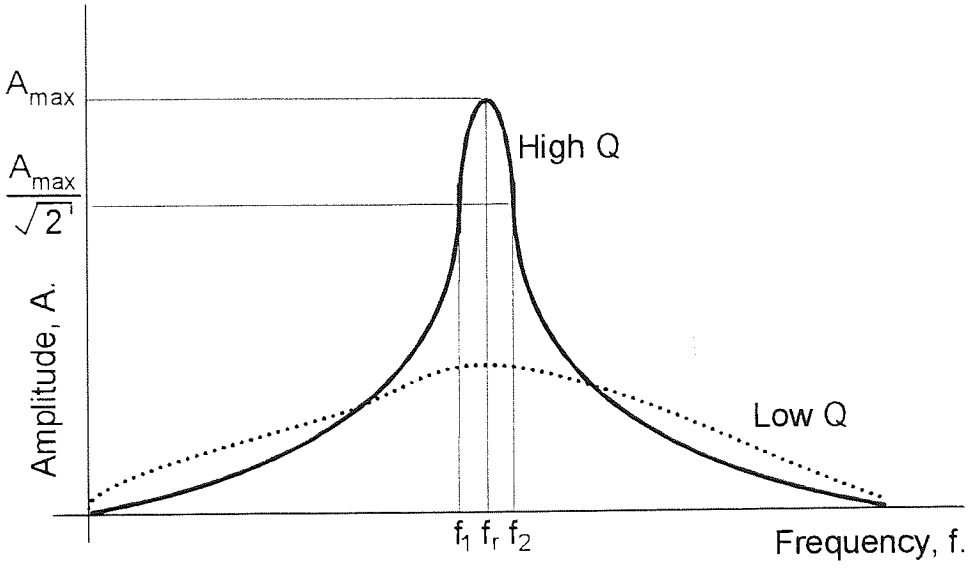

Figure 5.8: Frequency response curves for velocity amplitude

The mechanical quality factor Q_m can be described in one of two ways as defined by equations 5.15 and 5.16

$$Q_m = \frac{\omega_r}{\omega_2 - \omega_1} \qquad \text{Equation 5.15}$$

where ω_1 and ω_2 represent angular frequencies $1/\sqrt{2}$ of the maximum value on either side of ω_r.

The mechanical quality factor can also be defined by equation 5.16

$$Q_m = \frac{\omega_r M}{R_m} \qquad \text{Equation 5.16}$$

where R_m is the mechanical resistance to vibration, M is the mass being displaced and ω_r is the angular frequency at maximum velocity amplitude.

The electrical quality factor is related to the mechanical quality factor by equation 5.17

$$Q = \frac{\pi^2 \cdot 2K_c^2}{Q_m}$$ Equation 5.17

where K_c is the electromechanical coupling factor. K_c characterises the conversion of electrical to mechanical energy and provides of a measure of the losses associated with a transducer.

5.2.3 Transducers for ultrasonic propagation

There are many types of crystal that display the piezoelectric effect. The choice of crystal will depend on the application for which it is required. For ultrasonic propagation some general points for consideration with respect to choice of transducer (57) are that the material is readily machinable, robust and stable both chemically and physically within the operational parameters of the experiment. It must have suitable piezoelectric characteristics for the operation or operations for which it is required. For high power ultrasonic propagation there are some more specific points that need to be considered: it must be a material of low impedance that can be satisfactorily matched with the electrical circuit to operate at maximum efficiency. It should have high piezoelectric constants (i.e. d and Curie temperature) and a high quality factor.

5.3 CRYSTAL HOLDERS FOR ULTRASOUND PROPAGATION

5.3.1 Mounting the transducer

Ceramic transducers are manufactured with a deposit of electrical conducting film on their two radiating surfaces. These surfaces must be fitted with electrodes to supply the necessary electrical driving force. These electrodes must be designed to ensure that ultrasonic propagation is not impeded. A variety of ways of achieving this has been reported in the literature (58). One of the most perfect ways of accomplishing it is to cut a nodal groove in the sides of the transducer and create a screw attachment to it (59). Other methods include attaching springs or very thin sections of metal wire or foil to the transducer.

5.3.1.1 Quarter wavelength backing

The mechanical resistance, R_m, of a transducer has two components associated with it: the loading of the transducer by the medium into which the ultrasound is propagating and energy losses arising from the method of mounting the transducer. Maximum power output, at mechanical resonance occurs when the transducer is backed by an infinite acoustic impedance (60). This condition can be approximated by mounting the transducer such that it is has an quarter wavelength air backing of zero impedance i.e. $l = \lambda/4$, where l is the thickness of the transducer. This condition ensures that the transmission coefficient tends to zero and that maximum power output from the front face of the transducer is achieved. In practise, as outlined fully in chapter 7, with respect to the design and construction of transducer holding devices; a solid reflector is placed in

parallel with the rear surface of the transducer at a distance from it of exactly a quarter wavelength.

5.3.2 Focusing ultrasound

An ultrasonic lens can be used to focus the power of the ultrasound into a localised region (61)(62). The lens should be flat on one side and curved on the other, the radius of curvature of the lens is given by equation 5.18,

$$f = r\left(\frac{n}{n-1}\right) \qquad \text{Equation 5.18}$$

where r is the radius of curvature, f is the focal length (i.e. distance from focal bowl to the required convergence point), n is the index of refraction and equals V_p/V_W , where V_p is the velocity of sound in the lens material and V_W is the velocity of sound into the medium.Figure 5.7, shows how the lens can be set up to converge the ultrasonic energy. The lens should be constructed to be as thin as possible (not more than a few millimetres) to minimise absorption and save on material.

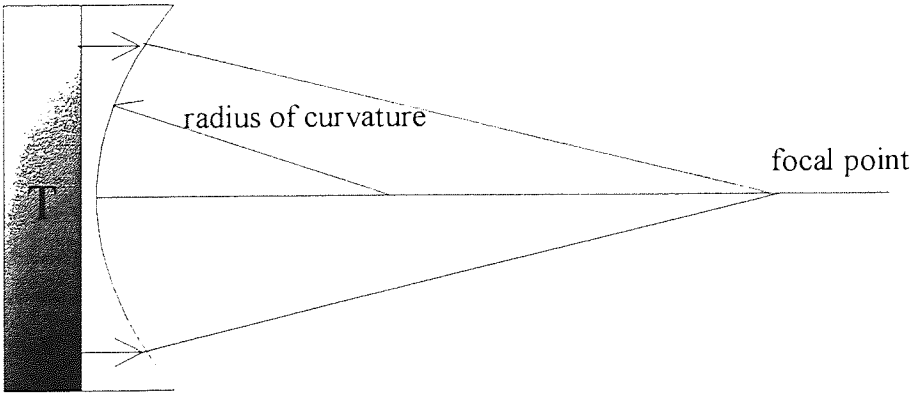

Figure 5.9: Using a lens to concentrate the energy from a transducer into a small volume

5.3.3 The amplification of sound

Solid horns can be used to amplify the displacement or particle velocity of ultrasound (63). Ultrasonic power intensity (in Wcm^{-2}) can be defined as the electrical power into the transducer divided by the surface area of the transducer, or if a horn is used, then the area of the end transmission tip. Figure 5.10, shows some typical ultrasonic horns. The displacement amplitude of the ultrasonic wave increases as the area of the end tip decreases. The exponential horn offers the highest amplification factor, and its narrow tip area makes it suitable for irradiation into small sample tubes. The horn should be manufactured from a material of similar acoustic impedance to the transducer material, in order to maximise forward power generation.

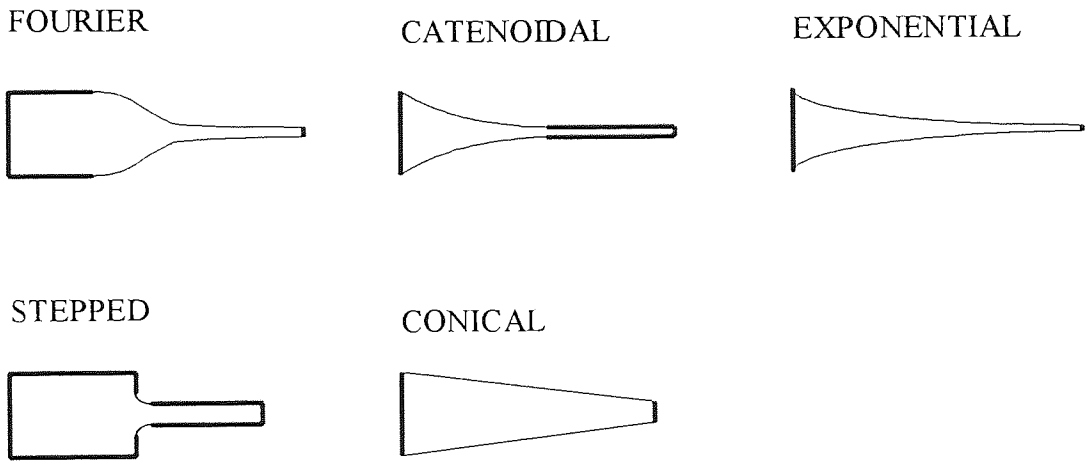

Figure 5.10: Solid horns for ultrasonic intensity amplification

5.4 HIGH INTENSITY ULTRASOUND AND ITS EFFECT

At high acoustic intensity (intensities greater than 0.5 Wcm^{-2} (64)), the passage of the acoustic wave through a liquid medium can have a profound effect on the medium that results in acoustic streaming, shock waves and cavitation (65).

5.4.1 Cavitation

Cavitation (66) literally means "the formation of a cavity". It has been observed that a bubble of radius, R, will be stable within a liquid if the pressure of the liquid p_0 is related to, P_i the pressure inside the bubble by

$$p_0 = p_i - (2\sigma / R) \qquad \text{Equation 5.19}$$

where σ is the surface tension of the liquid. For cavitation to occur, p_i must equal p_v, where p_v is the vapour pressure of the liquid. This means that the cavitation bubble can only be stable if the liquid pressure is less than the vapour pressure by $2\sigma/R$. This would require a huge negative pressure to form minute bubbles. This has lead to the development of a number of theories for proposed mechanisms for the bubble stabilisation. Harvey et al (67) proposed a theory later developed by further workers (68), (69), (70) suggesting that air is trapped on suspended hydrophobic particles within a water medium. Fox & Herzfield (71) proposed a theory suggesting that thin organic films develop on the bubble surface to stabilise it. Thus, a nucleation centre (72), as required for cavity formation, can be in one of many forms, for example, a bubble already existing in the liquid, a small pocket of gas existing on a solid or a particle of dust.

Ultrasonic waves cause cavitation by creating pressure fluctuations above and below the ambient pressure of the liquid. The liquid will experience a tensile stress during the negative half of the wave cycle followed by a compression during the positive half. The drop in pressure within the liquid caused by a period of compression encourages the growth of a sub microscopic bubble whereas a rise in pressure within the liquid discourages bubble growth, thus bubbles present in the liquid will expand and contract alternately. Stable cavitation can occur which results in the cavitating bubble pulsating over many acoustic cycles until it either dissolves, drifts out of the acoustic field or

becomes a transient cavity. A transient cavitation bubble is formed when the applied acoustic pressure amplitude is sufficient to satisfy the resonance condition of the bubble. Under this condition and during the wave cycle, the surface area of the bubble will be slightly larger during the expansion period compared to the compression period, as the amount of gas that diffuses into or out of the cavitation bubble is dependent on the surface area, progressively more gas will diffuse in than diffuse out. Therefore over a number of cycles the cavity grows until it reaches a resonant size. The critical size of this resonant cavity is dependent upon the frequency of the ultrasound, according to equation 5.20.

$$R_r = \frac{1}{2\pi\upsilon}\left(\frac{3\kappa P_0}{\rho}\right)^{\frac{1}{2}}$$ Equation 5.20

where R_r is the resonant cavity radius (mm), υ is the ultrasound frequency (Hz), κ is the polytropic constant which varies between unity and the ratio of specific heats, these being the limits for isothermal and adiabatic conditions, respectively , P_0 is the ambient pressure of the liquid (Pa) and ρ is the liquid density (kg m^{-3})

Once a bubble has reached its resonant size bubble growth occurs more rapidly due the ability of the resonant cavity to efficiently absorb energy from the sound field, the bubble expands very rapidly until it can no longer efficiently absorb energy from the sound field. The cavity is unable to sustain itself once it becomes unable to absorb more energy, at this point the cavity implodes. If any vapour is present in the collapsing cavity, it will cushion the collapse. Conversely if the cavity contains trapped gas the cavity implodes violently. The cavitation force is highest in intensity at the centre of the collapsing bubble (73) although its effect is felt in the immediate vicinity of the liquid because the liquid

will transmit shock waves very readily (74). The intensity of the radiated shock wave decreases with the square of the distance from the sound source, but the pressure decreases only in inverse proportion to the distance.

Imploding cavitation bubbles can generate a moving jet of liquid, a microjet, if the collapse of the bubble occurs near a solid surface boundary (75). The presence of the boundary distorts the imploding bubble such that the collapse is directed at high speed (in the order of $100ms^{-1}$ (76)) towards the solid boundary as shown in Figure 5.11.

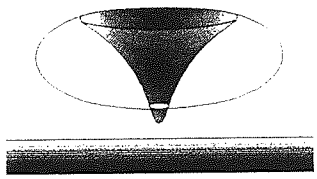

Figure 5.11: Microjetting action

It has been shown that the minimum power required to cause cavitation is frequency dependent and that there is an increase in this threshold intensity with frequency (77)(78).

The high temperatures and pressures produced during cavitation are thought to be responsible for ultrasonic phenomena such as sonoluminescence (79) (80) (81) and chemical reaction initiation, for example (82) (83). Two theories have been proposed in an attempt to explain this phenomena. The first is that cavitation processes cause "hot spots" (84) (85) (86) within the liquid: the high temperature produced as a cavity implodes results in the formation of excited atoms and radicals. Energy is released as these excited entities return to lower energy levels. Secondly, the electric charge theory (87) (88) proposes that electric charge accumulated around a large cavitation bubble can

be transferred and concentrated onto a smaller bubble, as it is being detached from the larger one. As the smaller bubble grows it is unable to sustain the growing charge which gets released as an electric discharge.

5.4.1.1 Other factors that affect cavitation

There is a minimum input power required to facilitate cavitation, known as the cavitation threshold (89). Increasing the power intensity beyond this threshold value increases the cavitation process within the liquid. The physical properties associated with certain liquids can also affect the cavitation threshold intensity. This is because acoustic forces are required to overcome the inertia of the surrounding liquid to assist bubble growth and during bubble collapse. Thus liquids which have small intermolecular forces, low viscosity and low vapour pressure will have reduced cavitation thresholds. In this respect maintaining a low temperature keeps the vapour pressure low to help reduce the cavitation threshold. The presence of dissolved gases or particulate matter in the liquid also lowers this threshold value (90), this is due to the fact that they provide a nucleation centre for bubble formation. Cavitation can only occur in gas and particulate free liquids once the acoustic pressure has exceeded the hydrostatic pressure, as under this condition the acoustic wave can overcome the forces of cohesion associated with the liquid thus creating voids in the structure of the liquid, which can grow in size to become resonating cavities.

A comprehensive review on cavitation has been carried out by Flynn (91)

5.4.2 Possible mechanisms for causing incoherent particle motion

As stated previously the SINNMR technique uses ultrasound to impart an incoherent motion to solid particles suspended within a support liquid (92), such that the solid particles mimic liquid behaviour. This is thought to occur for a number of reasons. Microjets could impart a translational motion to the particles by hitting them towards the centre of their mass. However, if the microjet hits the particle off of the centre of its mass it is thought possible that this action will cause the particle to rotate. A number of microjets hitting from all directions will create incoherent particle motion.

A second possible mechanism for incoherent particle motion is the action of the cavitating bubbles on the particles, again hitting the solid particles off centre of their mass to impart an rotational motion. Also, if the collapse speed of a resonant cavity is greater than the speed of sound, this will create a pulse of pressure which travels through the liquid medium as a shock wave. This creates a turbulence in the liquid which can cause incoherent particle motion.

Thirdly incoherent particle motion is thought to be facilitated by the particulate suspension following the motion of the wave, it is thought that whereas large particles will move out of phase with the wave front, smaller particles will translate more easily with the motion. A mismatch of these events would make collisions more likely

In totality a mismatch of all these events is a possible cause for the total incoherent motion of the particles.

5.4.3 Particle buoyancy

Dsythe (93) showed that a particle subject to an acoustic wave will have three equilibrium positions of stability within that wave. The most stable, and therefore the preferred orientation, occurs when the major principal axis of the particle is parallel to the direction of propagation of the wave. The particle will reorientate itself in order to achieve its most stable orientation. Particles suspended in a support medium, such as in the SINNMR experiment will encounter other forces that will determine their position within that support liquid. It should be possible, by suitable choice of ultrasonic power to manipulate the solid particles into a position so that they are aligned within the coil region of the NMR probe. By reference to Figure 5.12 it can be seen that if ultrasound is applied from above the sample the particle will reach an equilibrium position when the main opposing forces of upthrust (Fu) and particle buoyancy (Fb) equal out.

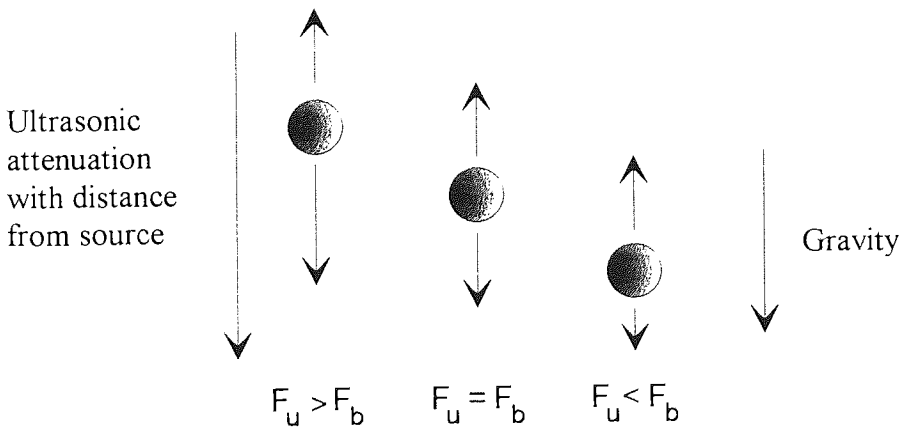

Figure 5.12: Particle buoyancy in an acoustic field

5.4.4 Streaming

When ultrasonic waves pass through a fluid medium, ultrasonic energy will be absorbed, thus setting up an intensity gradient with an associated ultrasonic energy gradient (94). This means that there will be a pressure exerted on the liquid that will cause it to flow in the direction of propagation of the ultrasonic radiation and return by the path of the least or no ultrasonic intensity.

5.4.5 Standing waves

Figure 5.13 shows how a wave travelling through a medium will be reflected back to its source on contact with a reflecting boundary (95). The forward and reflected waves reach a state of equilibrium as the sum of the energy becomes stable. The sum of this energy may differ at certain points of the path of travel and minima and maxima may be established (nodes and antinodes). The ratio of the amplitude of the wave at the maxima to that at the minima is known as the standing (or stationary) wave ratio. This quantity depends on the reflection coefficient at the boundary and the attenuation coefficient of the medium and can be manipulated to obtain high intensity sound waves.

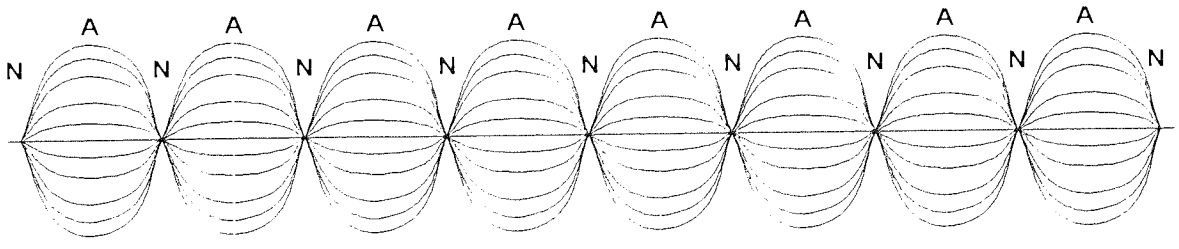

Figure 5.13: Standing waves

5.4.6 Ringing and NMR

Ringing (96) (97) is a large amplitude acoustic standing wave that can occur in metals, persisting for about 2 milliseconds The source of a ringing signal is the electromagnetic generation of ultrasonic standing waves in metals, if this occurs during NMR signal acquisition it can and can totally obliterate the desired signal. The amplitude of this ringing depends upon B_0, and B_1 the length of the radio-frequency pulse.

The external radio-frequency field penetrates the metal within its skin depth, δ, and induces eddy currents, j(z), in that region. As B_0 is along the z axis j(z) experiences a Lorentz force. This force is the driving force for a shear wave which propagates through the metal in the z direction. A reciprocal mechanism then converts the acoustic energy, in the presence of the static magnetic field, to an oscillating magnetic field which is consequently picked up by the coil as a ringing signal.

The amplitude of the generated acoustic wave, given by equation 5.21 is:

$$\mu = \frac{\left(B_0 / 4\pi m v_s \omega\right) B_1}{\left(1+\beta^2\right)^{\frac{1}{2}}} \qquad \text{Equation 5.21}$$

Where $\beta = (q\delta)^2/2$ and $\delta = (2\rho/\mu\omega)^{1/2}$,ω is the angular frequency, B_O is the static magnetic field, B_1 is the amplitude of incident radio-frequency magnetic field, m is the mass density, V_S is the acoustic velocity of the material, ρ is the resistivity and q is the acoustic wavenumber.

The theory of reciprocity then shows that the radio-frequency signal induced in the coil is proportional to the initial amplitude B_1 and the conversion efficiency given in equation 5.22

$$E = \frac{kB_0^2}{mv_s\left(1+\beta^2\right)}$$ Equation 5.22

where k is a constant

When designing the acoustic NMR probe, the materials out of which to construct the probe were carefully chosen to help eliminate any ringing problems. There are two factors that dictate how effective a particular metal is at producing the acoustic ringing effect. First is its conversion efficiency (E in equation 5.22) for the electromagnetic generation of acoustic waves, and second is its efficiency at transmitting these waves. From equation 5.22: conversion efficiency can be reduced by choosing materials with large β^2 or large mV_S. From Table 5.2 it can be seen that suitable metals to help eliminate the ringing effect are brass, platinum and tungsten.

Table 5.2: Table showing the best materials to choose to eliminate ringing (98)

Material	mv_s/mv_s(Al)	β^2 at 5MHz
Aluminium	1.0	0.005
Brass	2.2	0.121
Copper	2.5	0.007
Stainless steel	3.0	3.61
Tungsten	6.2	0.042
Platinum	4.5	0.783
Gold	2.9	0.173

For a given probe material, (especially piezoelectric materials, which are susceptible to mechanically deform in the presence of an electric field (99)) acoustic ringing effects can also be minimised by maximising the distance between the NMR coil and the probe body (100).

CHAPTER 6 INSTRUMENTATION

6.1 BRUKER WM250 NMR SPECTROMETER

Experiments were performed on a Bruker WM 250 FT spectrometer, linked to a super conducting magnet at 250 MHz (5.8 T). Two broadband probes, with axes in line with the magnetic field direction were used, one capable of observing nuclei up to ^{31}P, and a second broadband probe that was to be adapted into an acoustic NMR probe with a tuning range that was capable of observing nuclei from ^{2}H to ^{23}Na.

A list of the resonant frequencies for the nuclei observed is given in Table 6.1

Table 6.1: Resonant frequencies for some nuclei in a 250MHz spectrometer.

Nuclei	Nuclear Spin	Sensitivity to ^{1}H=1	Frequency/ MHz
^{31}C	1/2	$1.76*10^{-4}$	62.860
^{2}D	1	$1.45*10^{-6}$	38.376
^{23}Na	3/2	$9.25*10^{-2}$	66.128
^{27}Al	5/2	$2.1*10^{-1}$	65.143

The probes used were 10 mm internal diameter with an excitation/detection coil. The unadapted probe also had a decoupler/lock coil (^{2}D internal only), but the adapted probe had its decoupler and lock assemblies removed. The spectrometer was controlled by an Aspect 3000 computer fitted with a pulse programmer.

Further information about the adaptations and capabilities of the Acoustic NMR probe can be found in Chapter 7.

The probe temperature is maintained by a B-VT1000 variable temperature unit capable of operating between 64K-574K (-209-301^{0}C), and the experimental temperature was monitored by a copper/constantin thermocouple. The temperature of the probe can be set, by the operator, using a pulse program for variable temperature work.

All spectra obtained on the Bruker spectrometer were transferred to a PC computer using a "NMRLINK" and processed on "WINNMR".

6.2 ULTRASOUND

6.2.1 Transducer mounting

Ultrasound was applied to the liquid medium by piezoelectric transducers of various frequencies, that were driven by a generator of suitable frequency via connections of low electrical resistance It was necessary to arrange for the transducer to be able to oscillate freely and be resistant to chemical attack. To prevent the interference of ultrasonic frequencies with the NMR FID, from the r.f. power supplied to the transducer, a distance of at least 10 mm was maintained between the transducer holder and the NMR probe coil. Failure to do so resulted in a sinusoidal base line on the transformed spectrum at the frequency of the ultrasound; variable temperature equipment was used to prevent overheating of the sample.

6.2.2 Frequency generation

All the ultrasonic frequencies used were in the MHz region and synthesised using a radio frequency generator. The equipment, capable of generating frequencies in the range of 0.1-30 MHz with a maximum power delivery of 100W, is show schematically in Figure 6.1

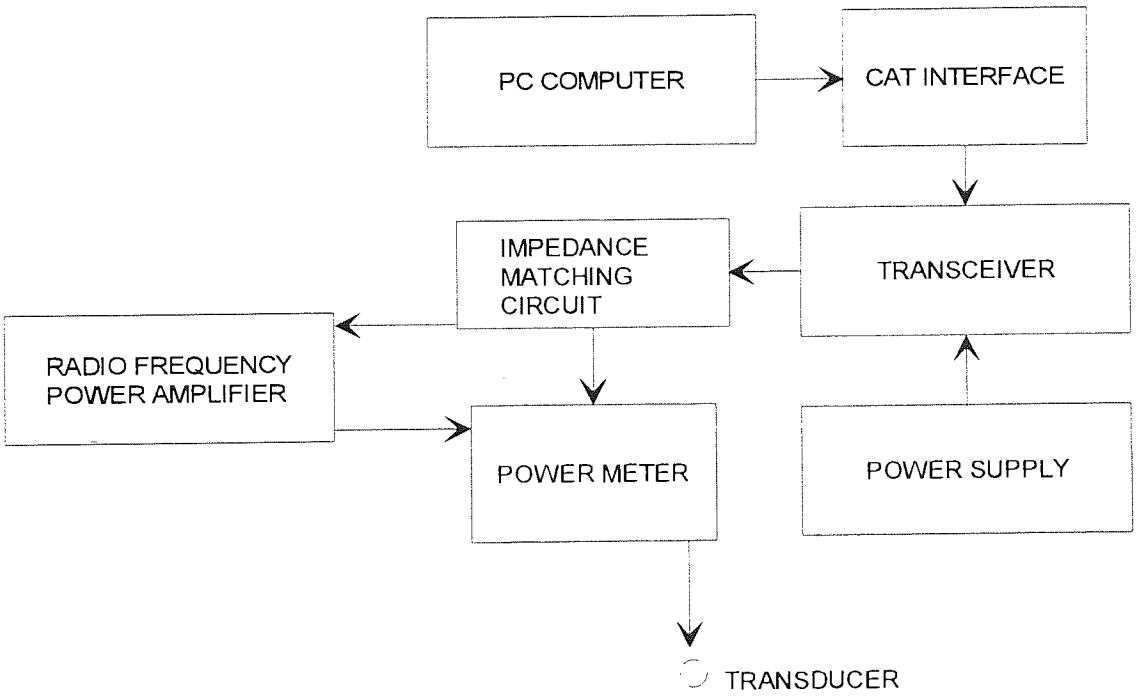

Figure 6.1: System schematic for the generation of radio frequencies

The system is based around a Yaesu FT840 transceiver driven by a suitable 13.5 V DC power supply of up to 20 A. Power delivery was maintained at a maximum by impedance matching of the circuit to the transducer. This was achieved by using a manual tuner, MJF-949E or an automatic antenna tuner, Yaesu FC-800. Additional power amplification was possible using a BNOS radio frequency 10 fold power amplifier: the

maximum power that could be delivered to the transducer was a 150 W, as above this the transducer material broke down.

The transceiver was computer controlled by an Amstrad PC 1512 SD, via a Yaesu FIF-232 CAT (computer aided transceiver) interface. This allowed the ultrasound to be delivered in continuous wave, pulsed, frequency sweep and random frequency modes. Details of the computer programme can be found elsewhere (101).

6.2.3 Transducers

The ultrasound was generated by piezoelectric crystals manufactured by Morgan Matroc Ltd. The crystals used were lead zirconium titinate (PZT) 5 mm diameter discs, silvered on both faces. PZT-4 transducers were chosen as they have a high quality of resonance, Q_m=500, and are designed for use in high power applications: their Curie temperature is 325^0C. The various crystals used for the experiments resonate at fundamental frequencies of 2.0, 3.0, 5.0 and 10.0 MHz.

6.3 THE PRODUCTION OF SPECIALIST WORKSHOP ITEMS

The custom made transducer holders and adaptations to the multinuclear probe to incorporate a facility to run ultrasound were manufactured by the author, using an EMCO Maier Compact 8 lathe.

Most jobs were held in an appropriate collet from a comprehensive collection of collets, while oversize jobs were held using a 4 jaw chuck. The lathe had a steady turning down facility that enabled the operator to part jobs down to a fine finish. The turning speed

used was dependent upon the material being machined. Table 6.2 shows the turning speed for each material used in this work.

Table 6.2: Turning speeds for different materials

Material	Turning Speed/ Revs/m
Stainless Steel, Titanium	350
Brass	500
Insulating materials (e.g PTFE, Tufset)	850

6.3.1 Specification for threading

External threads were created using the appropriate size die stock, which was threaded externally down the material, while the job was held perfectly vertical in the lathe collets. The corresponding internal thread was made by drilling out the job to the specified diameter for that thread size, as shown in Table 6.3, and the thread was then made by screwing in the threading tap.

Table 6.3: Threading specifications

External diameter/ mm	Internal diameter/ mm
2	1.6
3	2.4
4	3.2
5	4.1
6	5.2
7	6.2
8	7.2
9	8.2
10	9.2

6.4 SAMPLE PREPARATION

Samples required for the SINNMR experiments were first ground, using a pestle and mortar, to break down the larger particles into smaller ones. The particles were then graded using sieves obtained from Endecotts Ltd, manufactured to standard BS419/1986, to give the desired particle range.

In order for the particles to remain in the NMR probe detector coil region the conditions were manipulated to give the particles zero buoyancy: this was achieved by density matching them in a support medium of chloroform and bromoform (obtained from Aldrich Chemical Company, stock numbers: $CHCl_3$-31,998-8, $CHBr_3$-13,294-2). These chemicals have densities of 1.49 and 2.89 g/cm respectively and when combined in varying proportions the mixture can be arranged to have a density similar to that of the

solid particles. It was found that the density of the liquid mixture needed to be slightly higher than that of the particles to allow for a possible reduction in density due to heating. The sample was then placed in a Goss 10 mm NMR sample tube (type 1005-P). If the glass tube contained the nucleus that was under observation then a home made 10 mm PTFE tube was used. In order to maintain the particles in the desired size range a few drops of octanol (Aldrich-29,324) were added as a surfactant to prevent particle aggregation. Any deuterium lock solvent was usually omitted due to the large amounts required effecting the density of the mixture.

6.4.1 DESPOT calculations

Where necessary values of T_1 were measured using the DESPOT technique (3.1.2.1). Calculations using the DESPOT sequence for the measurement of T_1's were carried out using a custom designed programme to calculate the T_1's from pulse angles and intensity measurements, on an Amstrad PC 1512 SD, running GEM Desktop software v2.0U with Basic2 v1.0. Details of this programme can be found elsewhere (102).

CHAPTER 7 DESIGN AND STRUCTURE OF AN ACOUSTIC NMR PROBE SYSTEM

7.1 ASPECTS OF DESIGN

Transducer holders have been developed and fabricated which are suitable for ultrasonic propagation in an NMR tube such that the sample under investigation can be irradiated with ultrasound from either the top or the bottom. The work was carried out in collaboration with S. Reynolds. The machining and fabricating of the devices outlined in this chapter was carried out by the author on an EMCO Meier lathe, so that first hand experience of the design problems to be encountered could be better understood and remedied.

Many of the design features are general to the construction of both "top" and "bottom" mounted transducer holders. This chapter is concerned with providing the reader with an overview of the development of the transducer holders for various applications, concentrating primarily on the bottom mounted design which is essential to the final design for an ultrasonic probe. The latter half of the chapter describes the redevelopment of the probe head area to incorporate the transducer holder.

7.2 HISTORY OF TRANSDUCER MOUNTING

Early high frequency work, achieved by Howard (22) and by Patel (25) was carried out using a transducer device mounted within the sample, as shown in Figure 7.1.

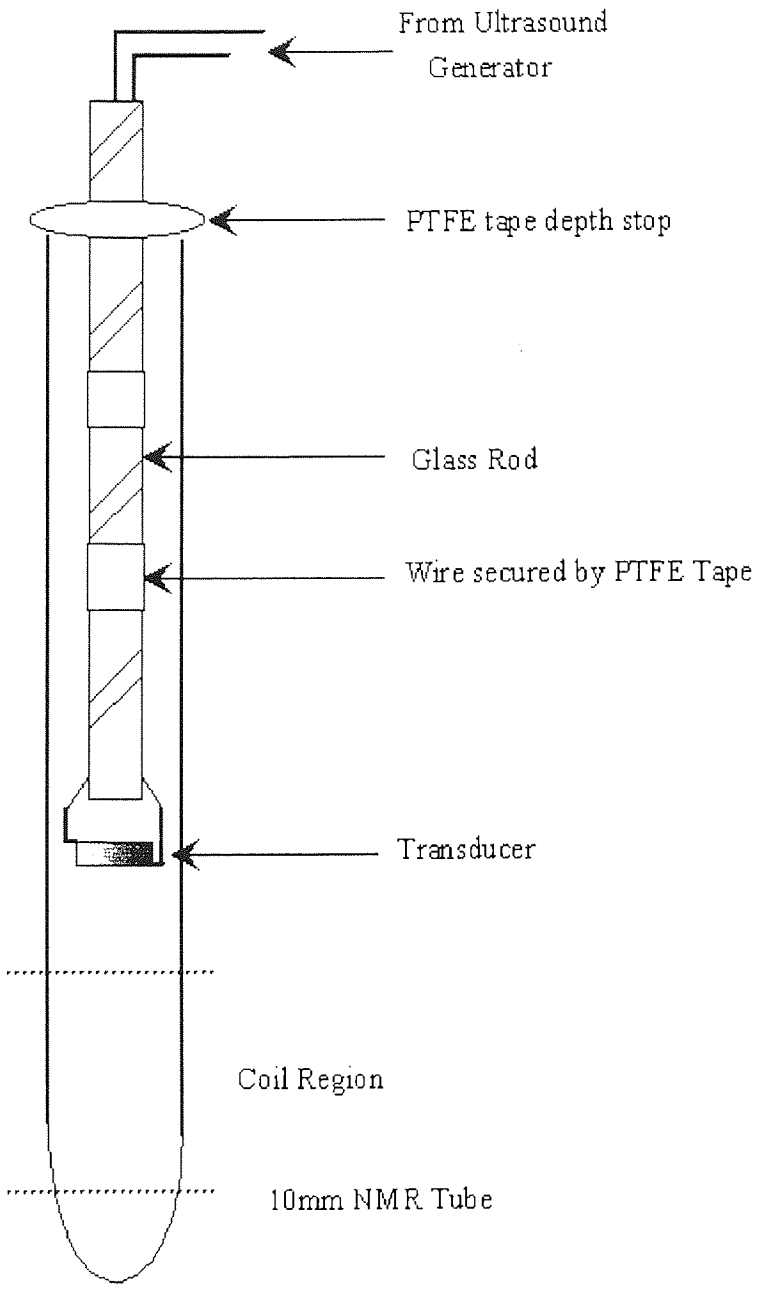

Figure 7.1: Mounting arrangement for transducer to a glass rod

This system was rather limited in its capabilities and had associated problems. One such problem was in the soldering of the copper wires directly to the upper and lower surfaces of the transducer. As it is not possible to achieve an even distribution, or equal mass of solder, every time the operation is performed, the efficiency of ultrasonic propagation of

a transducer will be impeded by the restraint that the solder places on it. This occurs because the solder changes the loading and thus the resonance frequency of the transducer, and this results in a lowering of efficiency of transmission and will ultimately attenuate ultrasonic propagation

Application of the solder tended to strip the conductive silver paint from the outer surfaces of the transducer. This was due over time, to the ultrasonic vibrations breaking the solder and stripping off the paint at the same time. Solder putty was used as an alternative but proved as difficult to apply thinly, and no more robust than conventional solder.

A further problem with this system was that the unshielded wires carrying the electrical connections are rather close to the coil region of the magnet, and their influence could be detected in the spectra being acquired.

Finally as the transducer is being submerged in the solvents it is open to chemical attack.

It was therefore necessary to design and produce dedicated transducer holders for reproducible ultrasound generation.

7.3 Overview of design

A schematic of an early "bottom mounted" design can be seen in Figure 7.2. The total width of the holder is 8.8mm, as this is just less than the internal diameter of a Goss 10mm glass NMR tube. The idea behind this approach being that the transducer holder is bonded into an NMR tube that has had its bottom removed; so that its upper face is capable of radiating ultrasound into a sample.

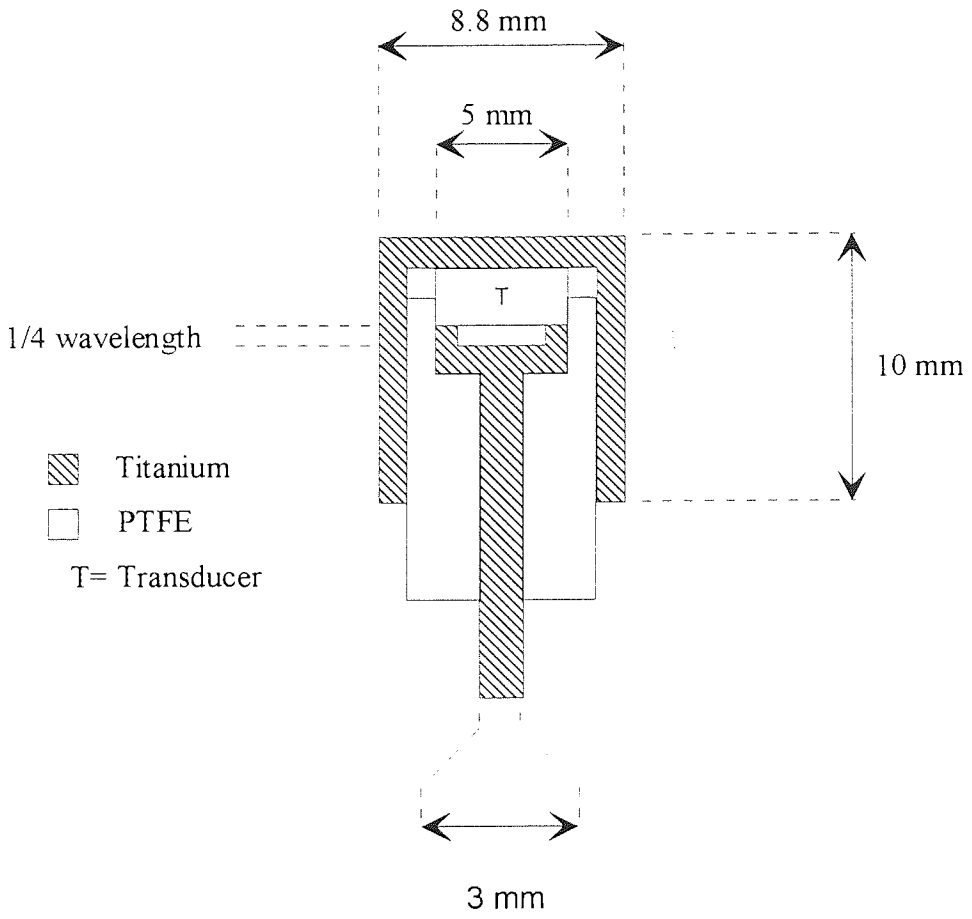

Figure 7.2: Early bottom mounted transducer design

The electrical connection to the transducer was made firm by screwing the outer face housing down onto the insulating piece so that a firm compressional contact was made by the transducer onto its front and back metal contacts. The inner and outer connections were then connected via a coaxial cable to the tranceiving equipment and power supply.

7.4 MATERIALS

The materials used for the construction of the transducer holders had to be carefully selected. The design of the holders was based around the dimensions of the transducers, which were selected for high frequency, high power ultrasound propagation.

7.4.1 Transducers

The piezoelectric transducers, (see 5.2.1) that were to be incorporated into the holder design were 5mm ceramic disks with coated silver faces. The thickness of the disks was dependant on their fundamental resonant frequency, see Table 7.1.

Table 7.1: Transducer widths for given frequency

Frequency/ MHz	Thickness/ mm
2	1.4
3	1.0
5	0.5
10	0.2

7.4.1.1 Metal piece

Certain important factors have to be considered when selecting a material out of which to construct an ultrasonic holder. The material must be non magnetic, have a high dynamic fatigue strength, low acoustic loss, be resistant to cavitation erosion, chemically inert and be a suitable material to help reduce ringing (5.4.6).

Originally titanium was chosen as it not only fulfils all of the above criteria, but is also a fairly low density and relatively inexpensive material. Later it was realised that the titanium cell was distorting the line shapes of the spectra due to magnetic impurities within the metal.

Ideally either very low magnetic content titanium or a high quality stainless steel, as used in the probe head by the manufacturers, should be used. As this was unavailable, brass was used to construct both the holder and its contacts, because it fulfils the criteria stated above and is also easy to machine and distorts NMR spectra to a lesser extent than titanium. It should be remembered that brass has a tendency to tarnish over time and therefore requires regular cleaning.

7.4.1.2 Insulating piece.

An insulating material was required to keep the inner and outer brass connections apart. This material must be easy and safe to machine, stable over the relevant temperature and resistant to any solvents that my be present in the sample. By reference to materials catalogues, three were chosen as possible candidates: polyfluorotetraethylene (PTFE), Tufset and a ceramic, "Macor".

PTFE performed very well, although it tended to deform over time due to its soft nature. Tufset is a more rigid material than PTFE; it is easier to machine and more hard wearing than PTFE. It has the disadvantage that it tends to absorb solvents over time and expand. "Macor" was found to be very brittle in nature. It was very hard to thread and tended to chip easily with use. It was therefore decided that Tufset would be the best material to use so long as the experiment did not require the use of inappropriate solvents. Where solvents were to be used it proved better to use PTFE as the insulating material.

7.4.2 Choice of adhesive.

Glass is a brittle material and it was therefore not possible to thread the glass NMR tube to the brass casing of the holder. Thus a suitable adhesive was required to bond the brass casing to the outer body of the holder. The bonding agent to be chosen needed to be compatible for use with both brass and glass and solvent resistant over the operating temperature range of the system. A survey of available adhesives showed that most were not totally solvent resistant.

Three different adhesives were tested for performance: Araldite, an acrylic adhesive and titanium putty. They all worked over a short time period, usually about a week, before leaks started to occur. The leaks occurred for one of a number of reasons: firstly the ultrasonic vibrations were responsible for fatiguing the adhesive; secondly by the solvents dissolving the adhesive and finally by the process of the ultrasound heating the mounting causing the glass and metal to expand (and then to contract on cooling) at differing rates, causing the glass tubes to crack and leak. This problem resulted in a redevelopment of the mounting to incorporate a PTFE tube that could be threaded onto the outer brass casing. This cured the problem of leaking and permitted ^{23}Na spectra to be acquired in a sodium free tube environment. The main drawback of this system was due to the opaque nature of PTFE, which prevented the performance of the ultrasound cell from being monitored from the outside.

7.4.3 Choice of coupling adhesive

Another consideration when designing a transducer mounting was to find a suitable coupling adhesive (103). The coupling adhesive can be applied between the front face plate and the transducer to create a lubricated coupling. The coupling adhesive can also be used to improve the versatility of a transducer holder. A transducer holder designed for use with a 2MHz transducer will have a quarter wavelength air backing of 0.39mm (7.5.2): using a coupling adhesive will enable any transducer to be run within that holder, as an air backing of incorrect size will result in poor acoustic coupling and attenuation of transmission.

Any such adhesive must not dissolve the transducer and must have good electrical and mechanical properties. The resonant frequency and resistance of the transducer should not be affected by any coupling adhesive used. Various such compounds were used including motor oil, Vaseline, silicone oil and a heat sink compound. The differences in performance of these different compounds was found to be negligible.

7.5 TOP MOUNTED TRANSDUCER HOLDERS

The top mounted transducer holders were produced to enable SINNMR experiments to be conducted while the dedicated ultrasonic probe was being constructed.

Figure 7.3 shows the design for a "top mounted" transducer holder. Figure 7.4 shows how such a holder is installed within an NMR tube. This whole assembly, including the coaxial cables that connect to the transceiver, are then placed in through the top of the cryo-magnet in the conventional manner.

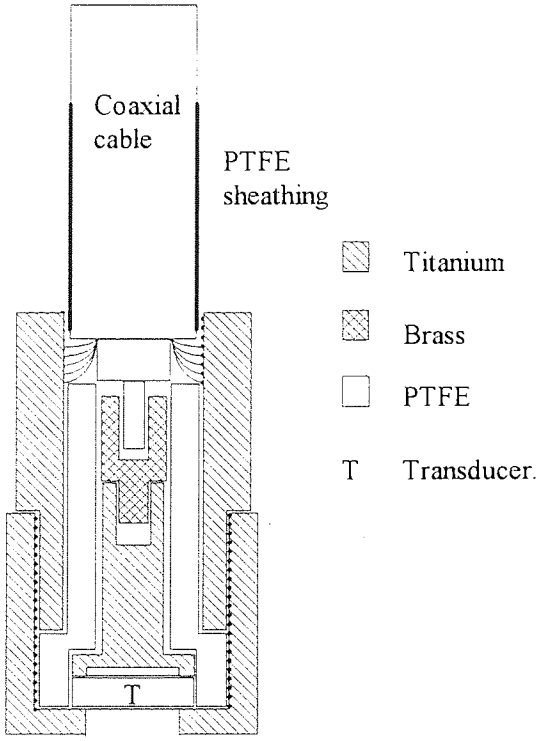

Figure 7.3: Transducer holder for ultrasonic propagation from above

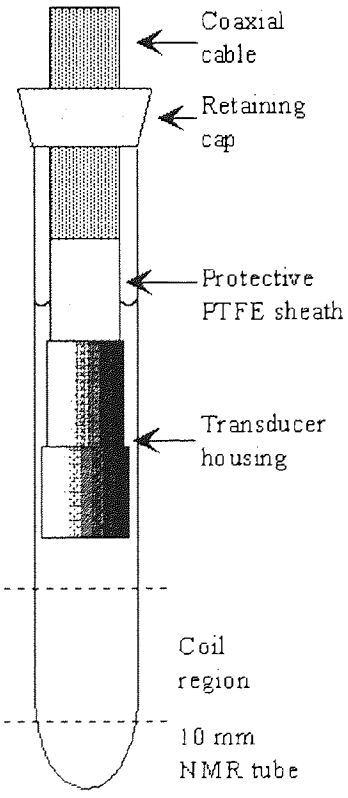

Figure 7.4: Mounting arrangement for the "top" mounted transducer

7.5.1 Problems with the top mounted transducer system

One problem with the top mounted transducer proved to be that the action of the ultrasound caused an air bubble to form beneath the radiating face; this resulted in poor acoustic coupling and impeded ultrasonic propagation. Another was that the action of the ultrasound from above tends to drive the particulate sample downwards, and if care was not taken, the particles accumulated at the bottom of the NMR tube, out of the NMR probe detection region. It was for these, and other reasons, that an acoustic probe capable of applying the ultrasound from beneath the sample was developed to benefit development of the SINNMR technique.

7.5.2 Mounting the transducer

The piezoelectric transducer needs to be suitably mounted so that it has good mechanical support as well as good electrical contact. An efficient method of mounting a transducer is to attach the transducer to a backing surface that ensures good electrical contact, does not impede vibration and fulfils the quarter wavelength conditions. As outlined in chapter five, the advantage of using a quarter wavelength backed system is that the forward power generation of ultrasound is enhanced by reflection from the backing plate. An experiment was devised to determine whether the condition for quarter wavelength backing did enhance the forward power produced by the ultrasound.

7.5.2.1 Experiment to determine the efficiency of the quarter wavelength backing.

A transducer holder was devised so that the backing plate position could be altered. This was achieved by having a screw thread on a movable backing plate which could be screwed up and down to alter the backing position, as depicted in Figure 7.5.

A receiving hydrophone was connected to an oscilloscope, while a transducer device such as that shown in Figure 7.3 was connected to a power supply. The faces of the transmitter and receiver were placed in parallel and facing each other, at a specified distance apart, as shown in Figure 7.6.

2 MHz transducers were used in both the movable backing device and the hydrophone. The backing position was set and the magnitude of the peak at 2 MHz was observed on the oscilloscope. The backing plate was moved and the experiment repeated.

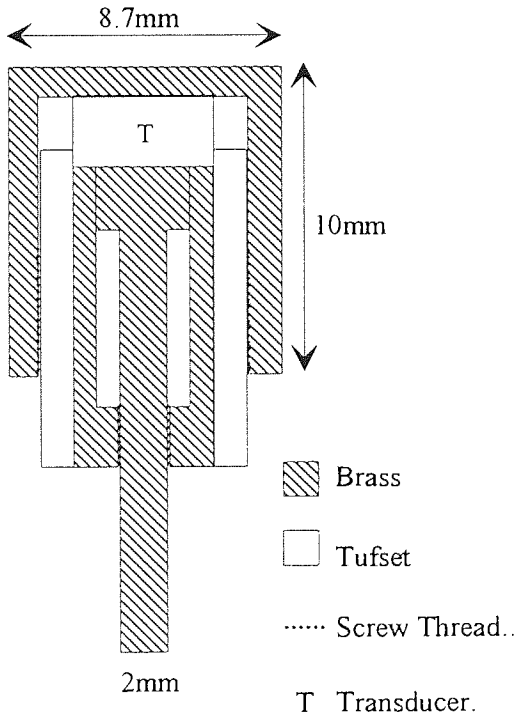

Figure 7.5: Quarter wavelength backing arrangement

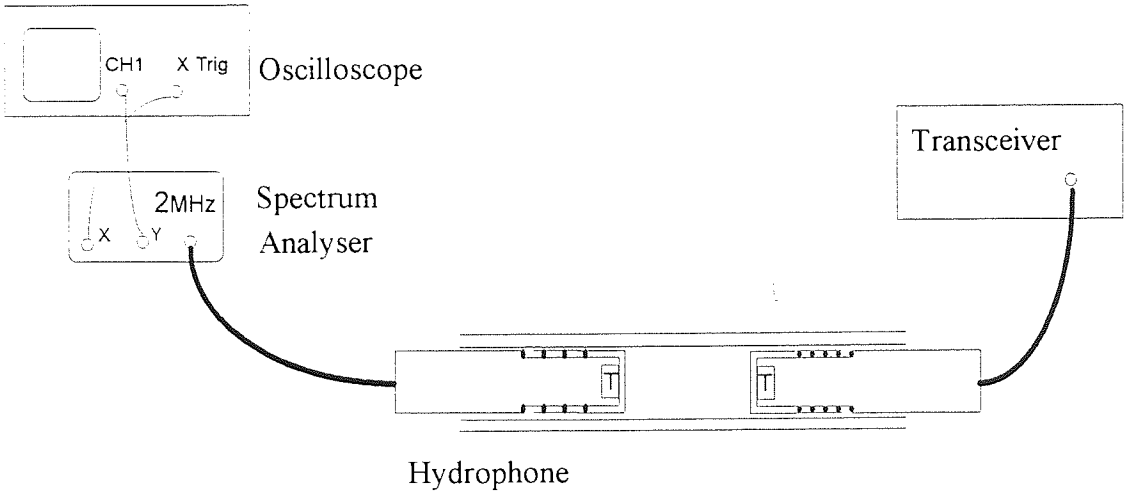

Figure 7.6: Quarter wavelength backing experiment

Within the experimental error and limits of the system, it could not be concluded whether or not the quarter wavelength backing did cause better ultrasonic propagation, as the received signal intensity did not seem to vary significantly enough with movement of the backing plate. It was decided to keep this feature in later designs as it was considered beneficial to transducer operation that the transducer be kept as unconstrained as possible.

7.5.3 Face plates

It was found during the course of developing the transducer holder assemblies that the fixed front face plate impedes ultrasonic transmission. Therefore, some experiments were performed to vary the thickness of the front face, to determine how this influenced the efficiency of ultrasonic propagation. Using a 2MHz transducer, face plates of four different thickness were tested: as thin as was possible (0.2mm), quarter wavelength,

(0.35mm) half wavelength (0.7mm) and full wavelength (1.4mm). It was found by visually inspecting the amount of particle motion within a support liquid, that the best ultrasonic propagation was achieved when the front face was as thin as possible.

Manufacturing a perfectly thin and flat inner front face by use of a conventional two fluted flat face drill proved difficult to achieve. If the inner front face was not totally flat, this led to problems with ultrasound transmission and also to problems of the transducers cracking when the front housing was screwed on. To overcome this problem a multi-fluted flat face drill piece was obtained, as it was supposed that this would produce a finer flat face finish than the two fluted drill piece that was used initially. This drill was found to improve the finish of the front face but not to cure the problem entirely. Therefore some re-design features were implemented to remedy this difficulty.

7.5.3.1 The parted down front face design

The parted down front face design, (see Figure 7.7), was developed as it proved easier to produce a fine finish on the front face if it can be parted down using a lathe, rather than drilling in with a flat bottom drill. It also proved easier to manufacture the thin finish required to assist ultrasonic propagation using this technique.

The edges leading downwards towards the transducer from above were slanted to avoid build up of particles on any ledges.

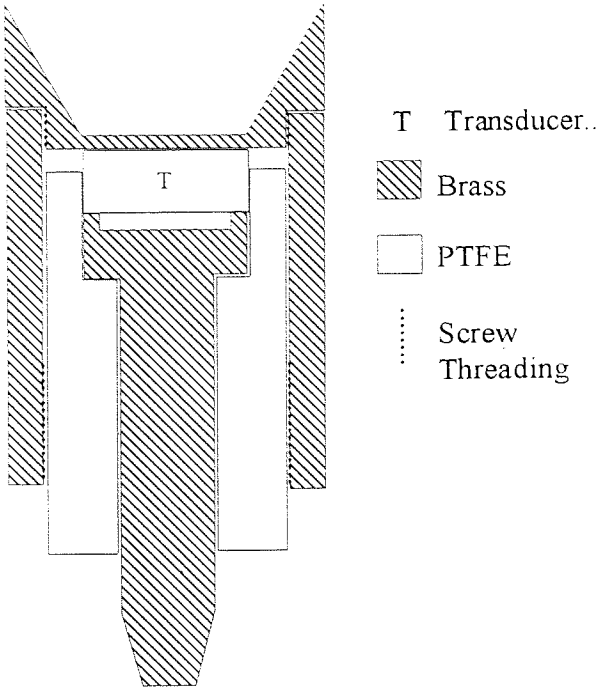

Figure 7.7: Parted down front face

This design was found to prevent any cracking of the transducers.

7.5.3.2 Incorporation of a spring

Figure 7.8 shows how the inner body design was altered to incorporate a spring. The purpose of incorporating a spring was to ensure that the restraint placed on the transducer was minimised. It was hoped that the spring would not be capable of absorbing any of the vibrations of the transducer which would be operating at frequencies of 2 MHz and higher.

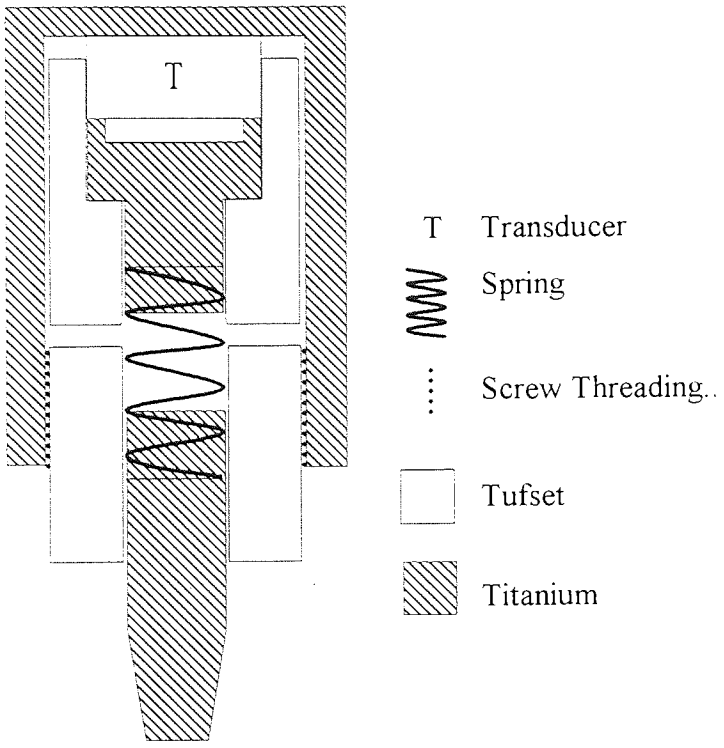

Figure 7.8: Spring backed transducer holder

This system proved very robust, and prevented transducers from cracking. The problem with it was found to be that although the spring was made of a "non-magnetic" stainless steel, it

7.5.3.3 The open face design

As discussed above, the top and bottom mounted transducer holders were developed in tandem. It was realised that the best solution to the problems caused by the front face was to remove it, leaving only a small ledge to hold the transducer in place. This is easy to achieve if the sample is being irradiated from above but not so easy to achieve with the bottom mounted design because the solvents drain through the cell body down the probe. It was found that this draining problem could be eliminated with the use of o-rings

to provide an internal seal. Viton o-rings were used as opposed to the standard nitrile o-rings as they are more resistant to solvents and have a wider operating temperature range. Figure 7.9 shows a schematic of this transducer design.

The efficiency of the ultrasonic propagation into a sample using the open face design was found to be an improvement on any fixed face system. Although this design leaves the transducer open to chemical attack.

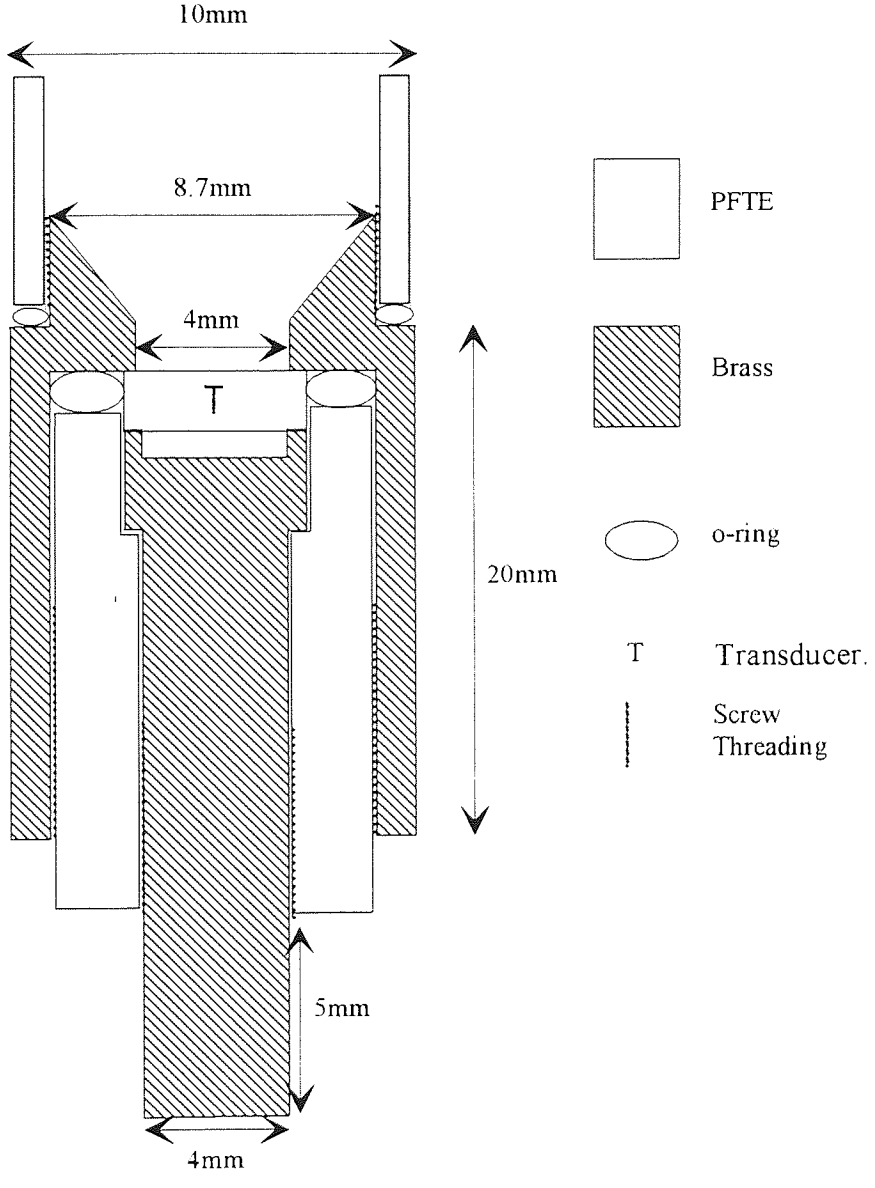

Figure 7.9: Open front transducer holder design

7.5.3.4 Metal foil

The use of a metal foil layer to cover the exposed, outer face of the transducer was investigated. A 5mm diameter of steel foil was cut and was placed on top of the transducer and clamped in place by screwing on the outer housing. A coupling adhesive was used in conjunction with the system to prevent any problems of poor coupling due to this sandwich system. This system proved to work well and not to impede ultrasonic propagation.

7.5.4 Variable temperature control unit

Application of ultrasound to a sample causes heating, therefore a variable temperature control unit was used to maintain the sample at a constant temperature.

The probe head area is cooled by two lines feeding up to the probe head area, one feeding up cold nitrogen and one feeding up compressed air to create circulation.

The use of Peltier effect heat sinks was investigated but it was found that they provided no better cooling effect than simply using the air lines.

7.5.5 Focusing bowls

A version of the design shown in Figure 7.2 was fabricated to include a focusing bowl face. It was thought that the forward power supplied to the sample could be maximised by focusing the energy towards the coil region of the probe (as outlined in section 5.3.2). It was found, through visual inspection of the turbulence produced, that there was a

reduction in particle agitation, probably due to the extra thickness required in the face to incorporate the focusing bowl, impeding ultrasonic propagation.

7.5.6 Running at harmonic frequencies

It is possible to run the transducers at upper harmonics of their natural frequencies (5.2.1.1). The piezoelectric effect can only occur when opposite charges appear on the electrodes, thus only odd harmonics can be generated. For example a 2 MHz transducer can be run at 6MHz (but not 4 MHz). It was believed that this would allow the frequency of ultrasound to be altered without taking the holder apart and changing the transducer. It was found in practice that the acoustic energy delivered by running at these upper harmonics was not sufficient to cause cavitation.

7.6 DESIGN OF THE NMR PROBE HEAD

The probe head of the probe needed to be adapted to incorporate compressional contacts to secure firm electrical connections to the body of the transducer holder.

7.6.1 Some original ideas

With the previously described designs of the transducer body in mind, it can be appreciated that an inner and an outer connection have to be made to the brass casing, when sited in the NMR probe head. An early idea to achieve this was to adapt a MAS probe, and use the compressed air lines that normally tip the coils over to the magic angle to tip some contacts towards both transducer assembly connections. This idea was subsequently deemed unsuitable due to problems that would be encountered such as the

need to replace the sinusoidal MAS coils with the orthogonal coils that are required if the sample is to be kept perpendicular to the field. It was also thought that the contact made would not be firm enough for high power ultrasound delivery.

It was therefore decided that it would be more practical to adapt a broadband high resolution probe.

7.6.2 The probe

A 300 MHz broadband was obtained and the lock, variable temperature and decoupler assembly removed, to maximise the space available. Only the tuning module was left in the upper probe body.

Firstly some brass supports for the coil assembly and tuning module were constructed (as shown in Figure 7.11).

Several ideas as to how to provide electrical connections were considered. First consideration was given to the possibility of incorporating brackets around the connections with a pneumatic clamping system to make the firm connections required for high frequency ultrasound delivery. This idea was eventually discarded due to the lack of space available. Another idea was to use a bed of brushes for the transducer holder to drop into, with the possible benefit that the sample could be spun within the brushes. The idea was soon discarded due to the fact that it would be impossible to secure a firm enough connection and it was thought that problems would occur with arcing across the connections especially if the sample was spinning. The design that eventually progressed to the manufacturing phase was the collet arrangement, shown in Figure 7.10, as this seemed practically the most feasible: the operation of this will be described later.

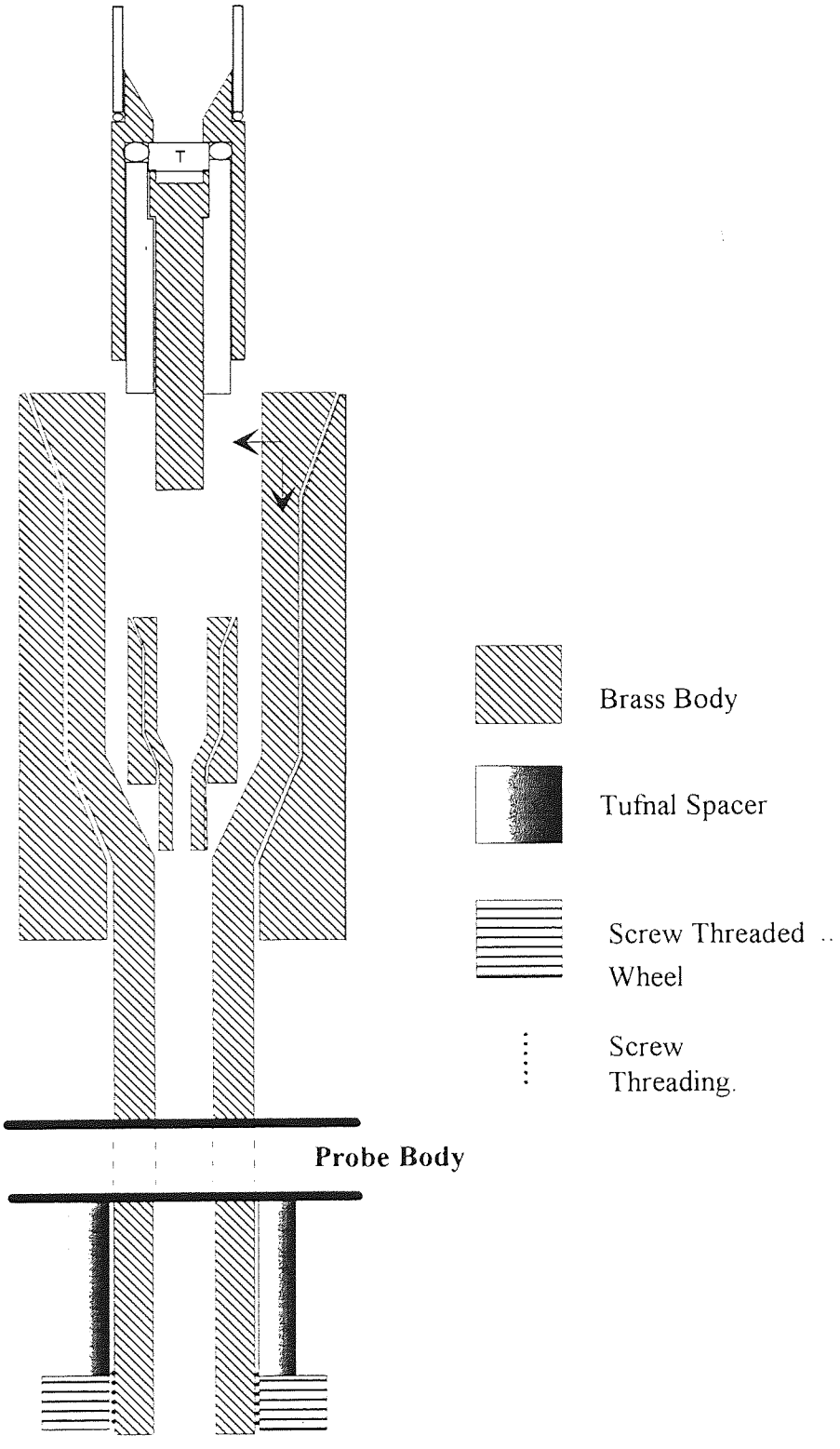

Figure 7.10: Collet arrangement

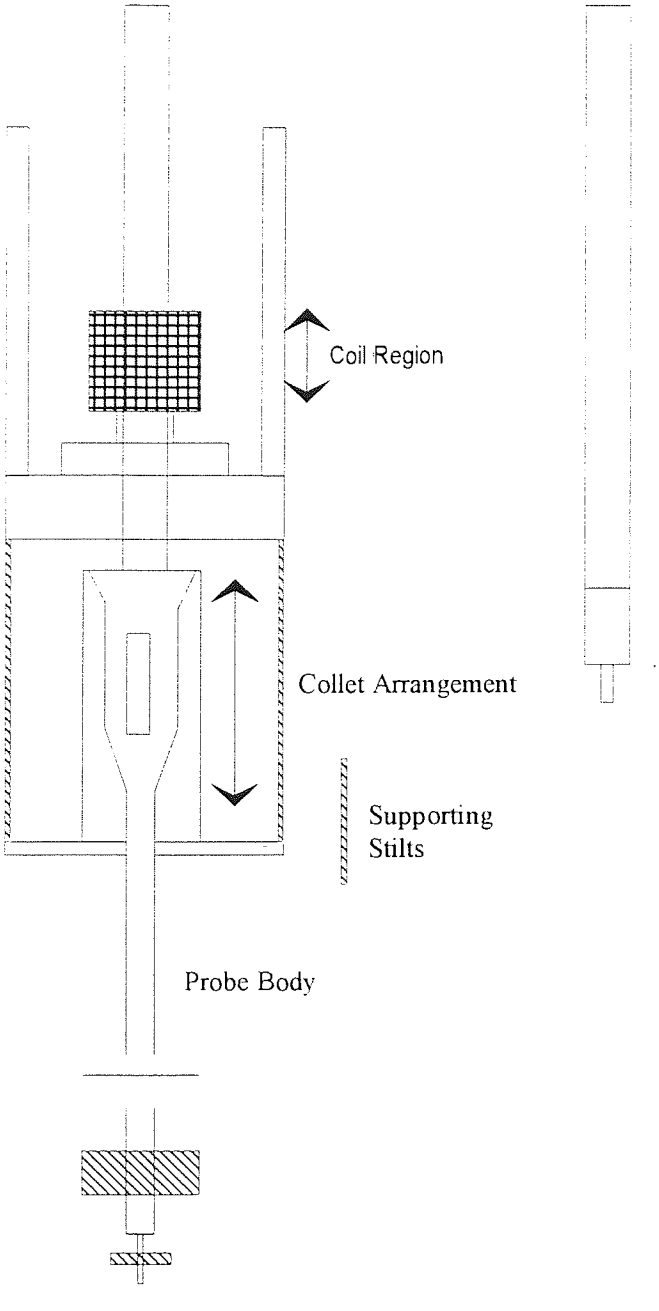

Figure 7.11: Overview of mounting arrangement

7.6.3 Experimental conditions

An overview of the system is shown in Figure 7.11 The NMR tube containing the transducer holder is dropped into the magnet in the conventional way. The holder drops inside the contacts which are made firm by screwing tight the inner and outer screw

mechanisms at the bottom of the probe. By reference to the arrows, (shown in Figure 7.10) it can be seen that the action of screwing tight the bottom screwing mechanisms (shown in Figure 7.11) "pulls down" the sloped inner contacts against the sloped, rigid, outer body. This action draws the inner contact inwards towards the transducer cell body where a firm connection is secured.

With the sample now in place within the magnet, NMR spectra can be obtained in the conventional way.

7.6.4 Notes on the mounting arrangement

Brass, (as the electrical contact) has a tendency to tarnish over time and, therefore, the power supplied to the transducer will be reduced if tarnishing has occurred. Therefore the collet and transducer mounting needed to be taken apart regularly and cleaned. A longer term solution to the problem would be to build the probe and transducer mounting out of a material such as a very high purity titanium or stainless steel, that would not distort the lineshapes and not tarnish over time.

CHAPTER 8 A PRELIMINARY INVESTIGATION INTO THE USE OF ULTRASOUND IN THE CRYOMAGNET

8.1 QUENCHING

An experiment was devised to prove that the application of ultrasound within the cryo-magnet would not quench the magnet. Fundamentally, this was the most important experiment to be performed, as its success or failure would determine the viability of running ultrasound within cryo-magnets.

8.1.1 Experimental conditions

A transducer of 1.5 MHz frequency had two copper wires soldered to it, one to its front and one to its back face, which were connected to the tranceiving equipment via the use of crocodile clips. The transducer was submerged in water and orientated within an NMR tube so that the direction ultrasound propagation was vertical to B_0 within the magnet. The transducer was run for 10 minutes at 5, 10 and 50 Watts forward power (which corresponds respectively to 25.5, 51.0 and 255.0 Wcm^{-2}) to assess whether quenching would occur. Cavitation bubbles were visually detected in the support medium, running at these powers and frequencies. This experiment was then repeated with the transducer horizontal to B_0.

The whole experiment was subsequently repeated using a 3MHz transducer.

8.1.2 Results

It was found that quenching of the magnet did not occur under these extreme conditions. Subsequent to this work ultrasound at 2, 5 and 10 MHz has been regularly run within the magnet which has further proved that even under the most extreme conditions of power and frequency, the magnet does not quench.

8.2 THE CAVITATION EXPERIMENT

As discussed in chapter 5 cavitation fields are thought to facilitate the incoherent particle motion of solids suspended within a support medium. This can be achieved by one of two possible mechanisms: firstly by shock waves colliding asymmetrically with the solid particles, hitting them off centre and thereby imparting rotational and translational motion to the particle. Secondly, cavitation is known to produce microjets as an unstable cavity collapses near a solid surface. The microjet consequently imposes a high energy density at the site of impact with the solid particle and again, if this is asymmetric with respect to the centre of mass of a particle, the rotational and translational motion of that particle will be enhanced.

Experiments were performed, using the Weissler reaction (104) as an ultrasonic dosimeter, to ensure that cavitation is taking place. The Weissler reaction was carried out both on the bench and within the magnet, to ensure that the presence of the magnetic field does not inhibit transducer oscillation or its ability to promote cavitation. This reaction relies on cavitation to occur to liberate iodine from potassium iodide solution and will turn a starch solution blue/black.

8.2.1 Reaction mechanism

It is thought that the mechanism that causes iodine liberation from potassium iodide, proceeds by cavitation causing radical formation in water (105). This radical formation then proceeds to activate oxygen ($O^{\bullet}$) that is dissolved in the aqueous medium. The reaction yield is increased by the addition of a small amount of carbon tetrachloride (106), as the activated oxygen, ($O^{\bullet}$), can react with the carbon tetrachloride to produce

free chlorine. The free chlorine then reacts with the potassium iodide to liberate iodine, as shown in scheme 8.1.

$CCl_4 + H_2O \rightarrow Cl_2 + CO + 2HCl$

$2HCl + O^{\bullet} \rightarrow Cl_2 + H_2O$

$2KI + Cl_2 \rightarrow 2KCl + I_2$

Scheme 8.1: Reaction mechanisms for the liberation of iodine

The iodine formation is detected by the inclusion of starch in the reaction mixture as starch will indicate its formation by turning the reaction mixture blue/black

8.2.2 Experimental conditions

8.2.2.1 Reaction mixture

A stock solution containing 0.7g of potassium iodide dissolved in 5ml of distilled water was prepared. 2ml of a 2% starch indicator was added to this solution and one drop of carbon tetrachloride.

8.2.2.2 Experimental

The Weissler reactions were first carried out in the acoustic NMR probe on the bench so that the minimum powers and times required to cause the reaction colour change for each frequency of transducer used, could be monitored.

The reactions were then repeated within the magnet using the times and powers known to be necessary to for the reaction to occur in order to ensure that the presence of the magnetic field did not inhibit the transducer oscillation. The probe was then removed from the magnet and the reaction colour observed in order to confirm that cavitation was no less efficient than doing the bench experiment.

8.2.3 Results

Table 8.1 shows the ultrasonic power intensity and time required for colouration of the reaction mixture to occur.

Table 8.1: The times and powers necessary to cause a solution of KI to liberate iodine, using starch as an indicator.

Acoustic Frequency, MHz	2	2	3	3	5	5	10	10
Power, W	5	10	5	10	5	30	5	40
Intensity, W/cm^{-2}	25.5	51.0	25.5	51.0	25.5	152.8	25.5	203.7
Time for colour change, s	134	6	149	6	_*	86	_*	98

* No reaction colour change observed

8.2.4 Discussion

Table 8.1 shows that the ultrasonic intensity required to liberate iodine from potassium iodide at frequencies of 2 and 3 MHz is much lower than the intensity required to cause

this reaction to occur at the higher frequencies. It can also be seen from these results that the time as well as the ultrasonic intensity required for the onset of cavitation to occur is greater for 5MHz and then higher still for 10 MHz. The colour change was not observed at all for an intensity of 39.8Wcm^{-2} at either of these frequencies.

Comparable experiments were carried out in the cryo-magnet. It was found after removing the acoustic probe from the magnet, visual inspection of the reaction colour change, showed that the times and powers necessary to cause cavitation within the magnet were comparable with the times and powers required to cause cavitation on the bench. Thus it was concluded that the presence of the magnetic field does not inhibit transducer oscillation or its ability to promote cavitation.

Colouration of the sample was not observed when the sample mixture was directly heated to the boiling point temperature of the mixture. Accordingly, the effect of temperature rises on the significance of the above experiment was eliminated.

Work was carried out in collaboration with S. Reynolds to run these cavitation experiments using a top mounted transducer holder, as discussed in chapter 7. The results (107) show that the times and powers necessary to cause cavitation using this radiating device, as opposed to the acoustic NMR probe, were comparable.

8.2.4.1 Undertones

In theory the PZT-4D transducers used for these experiments could be producing over or undertones. The possibility that undertones of the resonant frequency are responsible for the cavitation effects described above was addressed by observing the harmonic and sub-

harmonic frequencies using a spectrum analyser and an oscilloscope. Figure 8.1 shows a typical display as observed on the oscilloscope screen, the central peak seen is merely an artefact produced by the oscilloscope and not a real peak. Likewise, the negative peaks seen are simply ghost peaks of the real peaks.

This diagram shows that that only resonant or higher frequencies were produced for a given frequency transducer. It was thus concluded that only resonant or higher frequencies are responsible for cavitation to occur at a particular frequency.

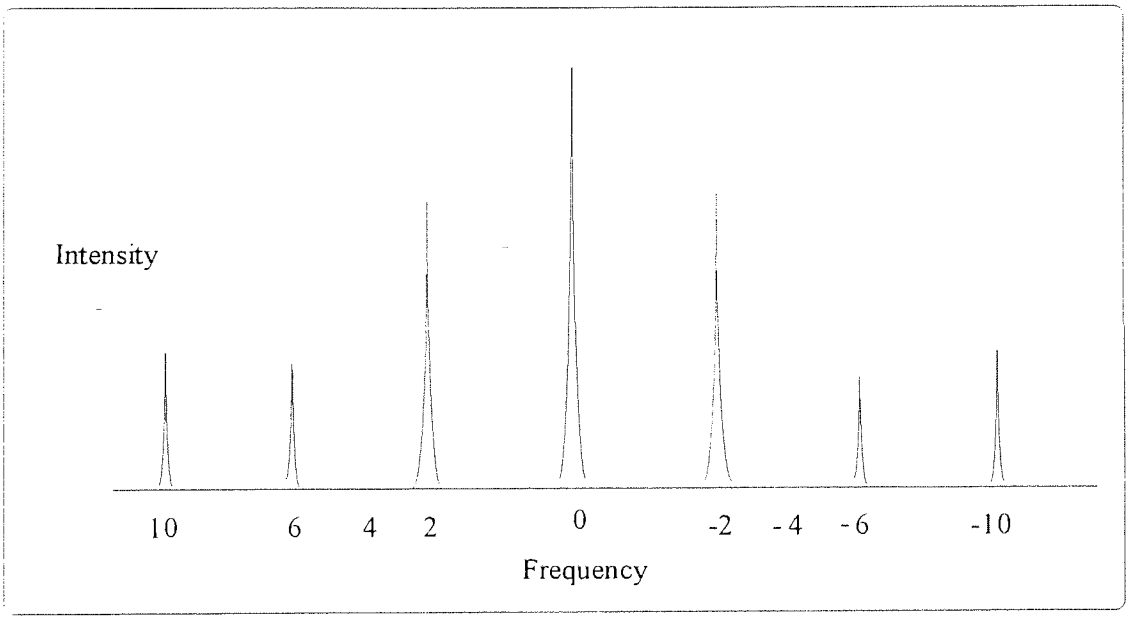

Figure 8.1: Overtones observed when operating a transducer at 2MHz

CHAPTER 9 LINE NARROWING OF TSP

9.1 INTRODUCTION

This chapter concerns SINNMR studies of trisodium phosphate dodecahydrate, (supplied by Aldrich). TSP is a translucent white crystalline solid with the chemical formula $Na_3PO_4.12H_2O$.

It was shown in preliminary experiments by Tilstone (108) and further experiments by Howard (21, 22) that the linewidth of both the ^{31}P and ^{23}Na spectra of TSP can be narrowed by the application of low frequency ultrasound at 20 kHz. Howard has also shown that the signal to noise obtained during a SINNMR experiment depends on the size range of the particles used. The following work was undertaken to determine if high frequency ultrasound can be used to improve the line narrowing and also determine if this linewidth reduction can be optimised with respect to the ultrasonic power delivered, the frequency of ultrasound and the particle size of TSP.

The power delivery needs optimisation so as to ensure the correct amount of ultrasonic energy is propagated into the sample to achieve a maximum reduction in linewidth. It is important to optimise the frequency of the ultrasound used, as the size of the cavitation bubble produced is dependant upon the frequency of ultrasound applied to the sample (see chapter 5). It is believed that the size of particles can then be optimised with respect to the frequency of ultrasound supplied as it is believed that maximum incoherent motion will be induced in the solid particles, suspended in a support liquid, if the cavitation bubble is smaller than particle size in order to hit the particle asymmetrically, thereby imparting a maximum rotational and translational motion to it. Howard (109) calculated that at 20kHz the size of the cavitation bubbles will be between 85-95μm. From equation 5.20 (taking an average support liquid density), it can be calculated that at 2MHz the

cavitation bubble size will be about 10μm and at 3MHz the cavitation bubble size will be about 7μm.

9.2 SAMPLE PREPARATION

The quantity of sample used in SINNMR experiments has been optimised by observing the signal to noise ratio compared to the mass of sample used (110) . The literature suggests that 1.2g of TSP suspended in 2.5ml of chloroform and bromoform mixture is optimum when using a 10mm NMR tube.

Three different particle sizes of TSP were sieved and separated: 75-104μm, 75-38μm and <38μm. The separations of these fractions was carried out in Endecott's test sieves complying to BS410, mounted in brass frames with stainless steel meshes.

TSP (1.2g) was suspended in 2.5 cm^3 of a mixture which contained chloroform and bromoform in a ratio of approximately 4:1 and 3 drops of a surfactant, octanol was added to avoid aggregation of the particles. The support mixture as stated above is an approximation: the exact ratio of chloroform to bromoform was carefully monitored for each individual sample to ensure that when the ultrasound was running, the solid particles were properly density matched and being incoherently agitated within the coil region of the NMR probe. Details of the NMR acquisition parameters used for this experiment can be found in appendix 2.

9.3 Optimisation of power delivery

A preliminary experiment was carried out at 2MHz ultrasonic frequency using a particle size range of 104 -75μm. The sample preparation was carried out as stated above.

A ^{23}Na spectrum of the static suspended solid, (no ultrasound applied) was taken first as a reference. The ultrasound was then applied in increasing power increments: Figure 9.1, shows the affect of the ultrasound on the linewidth of the spectra.

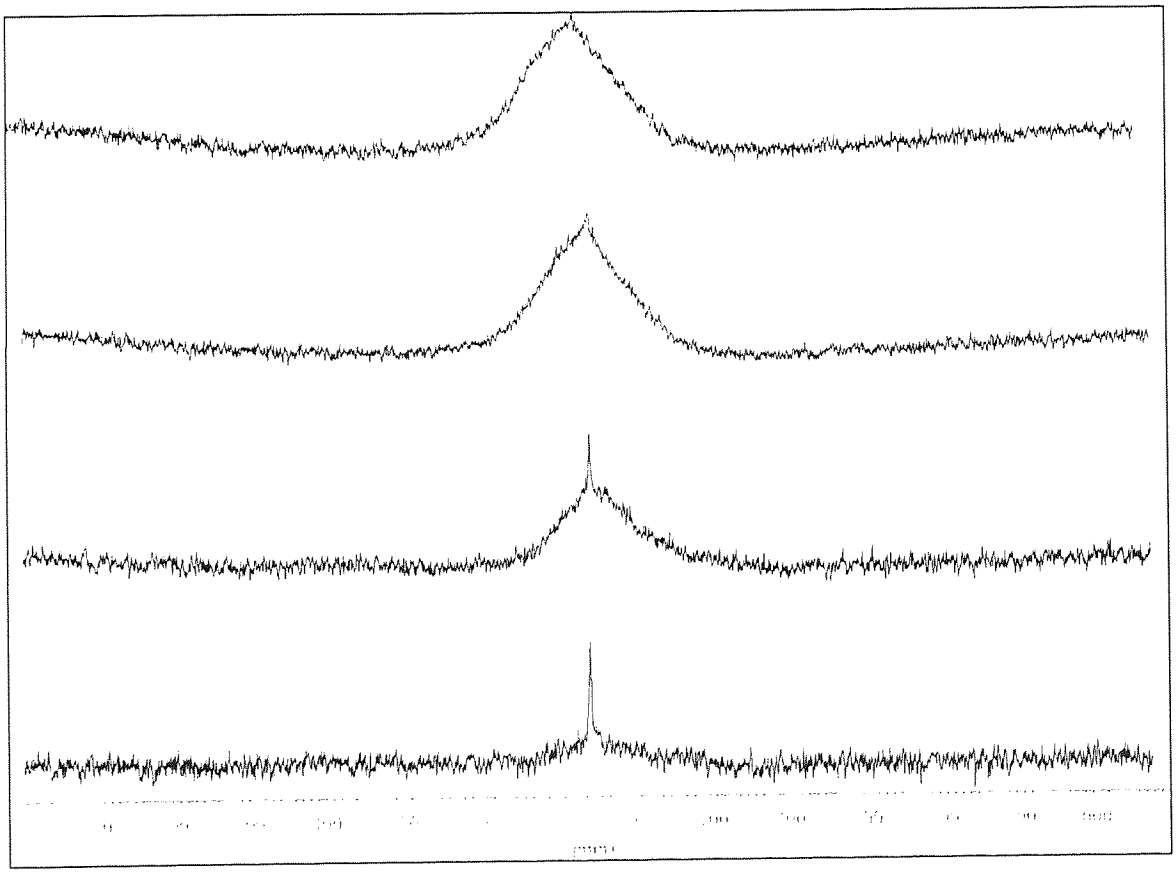

Figure 9.1: TSP line narrowing, at 2MHz frequency using 104-75μm particle size TSP: ultrasound supplied: from top to bottom 0, 20.4, 51.0, 61.2 Wcm^{-2}.

From Figure 9.1 it can be seen that the line narrowing at 51.0 Wcm^{-2} produces a broad based peak on top of which a narrowed SINNMR peak begins to show. Line widths at half maximum were measured for spectra measured with a variety of acoustic intensities: at the exact half total peak height, regardless of the shape of the peak. Shown graphically, a graph of frequency width at half peak maximum (FWHM) against ultrasonic power (Figure 9.2) was obtained.

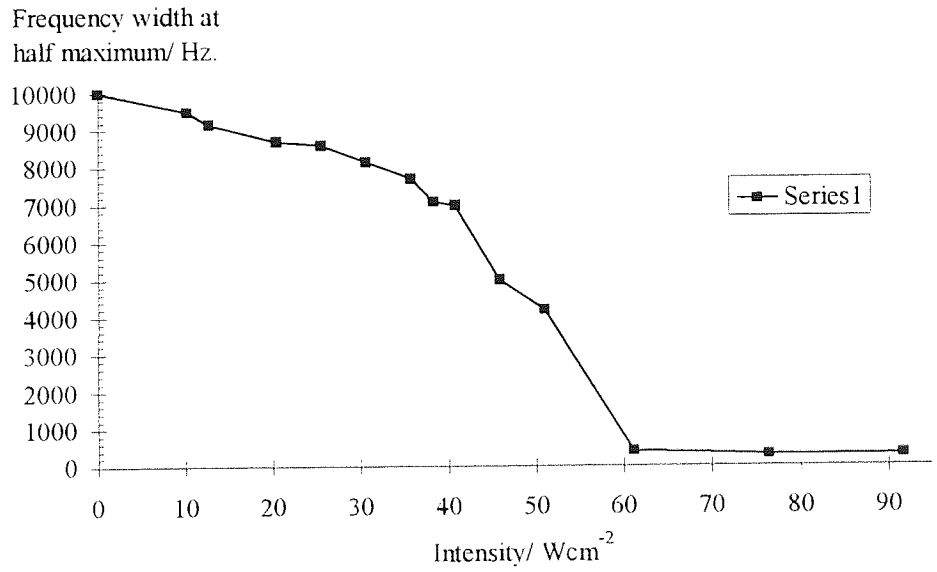

Figure 9.2: Change in frequency width at half maximum with ultrasonic power.

Linewidths at half maximum were also measured for these spectra by taking the half linewidth of the broad peak only. Shown graphically, a graph of frequency width at half broad peak maximum against ultrasonic power is shown in Figure 9.3.

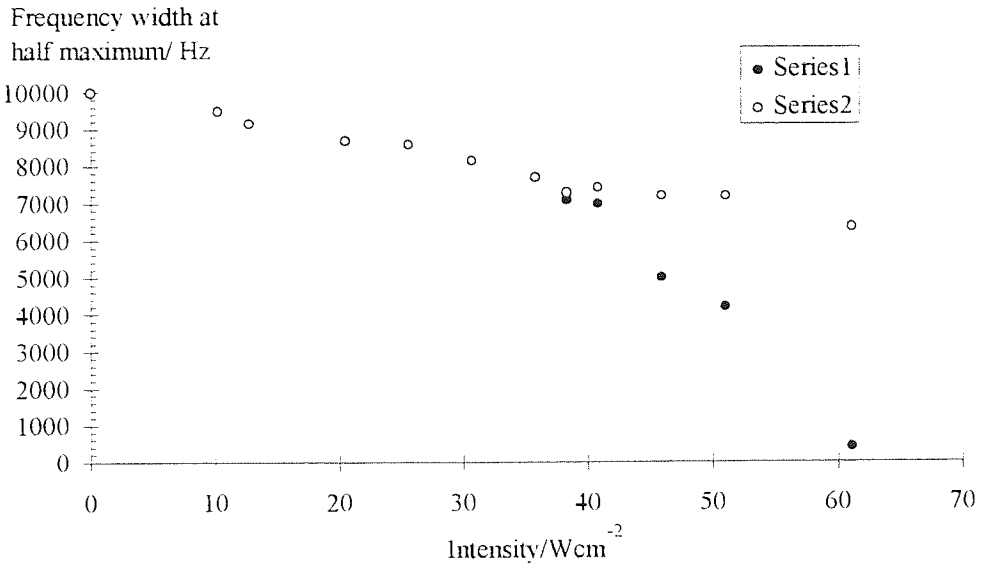

Figure 9.3: Frequency width at half maximum, shown for both the full peak (filled icons) and for the "un-narrowed" TSP spectra (unfilled icons)

9.3.1 Discussion

Figure 9.3, which shows the progressive narrowing of the broad peak, reveals that the SINNMR linewidth narrowing of TSP can be achieved progressively at high acoustic frequency.

The initial gradual rate of change of linewidth with power, between 1-6 Watts (5.1 -30.6 Wcm^{-2}), shown in Figure 9.2, is suggested to be due to the ultrasound providing an additional Brownian type motion, which, in addition causes more inter particle collisions. This is in agreement with work carried out by Yesinowski (111) and again later Kimura and Satoh (112) (113) who showed that Brownian motion, especially with a small particle size range, can be used to effect line narrowing of solid state NMR spectra.

For the power range 6-12 Watts, which corresponds to power intensity ranging from 30.6- 61.2 Wcm^2, the rate of change of linewidth with ultrasonic power starts to

decrease more sharply. This additional narrowing is thought to be due to the onset of cavitation and shock wave effects. Reference to the data in Table 8.1 indicates that cavitation is difficult to achieve with power levels of less than 5 Watts.

Beyond power levels of about 12 Watts ($61.2Wcm^{-2}$), Figure 9.2 shows the graph levelling off. This occurs as the cavitation bubble field is now at a maximum and ultrasonic intensity is not necessarily increased by the addition of higher power ultrasound. This is because the waves are attenuated by reflection and refraction from the high bubble population and their additional effect no longer creates a higher intensity cavitation field.

Elsewhere, it has been considered that line narrowing, such as that discussed above, could result from a heating effect of the applied ultrasound. Ball (114) carried out an investigation into how heating affects the line narrowing of TSP spectra at four different particle size ranges (104-75μm, 75-53μm, 53-38μm <38μm). Using the variable temperature control facility on the NMR spectrometer, spectra of TSP in a suspension of chloroform and bromoform sample were taken for the different particle size ranges at four temperatures of 10, 25 and 35 and 50°C. Within the experimental errors of the investigation it was stated by Ball that "the linewidths showed no overall trend with increasing temperature". This is in agreement with the initial TSP line narrowing experiments carried out by Howard, who showed that the narrowing could not be due to "heating, melting or dissolution" (115).

9.4 PARTICLE SIZE AND FREQUENCY EXPERIMENTS

The TSP SINNMR experiment was run at three different particle sizes and at two different frequencies to determine if improved narrowing conditions could be achieved by adjustment of these parameters.

The experiments were set up as described in section 9.2

9.4.1 Results

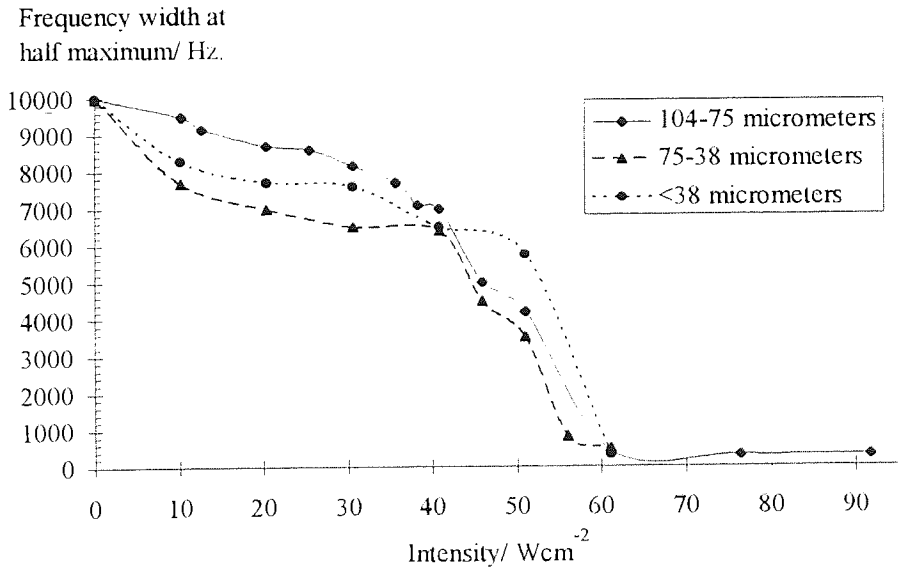

Figure 9.4: Change in FWHM with ultrasonic power for three different particle size ranges at 2MHz frequency.

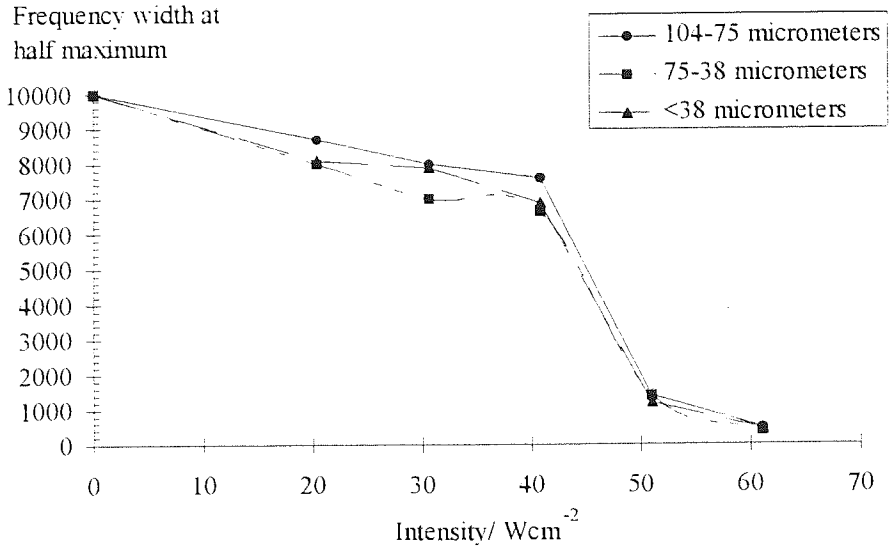

Figure 9.5: Change in FWHM with ultrasonic power for three different particle size ranges at 3MHz frequency.

9.4.2 Discussion

The results shown in Figure 9.4 and Figure 9.5 suggest that the particle size of the TSP particles was not a critical parameter in the SINNMR experiment.

Theoretically the larger particle sizes should have a higher probability than smaller particles of being hit off centre by a microjet action or a cavitation bubble, due to their larger surface area. As it is believed that the rotational and translational motion imparted to a particle can be enhanced if the particle has an asymmetric collision with such a microjet it was originally believed that using a larger particle size in the SINNMR experiment would optimise narrowing. However a larger particle will be subject to greater forces of viscous drag, which could reduce its rotational and translational motions.

A smaller particle would have a lesser probability of an asymmetric collision although due to it being subject to a lesser viscous drag could theoretically have a greater rotational and translational energy imparted to it.

Thus the totality of these events could account for the fact that no marked differences were observed when the particle size was altered.

Ultrasonic fragmentation of the particles (116) could account the fact that particle size seemed an uncritical parameters to the SINNMR experiment. Davies (117) has carried out some preliminary investigations, using a light scattering technique to determine particle size, and has observed that the application of ultrasound to a suspended sample of TSP seems to cause a reduction in particle size. These results suggest that the larger sized particles are broken down to a smaller particle size (~38μm), if this were happening, this could also offer an explanation as to why the optimisation of particle size could not be achieved.

9.4.3 Frequency

Comparison of Figure 9.4 with Figure 9.5 shows that varying the frequency between 2 and 3 MHz does not appear to significantly alter the narrowing of the ^{23}Na spectra. This could be due to there not being enough of a difference between the two frequencies, and in the effects they cause. A second point worthy of consideration is that the exact frequency of operation of a transducer does depend on its physical constraints. Thus the operation of a 2MHz or 3MHz transducer within the ultrasonic probe could be optimised by using a frequency analyser tuning circuit to determine the absolute frequencies at which they operate in the given environment. A transducer not running at optimum

frequency will not be operating at optimum efficiency, thus this event occurring could have masked any beneficial effect that changing the frequency may have had.

CHAPTER 10 SIGNAL ENHANCEMENT AND T_1 REDUCTION IN LIQUIDS USING ULTRASOUND

10.1 INTRODUCTION

Certain nuclei, such as quaternary carbon nuclei, have long spin lattice relaxation times, T_1, due to poor relaxation pathways. The relaxation delay, R_d, characteristic of pulse NMR experiments must be set at 5.3 times the longest T_1 in a molecule if quantitative results are required. Pulse experiments can, therefore, take a long time for these nuclei. However, if the value of T_1 can be reduced by the application of ultrasound, this could significantly reduce the total spectrometer time required for acquisition.

It is has been shown (118) that the passage of ultrasound through a liquid mixture can modify the translational motion of the liquid. These modifications alter the molecular rotational and translational correlation times, such as to enhance the spectral density of fluctuating fields at or near the Larmor frequency. Established theory (119) then predicts that these events will modify components of the spin lattice relaxation process, culminating in T_1 reduction and signal enhancement.

Homer and Patel (24) applied ultrasound *in situ*, at various frequencies and powers to ten different liquid mixtures and reported reductions of up to 60 % in the T_1 of these mixtures. The experiments carried out by Homer and Patel were reproducible in respect to the trends in T_1 reduction, although the absolute numerical values obtained often differed. However, the T_1 reduction of pure liquids, specifically bromoform and chloroform could not be achieved under the experimental conditions used by Homer and Patel

The aim of the present work was to optimise the approach of Homer and Patel for the application of ultrasound to mixtures and also pure liquids. For this purpose the dedicated acoustic probe (as described in chapter 7) was used to investigate the

enhancement of NMR signals, acquired with a fixed set of parameters, and so reduce T_1 times reproducibly, with respect to both the trend and the absolute values obtained.

Signal enhancement measurements were carried out on pure chloroform and a liquid mixture of 1,3,5-tri-methyl benzene, (mesitylene) and cyclohexane.

10.1.1 Experimental

A stock solution of 50 cm^3 of a 1:1 molar mixture of cyclohexane (molecular formula C_6H_{12}, relative molecular mass 84.16) and mesitylene (molecular formula C_9H_{12}, relative molecular mass 120.20), used in all experiments was prepared, and stored in a sealed container.

A $5cm^3$ sample of this mixture, taken from the stock solution, was used in each experiment. The sample was then placed inside the NMR tube in the dedicated acoustic probe and was irradiated at 0, 2.5, 5, 7.5 and 10 Watts (corresponding to 0, 12.7, 25.5, 38.3 and 51.0 Wcm^{-2}) ultrasonic powers at a frequency of 2MHz. The NMR acquisition parameters used for these measurements can be found in appendix 3.

10.1.2 Results: mesitylene/cyclohexane mixture

Figure 10.1 shows the ^{13}C spectra that were obtained for this mixture at the different ultrasonic power intensities.

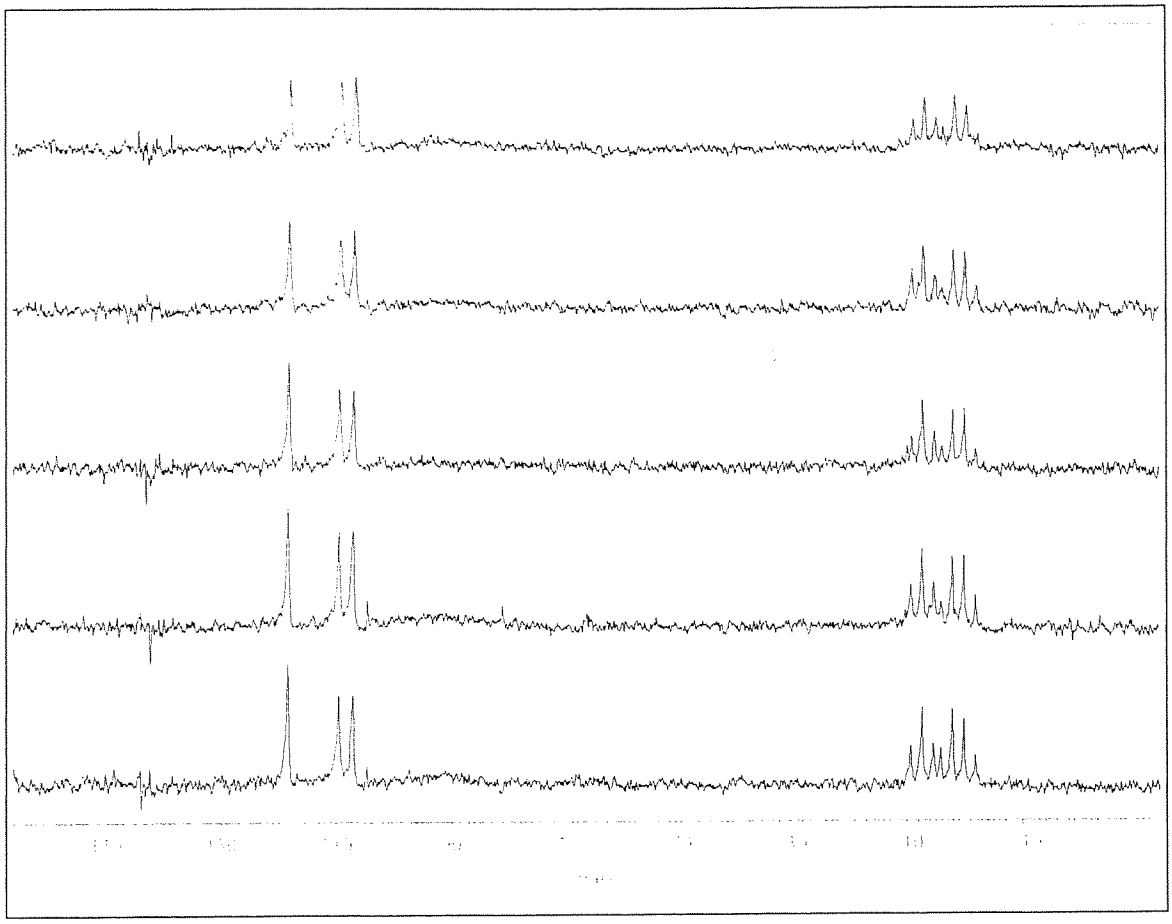

Figure 10.1: ^{13}C NMR spectra showing signal to noise enhancements with increasing ultrasound power for mesitylene/cyclohexane mixture: from top to bottom: 0, 12.7, 25.5, 38.3 and 51.0 Wcm^{-2} at 2 MHz applied ultrasound.

10.1.2.1 Spectra interpretation

The singlet shown in Figure 10.1, occurring at about 115ppm is due to the quaternary carbon of the mesitylene. The doublet shown at about 108ppm is due to the methyne carbon of the mesitylene. The peaks between 0 and 12ppm are due to the methylene carbons of the cylohexane and the methyl carbons of the mesitylene.

10.1.2.2 Results

Table 10.1 shows the calculated signal to noise measurements (taken by calculating, signal/√ noise) for the quaternary, aryl, methyl and methylene carbons at the different acoustic intensities. The values in parenthesis are repeat experimental data. The ^{13}C spectra for these measurements can be found in Figure A3.1.

Table 10.1: Signal to noise measurements for the different ^{13}C sites

		Signal to noise measurements Series 1 (Series 2)		
Power/Watts	Intensity/ Wcm^{-2}	Quaternary carbons	Aryl carbons	Methyl and methylene carbons
0	0	17.9 (18.0)	19.9 (20.5)	10.1 (10.8)
2.5	12.7	23.8 (22.7)	21.6 (21.8)	12.8 (11.7)
5	25.5	27.1 (27.2)	22.2 (24.3)	13.9 (14.7)
7.5	38.2	30.9 (30.4)	26.7 (25.1)	14.9 (15.7)
10	51.0	31.3 (30.8)	25.9 (26.7)	16.1 (16.4)

Graphs of signal to noise versus acoustic power were plotted to present this data graphically, as shown in, Figure 10.2, Figure 10.3 and Figure 10.4.

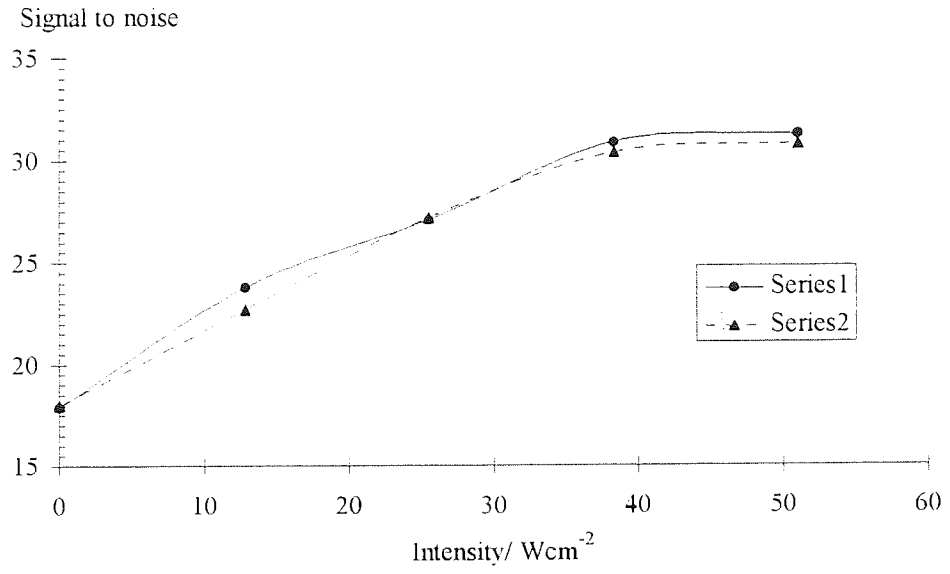

Figure 10.2: Signal to noise enhancements versus intensity for quaternary carbon

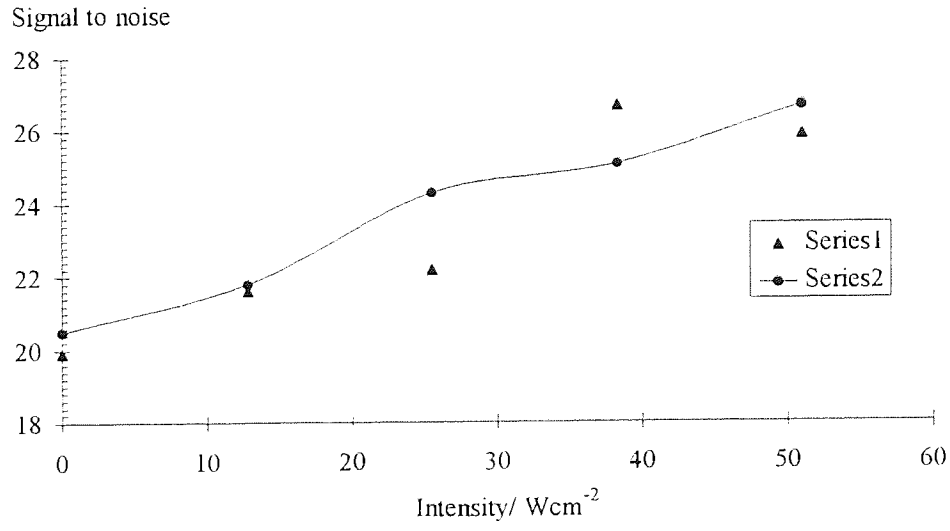

Figure 10.3: Signal to noise enhancements versus intensity for methyne carbons

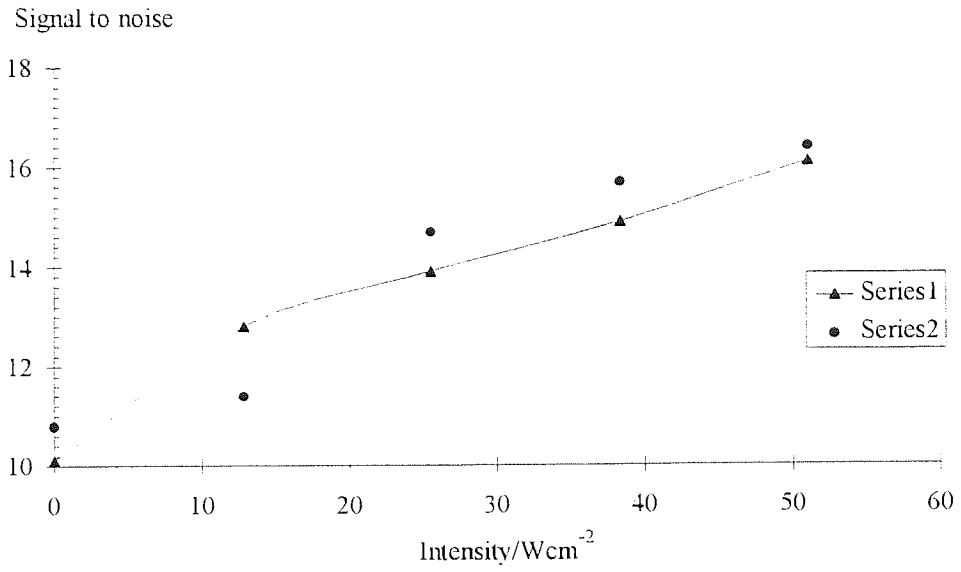

Figure 10.4: Signal to noise enhancements versus total absorption plotted for methyl and methylene carbons

10.1.3 Discussion

It can be seen from Figure 10.2, Figure 10.3 and Figure 10.4 above, that signal enhancement increases with increasing applied ultrasonic power. However, the enhancement generated for the quaternary and the methyl and methylene carbons by the passage of ultrasound through the sample appears to level off at around 7.5 Watts ($38.3 Wcm^{-2}$) as the processes responsible for causing the enhancement seem to optimise to a steady state.

From Table 10.1, it can be calculated that the maximum average percentage signal enhancement for the quaternary carbon nuclei is 72%, for the methyl and methylene carbons is 57% and for the methyne carbons is 30%

These results show, in agreement with those found by Homer and Patel (24), that each different carbon environment is enhanced to a differing extent by the passage of ultrasound. This suggests that the rotational and translational motion imparted to each different carbon environment, by the application of ultrasound, is unique to that environment.

The greatest enhancement that was seen was for the quaternary carbon, which has the longest T_1, and therefore the most to gain from the same extent of additional molecular motion imparted to the liquid mixture by the application of ultrasound. The quaternary carbon is the most hidden carbon environment in the molecule, which suggests that translation is less important than whole molecular rotation. By comparison of the enhancement observed for the methyl and methylene carbons to the methyne carbons, it can be seen that the methyl and methylene groups, with their additional hydrogen atoms show a greater enhancement than the methyne carbons. This could be due to ultrasonic accentuation of the bond rotation around the carbon-substituent bond, creating additional frequency components to enhance relaxation. The implication of this is that the ultrasound modifies a localised spin rotation contribution to the T_1.

10.1.4 Ultrasonic enhancement of the chloroform ^{13}C resonance

A $5cm^3$ sample of pure chloroform (molecular formula $CHCl_3$, molecular weight, 119.38), obtained from Aldrich was used for each experiment. This sample was placed inside the dedicated ultrasonic probe and irradiated with 0, 2.5, 5, 7.5 and 10 Watts (corresponding to 0, 12.7, 25.5, 38.3 and 51.0 Wcm^{-2}) ultrasonic powers at a frequency

of 2MHz. The NMR acquisition parameters used for these measurements can be found in appendix 3.

10.1.4.1 Results

Figure 10.5 shows the ^{13}C spectra that were obtained for this pure liquid at the different ultrasonic power intensities.

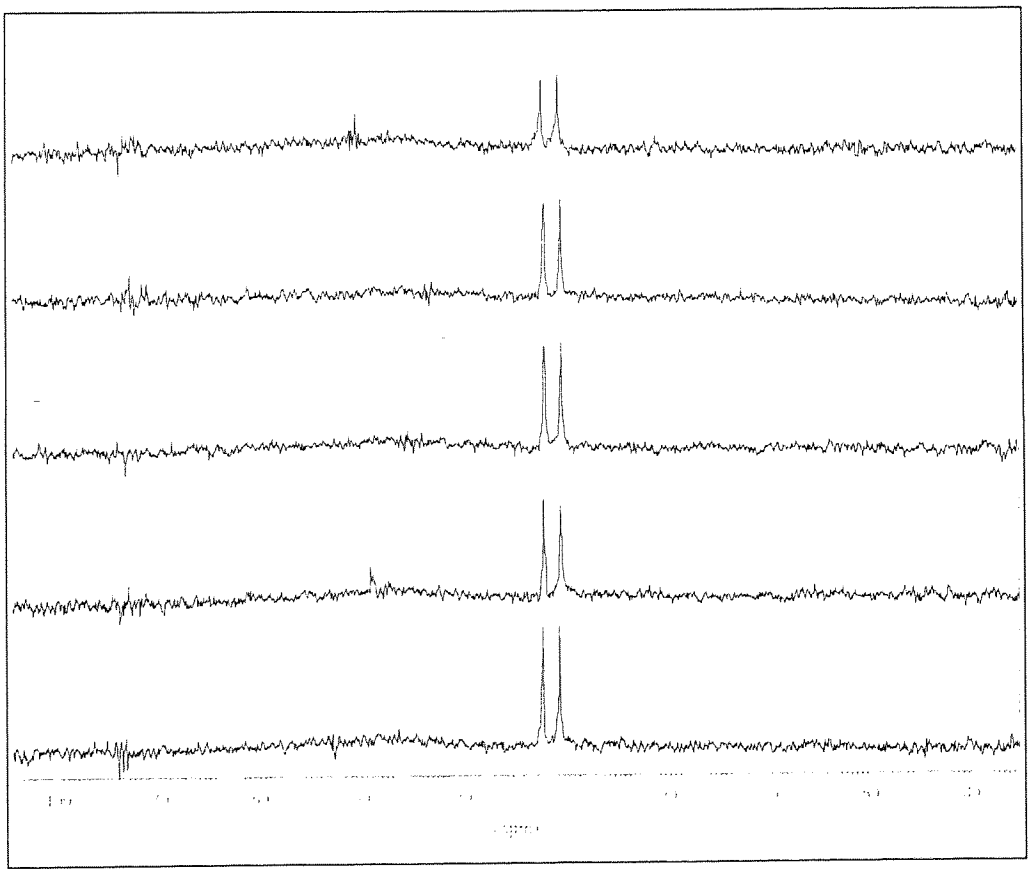

Figure 10.5: ^{13}C NMR spectra showing signal enhancements with increasing ultrasound power for chloroform: from top to bottom: 0, 12.7, 25.5, 38.3 and 51.0 Wcm^{-2} at 2 MHz acoustic frequency.

Table 10.2 below shows the calculated signal to noise measurements for the methyne carbon of chloroform at the different acoustic intensities.

Table 10.2: Signal to noise measurements for different ultrasonic powers for chloroform

	Signal to noise measurement
Intensity/ Wcm^{-2}	methyne carbon
0	17.6
12.7	23.1
25.5	28.5
38.3	31.7
51.0	29.2

A graph of signal to noise versus acoustic power are shown in Figure 10.6.

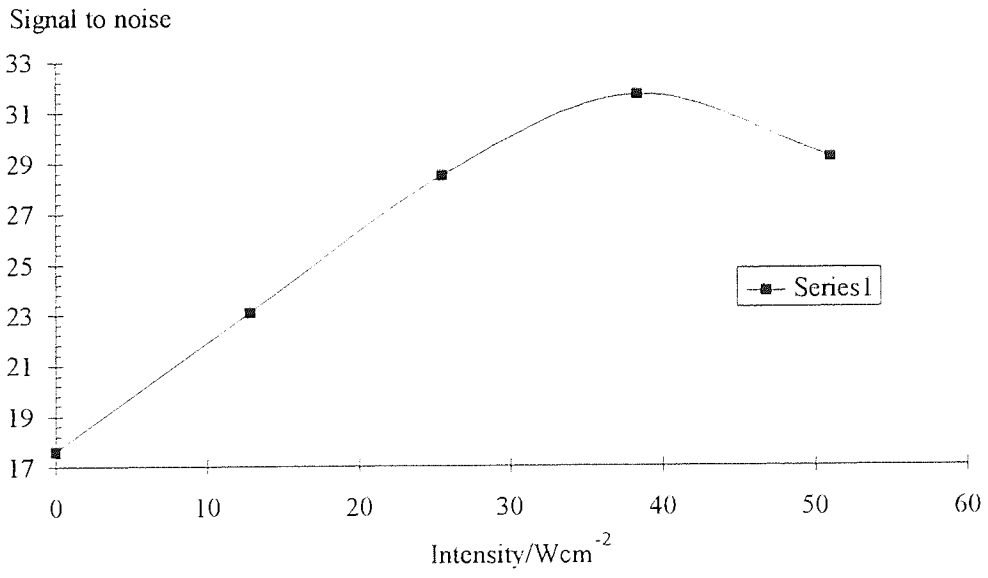

Figure 10.6: Signal to noise enhancement versus ultrasonic intensity applied for chloroform

10.1.5 Discussion of possible mechanisms for enhancement

The enhancement for the methyne carbon in chloroform is about 66%. This is greater than the enhancement for the aryl carbon of mesitylene, suggesting that the enhancement produced by the application of ultrasound is dependent not only on the nuclear environment, but on the type and size of the molecules. The carbon in chloroform is well exposed, which could explain why it shows a greater enhancement than the aryl carbon of the mesitylene molecule.

10.2 T_1 REDUCTION OF CHLOROFORM

The signal to noise results presented above merely provide a qualitative indication of T_1 reduction. To quantify the latter the DESPOT technique was used to determine the T_1 of the carbon in chloroform. Details of this technique can be found in Appendix 3. This technique was used in preference to other common methods for measuring T_1, such as inversion and saturation recovery due to the shorter time period required to perform the DESPOT experiment.

These DESPOT experiments were carried out 4 times without ultrasound to check the reproducibility of this technique. Table 10.3 shows the measured values for the T_1 of chloroform.

Table 10.3: Measured T_1 values against the power of ultrasound applied

Ultrasound applied/ Wcm^{-2}:	Measured T_1 Values/ s				
0	7.1	6.5	7.2	6.8	Average = 6.9
25.5	3.0	2.6			Average = 2.8
51.0	3.0	2.9			Average = 2.95

10.2.1 Discussion

The results shown above in Table 10.3 above suggest that the carbon T_1, in chloroform can be reduced by the order of 50-60% using ultrasound.

A possible mechanism for T_1 reduction in liquids is via an ultrasonically induced streaming effect (see section 5.4.4). While it is realised that streaming could be a contributing factor it is thought not to be the major mechanism, for two reasons. Firstly, Patel could not get a T_1 reduction for chloroform at 20 kHz and if the streaming effect alone was causing this reduction, it would have been observed at this frequency, which would provide a streaming action. Also this T_1 reduction was found to be independent of the power supplied, which again implies that the application of the ultrasound is not simply supplying a streaming effect as a higher power would promote more streaming, whereas this was not observed

Homer and Patel found that at high powers the T_1 of molecules in the liquid phase started to increase, this increase was not observed doing the present work, as shown in these results Table 10.3. The increase observed by Homer and Patel could have been due

to sample heating at these higher powers, as heating causes the T_1 for small molecules to increase as the temperature rises (see chapter 2).

The implication is that high frequency ultrasound induces changes to the rotational and translational motion of molecules. The detailed mechanism and extents of these effects remain to be fully elucidated.

CHAPTER 11 SAMPLE HEATING: A NOVEL ULTRASONIC DEVICE

11.1 ULTRASONIC HEATING

As outlined in section 7.5.4, the temperature in the ultrasonic probehead area was controlled by two gas inlet feeds. One fed in liquid nitrogen vapour and the other fed in compressed air to facilitate cooling and provide additional circulation of the nitrogen vapour. The temperature of the sample within the probe was monitored after NMR acquisition by removing the probe, with the ultrasound still running and taking the temperature using a thermocouple. It was found that running at low powers (5.1 - 20.4 Wcm^{-2}) the sample temperature was maintained at about 25°C (just above room temperature). Running at higher powers (between 20.4 - 45.9 Wcm^{-2}) the sample temperature stabilised at between 30-35°C, while running at even higher powers (51.0 - 61.2 Wcm^{-2}) the temperature stabilised at about 45°C. The ultrasonic experiments were generally not taken above 61.2 Wcm^{-2}, due to the fact that it was felt that to heat samples above a temperature of 45°C would be detrimental to the experiment and complicate the elucidation of results with regard to the origin of the SINNMR, signal enhancement and T_1 reduction experiments.

11.1.1 A novel ultrasonic unit, the drumskin device

To minimise sample heating a novel ultrasonic unit has been developed by the author in collaboration with Dr. J Robson.

Figure 11.1 shows a schematic diagram of the device.

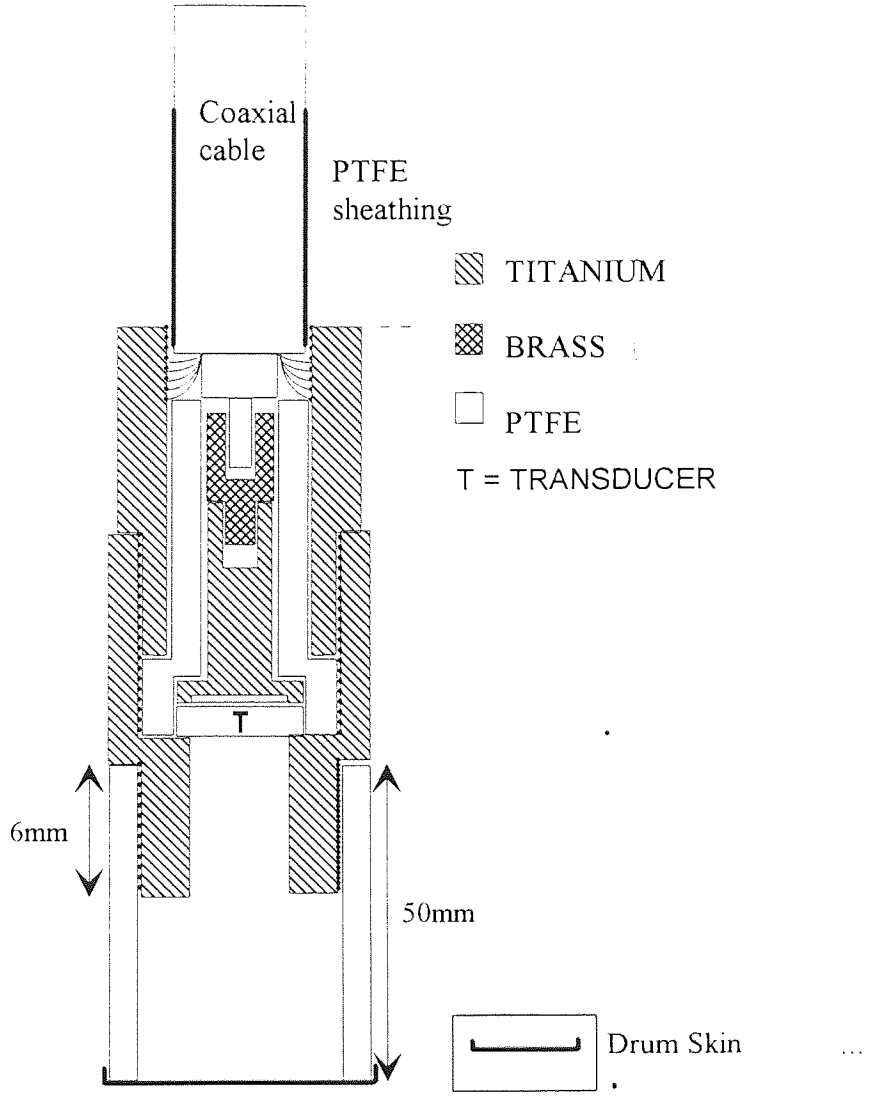

Figure 11.1: "Drumskin" transducer holder

The idea behind the device is that sample heating can be minimised if the ultrasound is delivered into the sample via a liquid filled tube that has a drumskin of parafilm^{TM} placed over the end to be in contact with the analytical liquid. The ultrasound passes thorough the intervening liquid medium and causes the drumskin on the end of the device to vibrate, such that the passage of ultrasound through into the sample is not impeded.

11.1.2 Experiment carried out to determine if cavitation is still possible using the drumskin device

Experiments have been carried out "on the bench" using the Weissler reaction (8.2.1), to ensure that cavitation in the sample beyond the device is possible.

11.1.2.1 Experimental

The Weissler reaction was set up out as outlined in 8.2.2.1. The reaction mixture was irradiated with 2 and 3 MHz ultrasound using the drumskin transducer holding device.

Table 11.1 shows the times and powers necessary to create a cavitation field and cause the reaction mixture to turn a characteristic blue/black using the drumskin device and are compared with the times and powers necessary for the reaction to occur when using a standard transducer holder (as shown in Figure 7.3).

11.1.2.2 Results

Table 11.1: The times and powers necessary to cause a solution of KI to liberate iodine, using starch as an indicator. (times in brackets are those for a regular custom made transducer holder, as originally shown in Table 8.1)

Frequency, MHz	2	2	3	3
Power, W	5	10	5	10
Intensity W/cm^{-2}	25.5	51.0	25.5	51.0
Time for colour change, s	(134) 139	(6) 8	(149) 142	(6) 7

11.1.3 Discussion

Table 11.1 shows that the times and powers necessary to cause cavitation by using the drumskin device are comparable with the times and powers necessary to cause cavitation, using the regular transducer housing arrangement.

The second important advantage to using the drumskin device is that the transducer is kept remote from the sample. As outlined in chapter 7, transducers may be deteriorated by the presence of certain liquids, specifically solvents, as these tend to strip the conductive paint from the transducer surface. As the power intensity supplied by a transducer depends on the surface irradiating area, if this is stripped away, the power output per voltage input (efficiency) may be reduced. It may be presumed that any loss of efficiency experienced by the transducer will result in an additional heating effect.

11.1.4 Experiment to measure sample heating using the drumskin device

An experiment was carried to measure the extent of heating produced by a normal custom made transducer housing, as shown in Figure 7.3, as compared to the amount of heating using the drumskin adaptation to the holder, shown in Figure 11.1.

11.1.4.1 Experimental

The experiment was set up in a 50ml beaker filled with 20ml of distilled water, as shown in Figure 11.2.

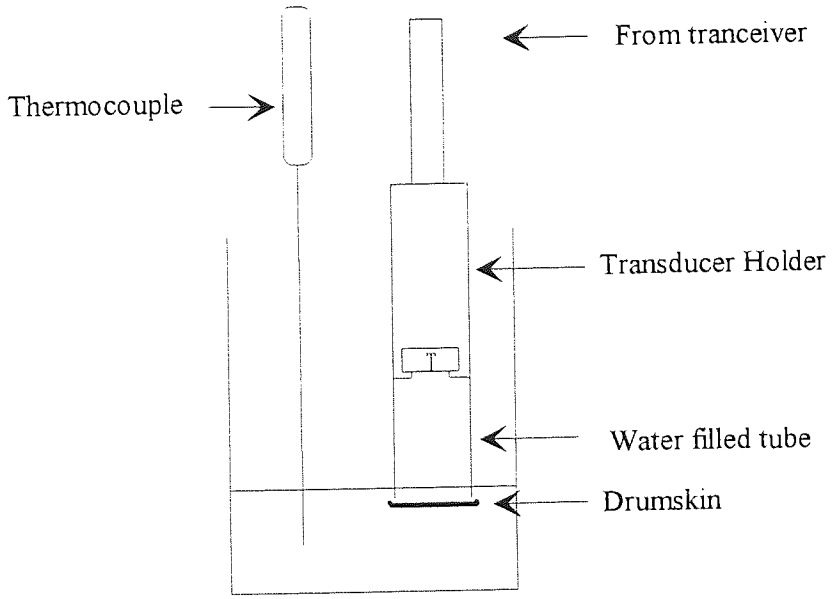

Figure 11.2: Experimental apparatus used for the heating experiment

A 3MHz transducer was used in both transducer devices and the ultrasound was run at powers of 25.5 and then 51.0 Wcm^{-2} . The temperature of the water was monitored at one minute intervals over a total time of 15 minutes using a Norma D1401 thermocouple capable of monitoring temperature in the range -50 to 199.9°C (± 0.05°C).

A monitoring time of 15 minutes was chosen for two reasons. First, that the heating effect seems to reach a steady state in this time, effectively because the rate of heating provided by the ultrasound equals the heat losses from the system. Second, a typical SINNMR spectrum, as outlined in chapter 9 generally takes no longer than 15 minutes to acquire .

11.1.4.2 Results

Table 11.2: Heating comparison between a regular transducer holder and the drumskin device

	Temperature/ °C			
Time/ Mins	25.5 Wcm^{-2} Regular Holder	25.5 Wcm^{-2} Drumskin Holder	51.0 Wcm^{-2} Regular Holder	51.0 Wcm^{-2} Drumskin Holder
0	18.0	17.9	17.8	17.8
1	18.5	18	19.1	18
2	19.7	18.1	20.6	18.1
3	20.7	18.2	21.9	18.3
4	21.5	18.2	23.5	18.4
5	22.0	18.3	24.8	18.7
6	22.6	18.4	26.2	18.9
7	23.0	18.5	27.0	19.1
8	23.4	18.6	28.0	19.3
9	23.9	18.8	28.9	19.5
10	24.4	18.9	29.8	19.7
11	25.0	19.3	30.6	19.9
12	25.3	19.0	31.3	20.1
13	25.8	19.1	31.7	21.0
14	26.1	19.1	32.1	21.1
15	26.2	19.1	32.2	21.1
Temperature Rise	8.2	1.2	14.4	3.3
Percentage Temperature Increase	45.6%	6.7%	80.9%	18.5%

Figure 11.3 shows a graphical representation of the temperature measurement data. The unfilled icons representing the heating effect (at 25.5 and 51.0 Wcm^{-2}) of the regular transducer holder, while the filled icons represent the heating effect again (at 25.5 and 51.0 Wcm^{-2}) of the drumskin device.

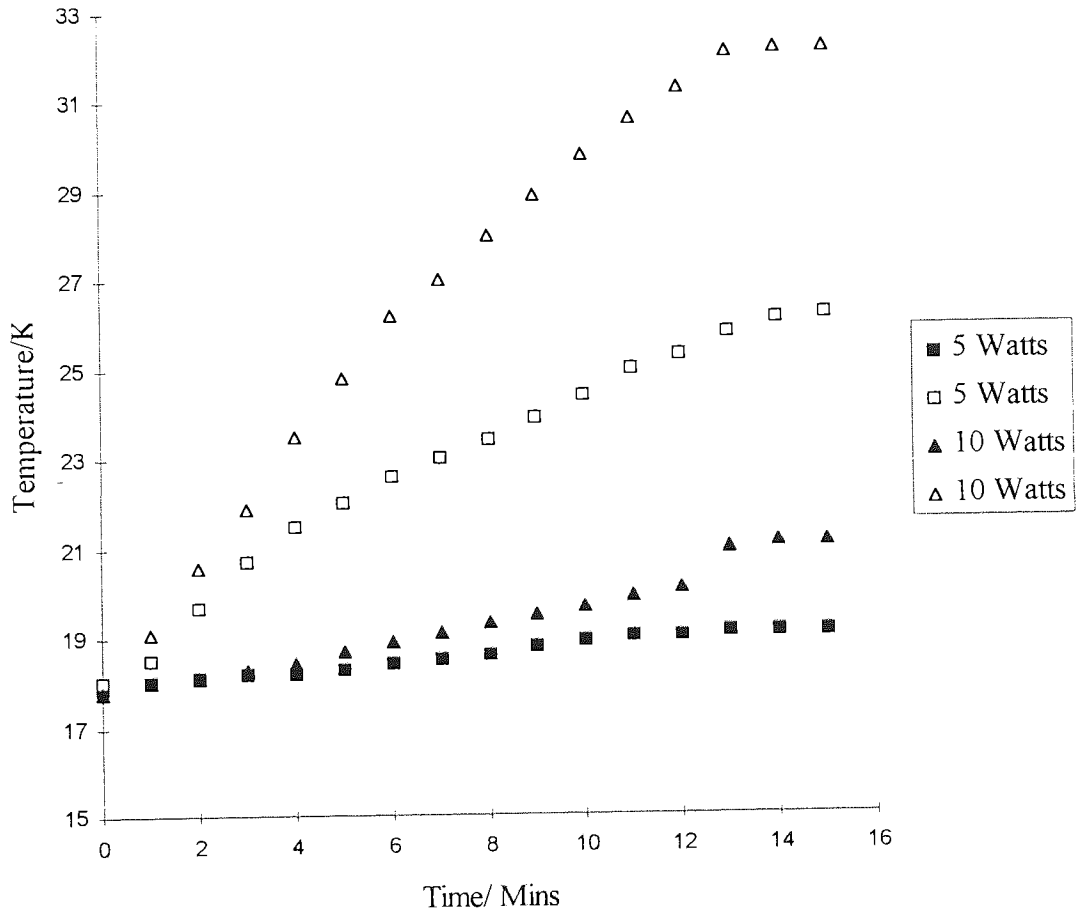

Figure 11.3: Heating effect using a standard transducer holder, (shown as unfilled icons) and using the drumskin adaptation, (shown as filled icons) at 35.5 and 51.0 Wcm^{-2} acoustic power.

11.1.4.3 Discussion

From Table 11.2 it can be seen that the percentage temperature increases at 25.5 Wcm^{-2} is approximately seven times greater for the regular transducer holder as compared to the drumskin device. At 51.0 Wcm^{-2} ultrasonic power the percentage increase for the regular transducer holder is about five times greater compared to the drumskin device. Presumably the low percentage temperature increase at these high powers is because the liquid behind the drumskin heats and transmits this heat to the analytical sample beyond the device. It is believed that this technique will eliminate the problem of localised heating effects due to the fact that any streaming effect (which is essentially an ultrasonic energy gradient) will take place in the liquid tube and not in the sample.

These results suggest that a significant reduction in heating can be achieved using the drumskin device, and its incorporation into the design of NMR and ultrasound experiments and ultimately the ultrasonic probe would benefit this work.

It was found, using this device that it is beneficial to run the device prior to use to deoxygenate the water, and prevent the formation of air bubbles in the liquid filled tube.

CHAPTER 12 CONCLUSIONS AND FURTHER WORK

12.1 CONCLUSIONS

The objective of this work was to design and construct a NMR probehead accommodating ultrasound irradiation facilities for use within a cryo-magnet NMR spectrometer. Such a dedicated probe has been developed and has been used for the T_1 reduction and signal enhancement of a liquid mixture and a pure compound as well as to facilitate the sonically induced narrowing of a solid state sample of TSP.

The initial experiment, fundamental to the whole progress of applying ultrasound *in situ* to samples placed within a cryo-magnet of a NMR spectrometer, has been completed with success: it has been proved that the application of 1.5, 2, 3, 5 and 10 MHz ultrasound at powers ranging from 1 to 50 Watts (5.1 -254.6 Wcm^{-2}) does not cause the magnet to quench.

It has also been proven using the well known Weissler reaction as an ultrasonic dosimeter that cavitation both inside and outside the magnet is possible. The Weissler reaction requires the onset of cavitation to facilitate the liberation of iodine from a solution of potassium iodide. This reaction has been carried out using 2, 3, 5 and 10 MHz ultrasound. The implication is that the magnetic fields do not affect ultrasonic cavitation (the times and powers required for the reaction to occur were similar when running the experiment both inside and outside the magnet). These results also show, in agreement with established literature, that cavitation at higher frequencies is harder to achieve as it requires a longer time and/or a higher power to initiate the colour change of the reaction.

Custom designed transducer holders suitable for the propagation of ultrasound from above the sample have been developed and constructed by the author. A transducer holder capable of irradiating the sample from below and a dedicated ultrasonic NMR probe have been developed, also by the author.

The main design features of the transducer holder used within the acoustic NMR probe design are that it was constructed from brass for the electrical contacts, (as other metals were found to distort the NMR signal lineshapes), and PTFE was used as an insulator. PZT4-D transducers were selected and used in the experiments as they are suitable for high power ultrasonic propagation, as required by the experiments carried out in this thesis. The design includes a quarter wavelength backing of the transducer to maximise forward ultrasonic power transmission and keep the transducer as unconstrained as possible. The front transmission face of the transducer holder was kept effectively open, having only a minimal lip to hold the transducer in place, as it was found that using a full front face impeded ultrasonic transmission. However the transducer was protected from chemical attack by a layer of thin stainless steel foil, placed over the transducer and kept in place underneath the retaining lip. Viton o-rings were used to seal the sample tube to the transducer assembly and prevent leakage of the sample through the holder body. A PTFE NMR tube threaded to the outer brass casing was found preferable to using a glass tube bonded to the brass casing as the glass to metal joint was prone to fracture and leaking.

The high resolution probe head area was redeveloped by stripping away the lock, decoupler and VT assemblies, to create space. Brass stilts were constructed to stabilise the tuning module and coil, which were kept in place. A collet arrangement of brass contacts that allow the bottom mounted transducer holder and sample tube to be dropped into the magnet in the conventional way was incorporated into the probe head area. The compressional connections required for high power ultrasonic propagation are made firm from outside the magnet by screwing tight the threaded wheels at the bottom of the probe The limitations of this probe are presently that there are several important nuclei outside its tuning range, such as boron, phosphorous and proton. Temperature stabilisation was achieved by the incorporation of two VT air lines, one feeding cold nitrogen into the probe head area and a second air line inlet to create efficient circulation and maximise cooling.

A novel ultrasonic device has been developed to minimise sample heating. This involves running the ultrasound though a liquid filled tube that has a drumskin on the end. The drumskin acts as a mechanical oscillator, passing the ultrasound through into the sample beyond the device. Preliminary bench experiments, utilising the Weissler reaction, have proved that cavitation in the liquid sample beyond the device is still possible without being significantly impeded by the presence of the drumskin. It has been shown, using this device, that sample heating is limited. An experiment set up to compare the amount of sample heating using a regular transducer holder compared to using the drumskin device has shown that heating reductions of up to 80% are possible using the drumskin holder.

The line narrowing of solid state TSP suspended in a support medium of chloroform and bromoform has been achieved using the dedicated acoustic NMR probe. Experiments were run at two frequencies of 2 and 3 MHz, with three different particle size ranges <38μm, 38 -75μm and 75 -104μm and acoustic powers ranging from 1 to 18 Watts (5.1 -.91.7 Wcm^{-2}). The narrowing achieved seemed not to be dependent on the size of particles used for the experiment or the frequency parameters, but did depend on the power supplied. The narrowing of the linewidth was achieved progressively with increasing power and seemed to occur in three phases: a linear decrease was observed for acoustic powers ranging from 1 - 6 Watts (5.05 - 30.1 Wcm^{-2}) which is thought to be attributed to the ultrasound providing an enhancement of Brownian motion type narrowing; a sharper increase in the amount of narrowing occurs at powers ranging from 6-10 Watts (30.1 - 51.0 Wcm^{-2}), which is thought to be due to cavitation and shock wave effects providing additional rotational and translational motion to the particles; finally optimum narrowing was achieved at ultrasonic powers of between 10-12 Watts, no further decrease in narrowing was observed with increasing power.

The signal enhancement of a liquid 1:1 molar mixture of mesitylene and cylohexane, was achieved using the acoustic NMR probe. The experiment was run at powers ranging from 0-10 Watts (0 - 51.0 Wcm^{-2}) acoustic power. A signal enhancement of approximately 72% was achieved for the quaternary carbon in this mixture, a 30 % enhancement was achieved for the methyne carbon, while the methyl and methylene carbons showed enhancements of 57%. Thus it was seen that the amount of signal enhancement is dependent on the environment of the carbon nuclei. The enhancement was found to increase with increasing acoustic power. The enhancement for the

quaternary, methyl and methylene carbons appeared to level off at acoustic powers of 8-10 Watts, this levelling off was not observed for the enhancement of the methyne carbon, presumably at higher acoustic powers more enhancement would be observed for this carbon environment, although it would be expected that this also would level off eventually.

Signal enhancement was also carried out on a sample of pure chloroform, the enhancement again showed an increase with increasing acoustic power, optimising to a steady enhancement at an acoustic power of 8-10 Watts (40.0 - 51.1 Wcm^{-2}).

It was shown, using the DESPOT sequence for measuring T_1, that the T_1 of the chloroform was reduced by approximately 67% by the application of ultrasound. This was found to be independent of the power supplied, which implies that the application of the ultrasound is not simply supplying a streaming type effect and that modulation of the rotational and translational motion that accompanies the T_1 reduction rises to a maximum at low powers.

12.2 Further Work

Further work on the ultrasonic probe can be achieved by reincorporating the lock and decoupler assemblies. Further to this it would be advantageous to replace the brass collet arrangement with an insulating type material that had minimised metal connectors in order to reduce distortion of the NMR lineshape. Ideally the transducer holder and connections to it should be made from a high purity titanium alloy or stainless steel, as used by NMR manufacturers to construct probeheads.

A light emitting diode type device could be incorporated into the probe design, which would light up outside the once all electrical contacts had been made. This would allow the user to see, (without removing the probe manually and checking), that the ultrasound was running within the magnet.

It is thought that the resonant frequency of the transducer may be altered by the restraint placed on it by its housing and that power delivery could be maximised if the resonant frequency of the whole assembly could be determined. If ultrasonic propagation can be increased for a given power supply then the amount of heating will be reduced.

With the use of appropriate cooling techniques such as the "drumskin" device it should be possible to radiate ultrasound into a suspended solid sample from more than one direction. This in theory should enhance the incoherent motion imparted to the solid particles and prevent effects such as standing waves. More than one frequency of transducer could be used to supply a greater size range of cavitation bubbles and wider range of events that lead to enhanced spatial averaging of the solid state SINNMR technique.

The signal enhancement and T_1 reduction work could be carried out on macromolecular liquids that possess nuclei with long relaxation times to facilitate the structural elucidation of these compounds. This technique might be used in a corresponding respect to produce enhanced signals in a shorter time than is possible in unsonicated sample.

Further studies could be carried out on many more pure liquids and liquid mixtures if the mechanism of T_1 reduction and the way in which the application of ultrasound has been seen to modulate different groups to different extent is to be fully elucidated

The ultrasonic probe can be used to monitor sonochemical reactions *in situ*. This information could be useful if the reaction pathway were not known as it would be possible to take "snap shots" of the reaction as it proceeded. It would also pinpoint the production of any unstable intermediates that either do not appear in the final reaction product or are unstable and break down before the reaction mixture can be sampled.

Further investigations into the use of the drumskin device could be carried out. For example, a heating investigation into how the length of the liquid filled tube affects the amount of heating reduction, would be profitable as would investigations concerning the properties of the liquid that is used in the liquid filled tube.

BIBLIOGRAPHY

NMR Texts

E. Fukushima S.B. Roeder, "Experimental Pulse NMR, A Nuts and Bolts Approach", Addison-Wesley, Reading, Mass. USA, 1981.

A.E. Derome, "Modern NMR Techniques for Chemistry Research", Pergamon, Oxford, 1987.

C. Brevard and P. Granger, "Handbook of High Resolution Multinuclear NMR", Wiley, New York, 1981.

C.A. Fyfe, "Solid State NMR for Chemists", C.F.C. Press, Ontario, 1983.

A. Abragam, "Principles of Nuclear Magnetism", Clarendon Press, Oxford, 1961.

J.W. Akitt, "NMR and Chemistry, An Introduction to modern NMR Spectroscopy", Third Edition, Chapman and Hall, London. 1992.

M. Mehring, "High Resolution NMR in Solids" 2nd Edition, Springer-Verleg, New York, 1993.

J.K.M. Sanders and B.K.Hunter, "Modern NMR Spectroscopy- A Guide for Chemists", 2nd Edition, Oxford, 1983.

S.W. Homans, "A Dictionary of Concepts in NMR", Clarendon Press, Oxford, 1992

C.P.Schlicter, " Principles of Magnetic Resonance", 3rd Edition, Springer-Verlag, New York, 1990.

J.W. Hennel and J.Klinowski, "Fundamentals of Nuclear Magnetic Resonance", Longman UK, Essex, England, 1993.

J.W.Emsley, J,Feeney, L.H.Sutcliffe, "Progress In NMR Spectroscopy" Volume 8, Pergamon Press, Oxford.1972.

T.C.Farrar, E.D.Becker, "Pulse and Fourier Transform NMR, Introduction to Theory and Methods", Academic Press, London, 1971.

G.Engelhardt and D.Michel, "High Resolution Solid State NMR of Silicates and Zeolites" John Wiley & Sons, Chicester, 1987.

R.M.Lyndon-Bell and R.K.Harris, "Nuclear Magnetic Resonance Spectroscopy" Thomas Nelson and Sons Ltd.,London. 1969.

G.A.Webb, Ed. "Annual Reports on NMR Spectroscopy" Volume 24. Acedemic Press, London 1992.

N. Bloembergen, "Nuclear Magnetic Relaxation" W.A Benjamin Inc. New York.1961.

R.K.Harris, "Nuclear magnetic Resonance Spectroscopy -A Physiochemical View". Pitman Books Ltd. London. 1983.

Ultrasound Texts

J.Blitz, "Fundamentals of Ultrasonics", 2nd Edition, Butterworths, London, 1967.

G.L.Gooberman, "Ultrasonics; Theory and Application", English University Press, London, 1968.

G.Price, Ed., "Current Trends in Sonochemistry", The Royal Society of Chemistry, Cambridge, 1992.

J.R.Frederick, "Ultrasonic Engineering", Wiley, New York.1965.

W.P.Mason, Ed. "Physical Acoustics" Volume 1 part B Academic Press, New York, 1965.

R.Goldman, "Ultrasonic Technology" Chapman and Hall Ltd, London. 1962.

T.J. Mason, Ed. "Chemistry with Ultrasound" Elseveir Applied Science, London. 1990.

I.S. Grigoriev & E.Z.Meilikhov, "Handbook of Physical Quantities" CRC Press Inc, London. 1997

J.Daintith, Ed. "A Dictionary of Physical Sciences" The Macmillan Press Ltd, London 1978.

R.T.Beyer, & S.V.Letcher, "Physical Ultrasonics" Academic Press, London 1969

13. REFERENCES

1 W. Pauli, "Zuschriften und varlaufige Mitteilungen", Naturwisschaften, 1924, **12**, 741.

2 E. M. Purcell, H.C. Torrey & R. V. Pound, "Resonance Absorption by Nuclear Magnetic Moments in a Solid", Phys. Rev., 1946, **69**, 37.

3 F. Bloch, W. W. Hansen & M. Packard, "The Nuclear Induction Experiment", Phys. Rev., 1946, **69**, 127.

4 R. M. Bracewell, "The Fourier Transform and its Applications", Mcgraw-Hill, New York, 1968.

5 D. Traficante, "Carbon -13 NMR Spectroscopy, It was not always easy", Concepts in Mag. Res., **3,** 1991, 13.

6 E.R. Andrew, A. Bradbury & R. G. Eades, "Nuclear Magnetic Resonance Spectra from a Crystal rotated at High Speed", Nature, 1958, **182**, 1659.

7 I. J. lowe, "Free Induction Decays of Rotating Solids", Phys. Rev., Lett, 1959, **2**, 285.

8 S. R. Hartmann & E. L. Hahn, "Nuclear Double Resonance in the Rotating Frame", Phys. Rev., 1962, **128**, 2042.

9 J. S. Waugh, M. L. Huber & U. Haeberlen, " Approach to High resolution NMR in Solids" Phys. Rev. Lett., 1968, 20, 180.

10 P, Mansfield, "Symmetrized Pulse Sequences in High Resolution NMR in Solids", J. Phys C: Solid State Phys., **4,** 1971, 1444.

11 W.K. Rhim, D.D. Elleman & R.W. Vaughan, "Analysis of Multiple Pulse NMR in Solids", J. Chem. Phys., **59,** 1973, 3740.

12 C. S. Yannoni, "High-Resolution NMR in Solids: The CPMAS Experiment", Acc. Chem. Res., 1982, **15**, 201

13 J. Schaefer, E.O. Stejskal & R. Buchdahl, "High Resolution Carbon-13 Nuclear Magnetic Resonance study of some Solid Glassy Polymers", Macromolecules, **8,** 1975, 291.

14 U. Haeberlan & J.S. Waugh, "Coherent Averaging Effects in Magnetic Resonance", Phys Rev, **175,** 1968, 453.

15 Burum D.P.. "Combined Rotation and Multiple Pulse Spectroscopy (CRAMPS)", Concepts in Mag Res., **2,** 1990, 213.

16 A.Samoson, E.Lippmaa & A. Pines, "High Resolution Solid State NMR. Averaging of second-order effects by means of a Double Rotor", Mol. Phys., **65**(4) 1988, 1013.

17 A. Samoson and A. Pines, "Double Rotor for Solid-State NMR", Rev. Sci. Instrum., 1989, **60**(10), 3239.

18 Y. Wu, D. Lewis, J.S. Frye A.R. Palmer & R.A.Wind, "Cross-Polarisation Double Angle Rotation", J. Mag. Res., **100,** 1992, 425.

19 A. Llor & J. Virlet, "Towards High Resolution NMR of more Nuclei in Solids: Sample Spinning with Time-dependent Spinner Axis Angle", Chem. Phys. Let., 1988, **152**(2.3), 248.

20 J. Homer, P. McKeown, W. R. McWhinnie, S. U. Patel & G. J, Tilestone, "Sonically Induced Narrowing of Solid State Nuclear Magnetic Resonance Spectra: A Possible Alternative to Magic Angle Spinning Nuclear Magnetic Resonance Spectra", J. Chem. Soc., Faraday Trans., 1991, **87**, 2253.

21 J. Homer & M. J. Howard, "Studies on the Origin of Sonically Induced Narrowing of Solid-State Nuclear Magnetic Resonance Spectra", J. Chem. Soc., Faraday Trans., 1993, **89**, 3029.

22 M.J. Howard, Thesis, "Evaluation of the Sonically Induced Narrowing of the Nuclear Magnetic Resonance of Solids", Aston University thesis, 1993.

23 S. Reynolds, "NMR Spectroscopy in the presence of Ultrasound and other Perturbations", Aston University thesis, 1997.

24 J. Homer & S.U. Patel, "Preliminary Observations on High Resolution Nuclear Magnetic resonance for Liquids subjected to Ultrasound" J. Chem. Soc., Faraday Communications, 1990, 215.

25 S.U. Patel, "Nuclear Magnetic Resonance and Ultrasound" Aston University thesis, 1989.

26 N.F. Ramsey "The internal Diamagnetic Field correction in Measurements of the Proton Magnetic Moment", Phys rev., **77**, 1950, 567.

27 N.F. Ramsey, "Magnetic shielding of Nuclei in Molecules", Phys. Rev., **78,** 1950, 699.

28 N.F. Ramsey, "Chemical Effects in Nuclear Magnetic Resonance and in Diamagnetic Susceptibility", Phys. Rev., **86,** 1952, 243.

29 J. I Musher, "Theory of the Chemical Shift", Adv. Mag. Res., Ed. J, Waugh Vol. **2.** 1966.

30 C.P Slichter, "Principles of magnetic Resonance", Springer-Verlag, New York, 1989, p.92.

31 W. Heisenberg, "Uber den anschaulichen Inhalt der quantentheoretischen Kinematik und Mechanik", Z. Phys., 1927, 43, 172.

P.W. Atkins, "Quanta: A Handbook of Concepts" Second Edition, Oxford University Press, Oxford, 1991

32 D. Traficante, , "Time Averaging: Does the Noise Really average Toward Zero", Concepts in Mag. Res., **3,** 1991, 83.

33 E. O. Brigham, "The Fast Fourier Transform", Prentice-Hall, London, 1974.

34 F. Bloch, "Nuclear Induction", Phys. Rev., 1946, **70**, 469.

35 J. Homer & M. S. Beevers, "Driven Equilibrium single pulse observation of T_1 relaxation. A re-evaluation of a rapid "new" method for determining NMR spin-lattice relaxation times", J. Mag. Res., 1985, **63**, 287.

36 J. Homer and J. K. Roberts, "Routine Evaluation of M_0 Ratios and T_1 Values from Driven Equilibrium NMR Spectra", J. Mag. Res, 1990, **89**, 265.

37 J. Homer and J.K. Roberts, "Conditions for the Driven Equilibrium Single Pulse Observation of Spin Lattice Relaxation Times", J. Mag.Res., **74,** 1987, 424.

38 S.A., Palke, W.E. & Gerig, J.T., "The Hamiltonians of NMR Part 1", Concepts in Mag. Res., **4,** 1992, 107.

39 S.A. Smith, W.E. Palke & J.T. Gerig, "The Hamiltonians of NMR Part 2", Concepts in Mag. Res., **4,** 1992, 181.

40 R.K. Harris, "Multinuclear magnetic resonance in liquids and solids- chemical applications", P.Granger & R.K.Harris (Eds). Kluwar Academic Publishers. 1990, p.279.

41 G. E. Pake, "Nuclear Resonance Absorption in Hydrated Crystals: Fine Structure of the Proton Line", J. Chem. Phys., 1948, **16**, 327.

42 F. Taulelle, "NMR of Quadrupolar Nuclei in the Solid State", Multinuclear Magnetic Resonance in Liquids and Solids-Chemical Applications, p. 393, (Eds.) P. Granger and R. Harris, Kluwer Academic Press, 1990.

43 J. Schaefer & E. Stejskal, Chapter 4 "Topics in Carbon-13 NMR spectroscopy", Vol. 3, Ed. Levy, G.C. 1979

44 E.R. Andrew, "Progress in NMR spectroscopy. **8**, 1.

45 A. Samoson & E. Lippma, "Sychronised Double Rotation NMR Spectroscopy", J. Mag. Res., **84,** 1989, 410.

46 K. T. Mueller, B. Q. Sun, G. C. Chingas, J. W. Zwanziger, T. Terao & A. Pines, "Dynamic-Angle Spinning of Quadrupolar Nuclei", J. Mag. Res., 190, **86**, 470.

47 D. Traficante, "Impedence: What it is and why it must be matched", Concepts in Mag. Res., **1,** 1989, 73.

47 E.J. Rathe, "Note on Two Common Problems of Sound Propagation", J. Vib. Sound., 10(3), 1969, 472.

49 W.P. Mason and H. J. McSkimn, "Attenuation and Scattering of High Frequency Sound Waves in metals and Glasses", J. Acoust. Soc. Am., **19,** 1967, 464.

50 W. P. Mason & H. J. McSkimn, "Energy Losses of Sound Waves in Metals due to Scattering and Diffusion", J. Appl. Phys., 1948, **19**, 940.

51 A.S. Ahuja & W.R. Hendee, "Effects of Particle Shape and Orientation on Propagation of Sound in Suspensions", J. Acoust. Am. Soc., Vol.63, No.4, 1978, 1075.

52 P. Curie and J. Currie, " Development, par presion, de l'electricite polaire dans les cristaux hemiedres a faces inclinees", Compt. Rend., 1880, **91**, 294.

53 K. Kawabata. & S. Umemura, "Use of Second Harmonic Superimposition to Induce Chemical Effects of Ultrasound", J. Phys. Chem., 1996, **100,** 18974.

54 J. Blitz, "Fundamentals of Ultrasonics", Second edition, Butterworths, London. 1967, p.49.

55 B. Jaffe, R. S Roth & S. Marzullo, "Piezoelectric Properties of Lead-Zirconate Titanate solid solution ceramics", J. Appl. Phys., **25** 1954, 809.

56 F. Kulcsar, "Electromechanical properties of lead titanate zirconate ceramics with lead partially replaced by calcium or strontium", J. Am. Ceram. Soc., 1959, **42**, 49.

57 P. Vigoureux, & C.F. Booth, "Quartz Vibrators and their Applications" H.M.S.O., London. 1950.

58 J. Blitz, "Fundamentals of Ultrasonics", Second edition, Butterworths, London. 1967, p.117

59 I.F. Zartman, "Ultrasonic velocities and absorption in gases at low pressures", J. Acoust. Soc. Am., 21, 1949. 171

60 J. Blitz, "Fundamentals of Ultrasonics" Second edition, Butterworths, London. 1967, p.51

61 G.W. Willard, "Focusing Ultrasonic Radiators", J. Acoust. Am. Soc., **21,** 1949, 360.

62 E. Fox. & V. Griffing, "Experimental investigations of Ultrasonic Intensity gains in Water due to Concave Reflectors", J. Acoust. Am. Soc., **21,** 1949, 352.

63 J.P. Perkins, "Power ultrasonic equipment for sonochemistry research", Based on a paper presented at the Sonochemistry Symposium Annual Chemical Congress, Warwick University, 8-11 April, 1986.

64 G.L. Gooberman, "Ultrasonics Theory and Application", The English Universities Press Ltd. London. 1968, p.94

65 T.G. Leighton, "Bubble Population in Acoustic Cavitation" Ultrasonics Sonochemistry. Vol. 5 ,No. 2, 1995, s123.

66 E.A. Neppiras, "Acoustic Cavitation" , Phys. Rep., **61,** 1980, 159.

67 E. N. Harvey, D. K. Barnes, W. D. McElroy, A. H. Whitely, D. C. Pease, and K. W. Cooper, "Bubble formation in animals: Physical factors", J. Cell. Comp. Physical, 1944, **24**, 1.

68 D.E. Yount,. "Skins of Varying Permeability: A Stabilisation Mechanism for Gas Cavitation Nuclei", J. Acoust. Am. Soc., Vol. 65, No.6, 1979, 1429.

69 M. Strasberg, "Onset of Ultrasonic Cavitation in Tap Water", J. Acoust. Am. Soc., Vol.31, No.2, 1959, 163.

70 L.A. Crum, "The Tensile Strength of Water", Nature. Vol. 278, No.8, 1979, 13

71 F.E. Fox & K.F. Herzfeld, "Gas Bubbles with Oragnic Skin as Cavitation Nuclei", J. Acout. Am. Soc., Vol. 26, No.6, 1954, 984

72 R. J. Apfel, "The role of Impurities in Cavitation-Threshold Determination", J. Acoust. Am. Soc., 1970, **48**, 1179.

73 Lord Raleigh, "On the Pressure developed in a Liquid during the Collapse of a Spherical Cavity, " Phil. Mag., Ser. 6, **34**, 1917, 94.

74 G. L. Gooberman, "Ultrasonics theory and application", The English Universities Press Ltd. 1968, p.94

75 C. F. Naudè & A. T. Ellis, "On the Mechanism of Cavitation Damage by Non hemispherical Cavities Collapsing in Contact with a Solid Boundary", J. Basic. Eng., 1961, **83**, 648.

76 M. S. Plesset & R. B. Chapman, "Collapse of an Initially Spherical Vapour Cavity in the Neighbourhood of solid Boundary", J. Fluid Mech., 1971, **47**, 283.

77 R.T. Beyer & S.V. Lecher, "Physical Ultrasonics" Academic Press. London. 1969, p.237.

78 V.R. Esche, "Untersuchung der Schwingungskavitation in Flussigkeitten" Acustica.1952, AB208.

79 V. Griffing & D. Sette, "Luminescence as a Result of Intense Ultrasonic Waves", J. Chem. Phys., 1955, **23**, 503.

80 H. Frenzel & H. Schultes, "Ultrasonic Luminescence in Water", Z. Phys. Chem., 1935, **27B(5/6)**, 421.

81 E.N. Harvey, "Sonoluminescence and Sonic Chemiluminescence", J. Am. Chem. Soc., **61,** 1939, 2392.

82 A. Weissler, "Depolymerisation by Ultrasonic Irradiation: The Role of Cavitation", J. App. Phys., **21,** 1950, 171.

83 S.L. Regen & A. Singh, "Biphasic Sonochemistry. Convenient generation of Dichlorocarbene", J. Org. Chem., **47,** 1982, 1587.

84 M.E. Fitzgerald, V. Griffing, and J. Sullivan, "Chemical effects of ultrasonic -"Hot Spot Chemistry" , J. Chem. Phys., 1956, **25**, 926.

85 D. Sette & F. Wanderlingh, "Nucleation by Cosmic rays in Ultrasonic Cavitation", Phys. Rev., **125,** 1962, 409.

86 K.S. Suslick, R.E. Cline Jr. & D.A. Hammerton, "The sonochemical hot-spot", J. Am. Chem. Soc., **108,** 1986, 5641.

87 M.A Margulis, "Study of electrical phenomena related to Cavitation. Electrical theories of chemical and physiochemical action of Ultrasound", Zh. Fiz. Khim., **55,** 1981, 154.

88 C.M. Sehgal & R.E. Verrall, "A review of the electrical hypothesis of sonoluminescence", Ultrasonics., **20,** 1982, 37.

89 E.A. Neppiras & B.E. Noltingk, "Cavitation Produced by Ultrasonics: Theoretical Conditions for the onset of Cavitation", Proc. Phys. Soc. B (Lond.), 1950, **63B**, 674. idem., ibid, 1951, **64B**, 1032.

90 R. J. Apfel, "The role of Impurities in Cavitation-Threshold Determination", J. Acoust. Am. Soc., 1970, **48**, 1179.

91 H. G. Flynn, "Physical Acoustics: Principles and Methods", Vol. IB, p. 58, W. P. Mason Ed., Academic Press, New York, 1965.

92 R.K. Gould. & W.T. Coakley, "The Effects of Acoustic Forces on Small Particles in Suspension"

93 J. B. Dysthe, "Force on a Small Inclusion in a Standing Acoustic Wave", J. Sound Vib., 1969, **10**, 157

94 G. L. Gooberman, "Ultrasonics Theory and Application", The English Universities Press Ltd. 1968, p.94

95 G. Whitworth & W.T. Coakley, "Particle column formation in a Stationary Ultrasonic Field", J. Acoust. Am. Soc., **91**(1), 1992, 79.

96 E. Fukushima & S.B.W. Roeder, "Spurious Ringing in Pulse NMR", J. Mag. Res., **33,** 1979, 199.

97 M.L. Buess & G.L. Petersen, "Acoustic Ringing effects in Pulsed nuclear magnetic resonance Probes", Rev. Sci. Instrum., **49(8),** Aug. 1978, 1151.

98 E. Fukushima & S.B.W. Roeder, "Experimental Pulse NMR A Nuts and Bolts approach", Addison-Wesley Publishing company. 1981, 465.

99 A.A.V. Gibson & R.E. Raab, "Proton NMR and piezoelectricity in tetramethylammonium chloride", J. Chem. Phys., **57,** 1972, 4688.

100 P.A. Speight, K.R. Jeffrey & J.A. Courtney, "A Probe modification for pulsed nuclear magnetic resonance to eliminate spurious ringing", J. Phys., E7, 1974, 801.

101 S. Reynolds, "NMR Spectroscopy in the presence of Ultrasound and other Perturbations" Aston University thesis 1997

102 J.K. Roberts "The use of Driven Equilibrium Conditions in the measurement of NMR relaxation Times" Aston University thesis 1989

103 J.R Frederick, "Ultrasonic Engineering", Wiley, New York.1965, p.284

104 A. Weissler, "Sonochemistry: The production of chemical change with sound waves" J. Acoust. Soc. Amer., 1953, **25**, 651

105 O. Lindström and O. Lamm, J. Phys. Colliod. Chem., 1951, **55**, 1139.

106 P. K. Chendke and H. S. Fogler, "Sonoluminescence and Sonochemical Reactions of Aqueous Carbon Tetrachloride Solutions", J. Phys. Chem., 1983, **87(8)**, 1362.

107 S. Reynolds, "NMR Spectroscopy in the presence of Ultrasound and other Perturbations" Aston University thesis 1997 138

108 G.J. Tilstone, "Sonically induced narrowing of solid state nuclear magnetic resonance spectra: A possible alternative to magic angle spinning", Final year undergraduate project. Aston university. 1991.

109 M.J. Howard, Thesis, "Evaluation of the Sonically Induced Narrowing of the Nuclear Magnetic Resonance of Solids" , Aston University Thesis, 1993 p.127

110 M.J. Howard, "The Sonically Induced Narrowing of Nuclear Magnetic Resonance Spectroscopy", First Year Postgraduate report, 1991.

111 J. P. Yesinowski, "High Resolution NMR Spectroscopy of Solids and Surface Absorbed Species in Colloidal Suspension: ^{31}P NMR Spectra of Hydroxyappatite and Diphosphonates", J. Am. Chem. Soc., 1981, **103**, 6266.

112 N. Satoh and K. Kimura, "High Resolution Solid State NMR in Liquids. 2. ^{27}Al NMR Study of AlF_3 Ultrafine Particles", J. Am. Chem. Soc.,1990, **112**, 4688.

113 K. Kimura, & N. Satoh, "High resolution solid state NMR of ^{27}Al particles observed by a conventional Fourier transform spectrometer", Chem. Lett. (Jpn). 1989, 271.

114 H.C. Ball, "Study of the NMR Line Narrowing Caused by Induced Brownian Motion in a sample of Suspended Solid Particles", Final Year Undergraduate Report, Aston University, 1995.

115 J. Homer and M. J. Howard, "Studies on the Origin of Sonically Induced Narrowing of Solid-State Nuclear Magnetic Resonance Spectra", J. Chem. Soc., Faraday Trans., 1993, **89**, 3030.

116 K.A. Kusters, S.E. Pratsinis, S.G. Thoma & D.M. Smith, "Ultrasonic Fragmentation of Agglomerate Powders", Chem. Eng. Sci., **48**(24), 1993, 4119

117 S. Davies, " Evaluation of the Sonically Induced Narrowing of Solids with respect to Organics", Unpublished Thesis, Aston University.

118 T.A. Litovitz, "Ultrasonic Spectroscopy in Liquids", J. Acoust. Soc. Am., 1959, **31**, 681.

119 H.S. Gutowsky & D.E. Woessner, "Nuclear Magnetic Spin-Lattice Relaxation in Liquids", Phys. Chem. Rev., 1956, **104**, 843.

Missing page(s) from the bound copy

Pages 196

Appendix 1 Introduction to Hamiltonian and Tensor Mathematics

Introduction to Hamiltonian Mathematics

A Hamiltonian, $\mathcal{H}$, can be described as an energy operator involved with an observable. Hamiltonian mathematics is central to NMR spectroscopy as it provides calculable resonance frequencies and intensities which account for all internal and external interactions of a particular spin system. The Hamiltonians of NMR are outlined in section 4.1.2. Given below is an outline of the derivation of the Zeeman Hamiltonian.

As outlined in chapter 2, the energy of a magnetic moment, μ, in a magnetic field, B_0, is given by:

$E = -\mu B_0$

The correct choice of wavefunction for this state must obey the Schrödinger equation:

$\mathcal{H}\psi = E\psi$

the function, ψ, is known as the eigenfunction of the operator, $\mathcal{H}$, where E is the eigenvalue. In the case of the Zeeman Hamiltonian the eigenvalue is the magnetic moment, μ, of a nuclear spin ,I, such that :

$$\mu = \gamma \hbar I$$

Thus the Zeeman Hamiltonian is given by:

$$\hbar \mathcal{H}_z = -\gamma I \hbar B_0$$

The eigenvalues for the Zeeman Hamiltonian are continuous, thus for an ensemble of spins:

$$\hbar \mathcal{H}_z = -\hbar \sum_i \gamma I B_0$$

Introduction to Tensor Mathematics

Vectors are first rank tensors possessing both magnitude and direction. A vector, I, has three components; Ix, Iy and Iz. The magnitudes of the x, y, and z components of μ to the applied field B_0 are written as $B_0\mu x$, $B_0\mu y$ and $B_0\mu z$, as shown in figure A1.1.

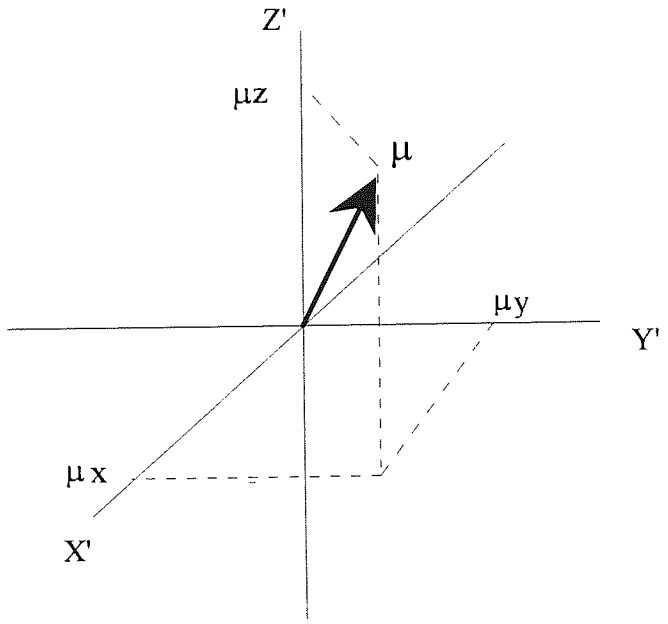

Figure A1.1: The components of a magnetic moment in a magnetic field

In general terms, a second rank tensor, R, in Cartesian co-ordinates links two such vectors in a 3*3 matrix that characterises the 3 dimensional nature of the interaction:

$$\begin{pmatrix} R_{xx} & R_{xy} & R_{xz} \\ R_{yz} & R_{yy} & R_{yz} \\ R_{zx} & R_{zy} & R_{zz} \end{pmatrix}$$

Tensors are often symmetric, even if they are not, anti-symmetric contributions have little influence on the NMR experiment and can generally be ignored. As such, tensors can be converted into diagonal form by correct choice of a co-ordinate system: this means that they only have elements along the diagonal of the co-ordinate system and thus are characterised by these "principal elements".

$$\begin{pmatrix} R_{xx} & 0 & 0 \\ 0 & R_{yy} & 0 \\ 0 & 0 & R_{zz} \end{pmatrix}$$

The terms, R_{xx}, R_{yy} and R_{zz} are known as the principal components, and provide the information of interest.

An axial tensor is one in which the z direction is chosen to be unique.

A traceless tensor is one which has an isotropic value of zero thus the interaction will completely vanish when averaged by fast random motion.

A secular expression is time dependent parameter and as such a secular term is one which will have a direct effect on the energy of the system.

Appendix 2 TSP Experiments

Table A2. 1: Parameters for obtaining the ^{23}Na Spectra in Chapter 9

PARAMETER	VALUE
SPECTROMETER	BRUKER WM 250
NUCLEUS	^{23}NA
OBSERVATION FREQUENCY/ MHz	66.13
OBSERVATION FREQUENCY OFFSET/ kHz	92.0
DATA POINTS	SI=16K: TD=16K
SWEEP WIDTH/ Hz	100000
DELAY/ μs	6.3
PULSE WIDTH/ μs	40
RELAXATION DELAY/ s	1
NUMBER OF SCANS	800
ACQUISITION TIME/ s	0.08192
LINE BROADENING	50

Table A2. 2: TSP linewidths at 3MHz acoustic frequency

Particle Size/ μm	104-75	75-38	>38
Powers/ Wcm^{-2}	Linewidth/ Hz		
0	10000	10000	10000
20.4	8700	8000	8100
30.6	8000	7000	7900
40.8	7600	6640	6900
51.0	1400	1390	1200
61.2	480	390	440

Table A2. 3: TSP linewidths at 2MHz acoustic frequency

Particle Size/ μm	104-75	75-38	>38
Powers/ Wcm^{-2}	Linewidth/ Hz		
0	10000	10000	10000
10.2	9500	7700	8300
15.3	9160		
20.4	8700	7000	7714
25.5	8600		
30.6	8160	6500	7600
35.7	7700		
38.3	7100		
40.8	7000	6400	6500
45.9	5000	4500	
51.0	4200	3520	5760
56.1	-	830	
61.2	415	500	340
76.5	310		
91.8	320		

Figure A2. 1: TSP spectra, 3MHz frequency using TSP of 104-75μm particle size; from top to bottom 0, 20.4, 51.0, 61.2 Wcm^{-2}.

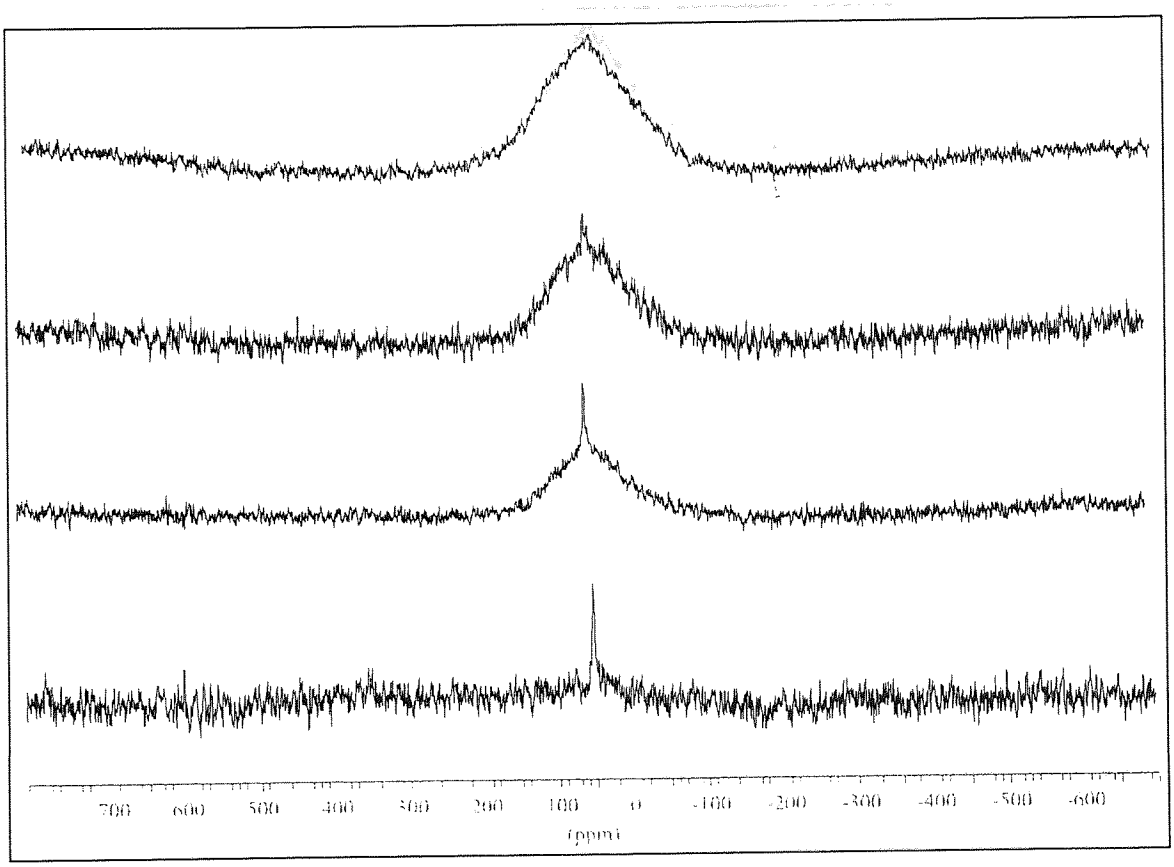

Figure A2. 2: TSP spectra; 2MHz frequency using TSP of 75-53μm particle size from top to bottom 0, 20.4, 51.0, 61.2 Wcm^{-2}.

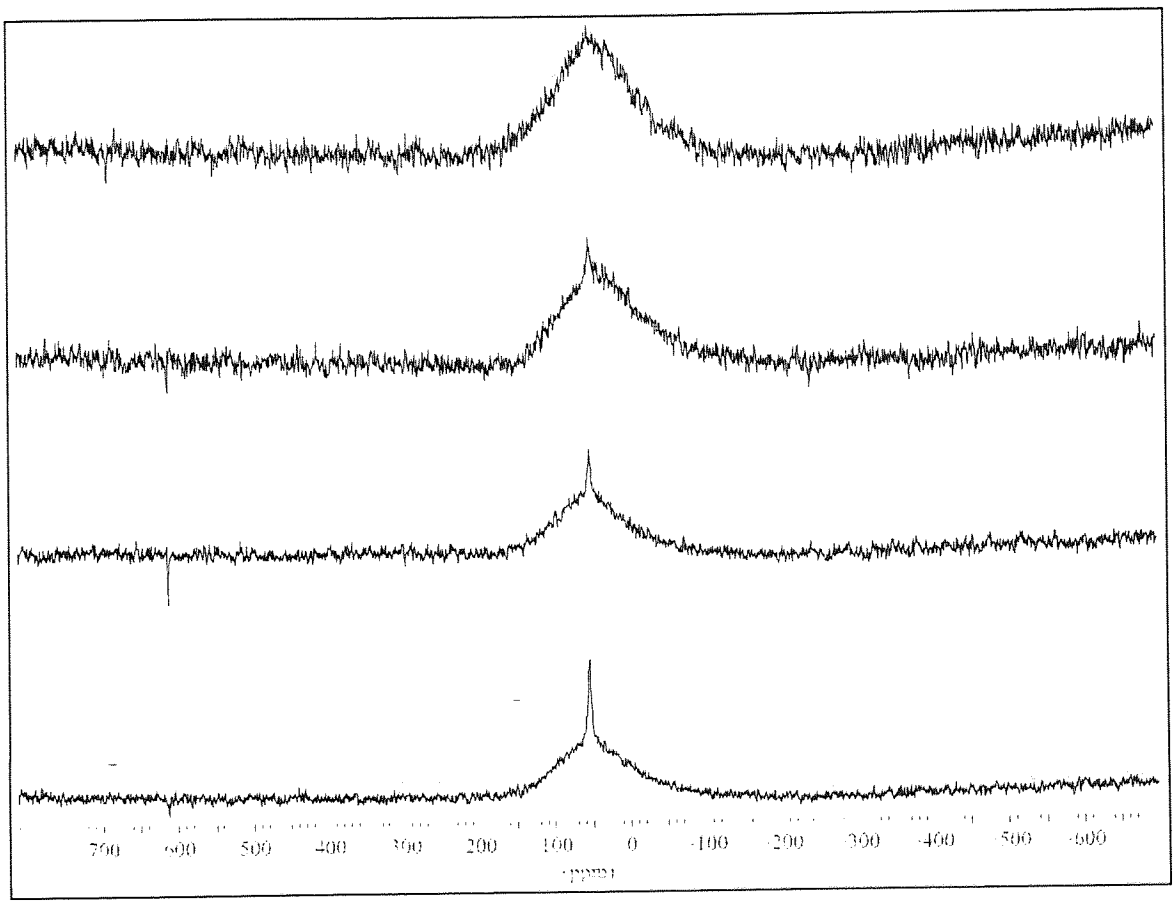

Figure A2. 3: TSP spectra; 3MHz frequency using TSP of 75-53µm particle size from top to bottom 0, 20.4, 51.0, 61.2 Wcm^{-2}.

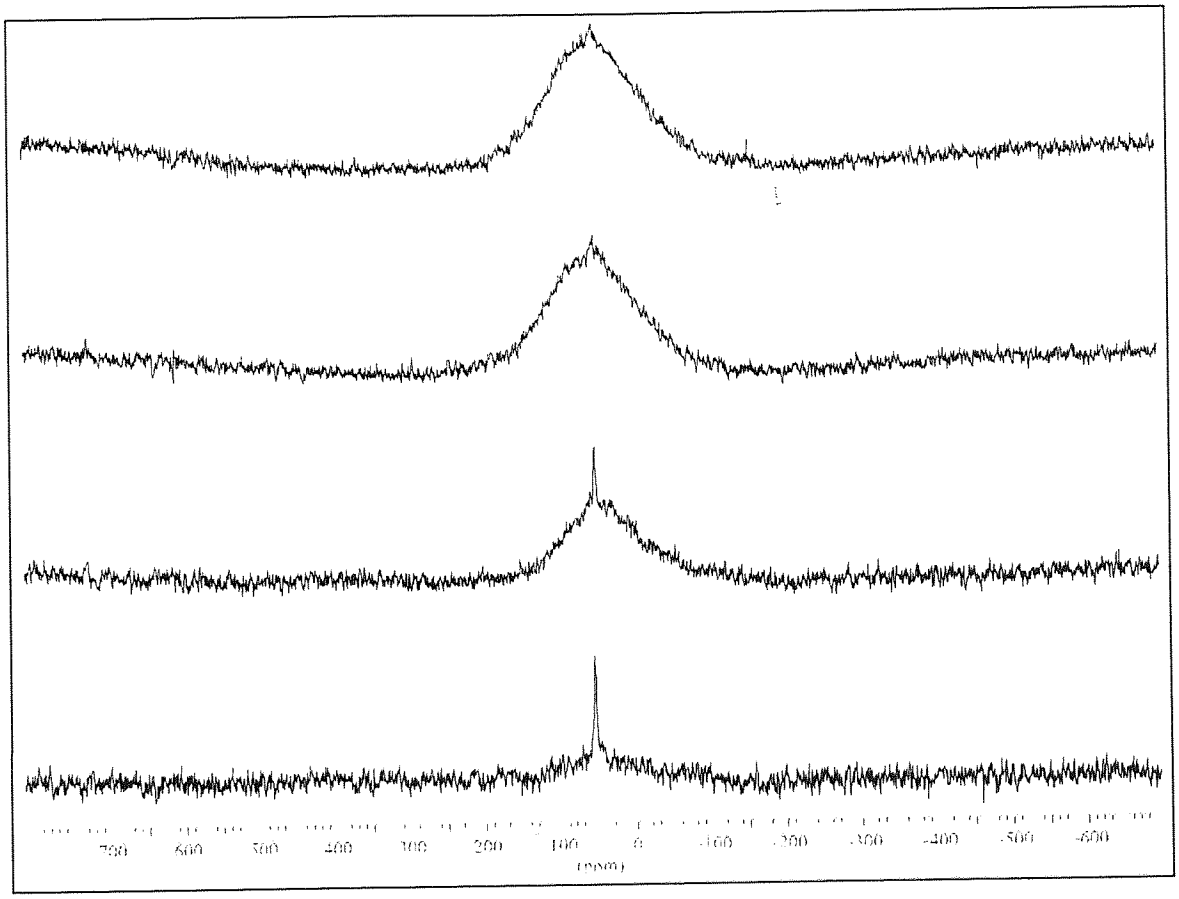

Figure A2. 4: TSP spectra; 2MHz frequency using TSP of <38μm particle size from top to bottom 0, 20.4, 51.0, 61.2 Wcm^{-2}.

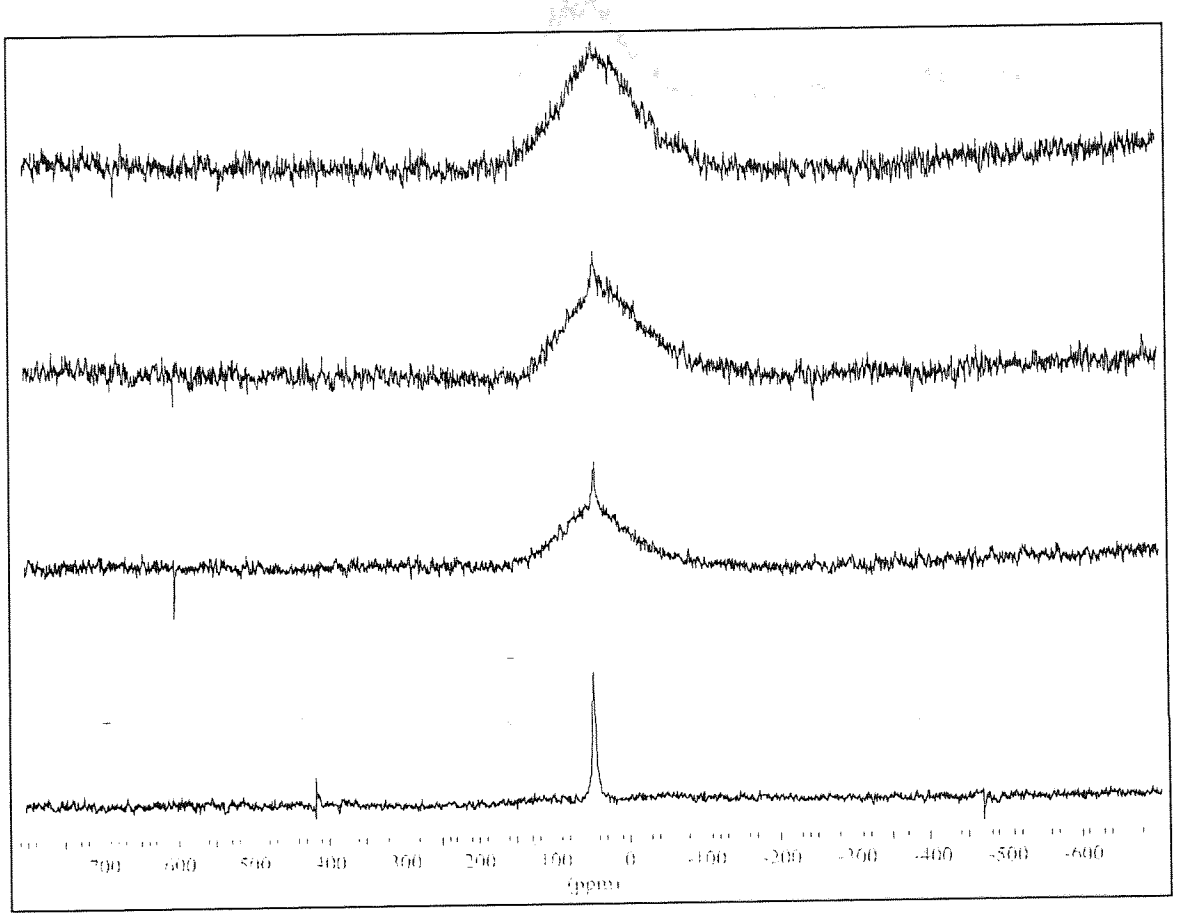

Figure A2. 5: TSP spectra; 3MHz frequency using TSP of <38μm particle size from top to bottom 0, 20.4, 51.0, 61.2 Wcm^{-2}.

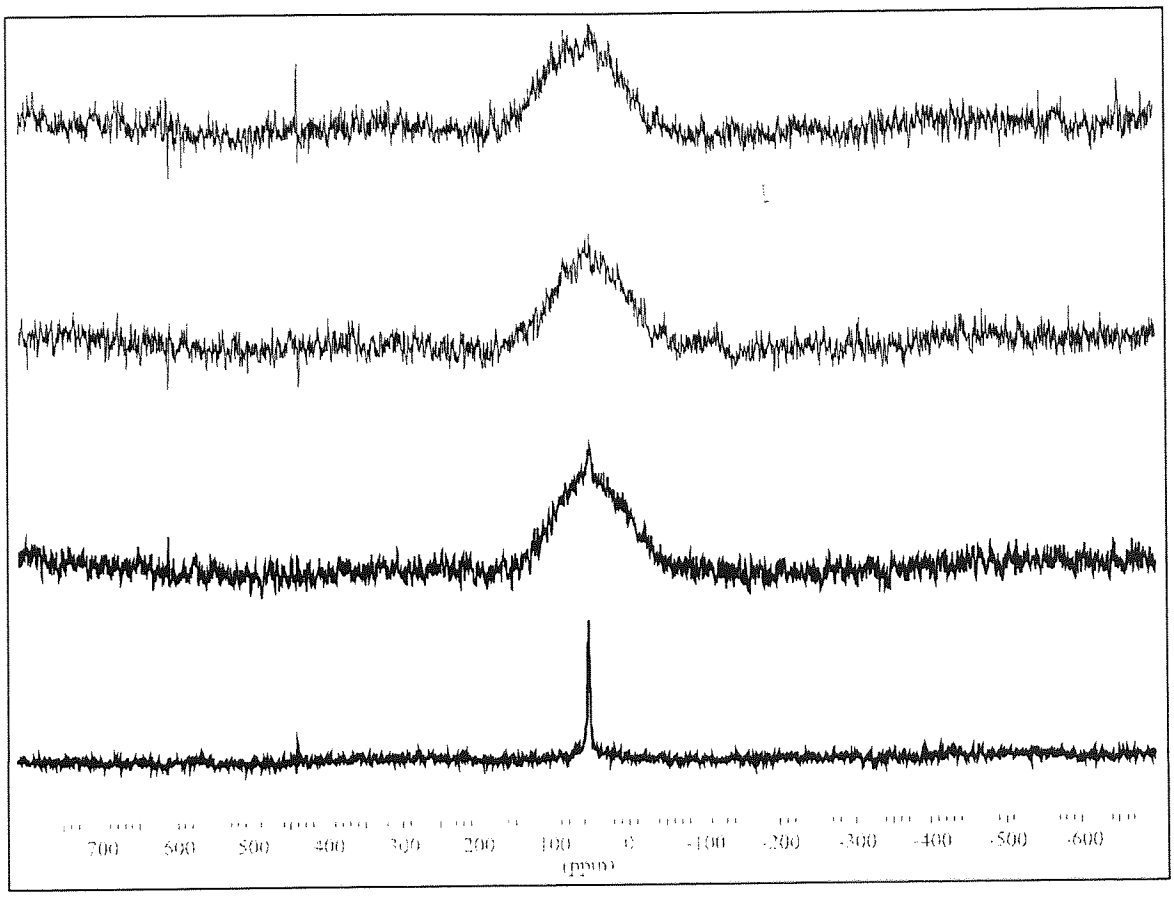

Appendix 3 T_1 Reduction and DESPOT

NMR Acquisition Parameters used in all Experiments in Chapter 10

Table A3. 1: Parameters for all ^{13}C spectra obtained as in sections 10.1.1 and 10.1.4.

PARAMETER	VALUE
SPECTROMETER	BRUKER WM 250
NUCLEUS	^{13}C
OBSERVATION FREQUENCY/ MHz	62.900
OBSERVATION FREQUENCY OFFSET/ kHz	93.96
DATA POINTS	TD=8K, SI=8K
SWEEP WIDTH/ Hz	12500
DELAY/, μs	50
PULSE WIDTH, μs	20
RELAXATION DELAY/ s	0.5
NUMBER OF SCANS	1232
ACQUISITION TIME/ s	0.3277
LINE BROADENING	10

Table A3. 2: Parameters for DESPOT Work as used in section 10.2

PARAMETER	VALUE
SPECTROMETER	BRUKER WM 250
NUCLEUS	^{13}C
OBSERVATION FREQUENCY/ MHz	62.900
OBSERVATION FREQUENCY OFFSET/ kHz	93.96
DATA POINTS	TD=8K, SI=8K
SWEEP WIDTH/ Hz	5000
DELAY/ μs	7.5
PULSE WIDTH/μs	VARIOUS, SEE A3.3
RELAXATION DELAY/ s	.1808
NUMBER OF SCANS	512
ACQUISITION TIME/ s	0.8192
LINE BROADENING	10
DUMMY PULSES	VARIOUS, SEE A3.3

Table A3. 3: Dummy pulses used

Nutation Angle	Pulse Width/ μs	Dummy Pulses Required
10	3	13
20	6	16
30	8.9	14
40	11.9	12
50	14.9	9
60	17.9	7
70	20.8	6
80	23.8	4

From table A3.2 it should be noted that the total acquisition time, as required for the DESPOT calculation is 0.8192 + 0.1808 =1 sec.

INTENSITY MEASUREMENTS FOR DESPOT CALCULATION

Table A3. 4: No ultrasound applied

Nutation Angle	Pulse Width/μs	Dummy Pulses	Intensity	
10	3	13	2.436	2.323
20	6	16	4.626	5.252
30	8.9	14	7.133	6.816
40	11.9	12	8.615	8.689
50	14.9	9	10.111	10.749
60	17.9	7	11.845	11.342
70	20.8	6	11.092	11.696
80	23.8	4	12.709	12.314

Table A3. 5: No ultrasound applied

Nutation Angle	Pulse Width/μs	Dummy Pulses	Intensity	
10	3	13	2.465	2.572
20	6	16	4.961	5.293
30	8.9	14	6.941	7.647
40	11.9	12	8.801	8.592
50	14.9	9	10.369	10.730
60	17.9	7	10.887	11.943
70	20.8	6	11.939	12.333
80	23.8	4	12.576	12.861

Table A3. 6: No ultrasound applied

Nutation Angle	Pulse Width/μs	Dummy Pulses	Intensity	
10	3	13	2.108	2.484
20	6	16	5.230	4.591
30	8.9	14	7.143	6.553
40	11.9	12	9.111	8.693
50	14.9	9	10.067	10.04
60	17.9	7	10.773	11.309
70	20.8	6	12.12	12.354
80	23.8	4	12.337	12.211

Table A3. 7: No ultrasound applied

Nutation Angle	Pulse Width/μs	Dummy Pulses	Intensity	
10	3	13	2.34	2.268
20	6	16	2.65	2.991
30	8.9	14	6.695	6.809
40	11.9	12	8.409	8.415
50	14.9	9	10.235	10.050
60	17.9	7	11.446	12.53
70	20.8	6	12.431	11.849
80	23.8	4	12.18	11.826

Table A3. 8: 25.5 Wcm^{-2} acoustic power

Nutation Angle	Pulse Width/μs	Dummy Pulses	Intensity	
10	3	13	1.505	1.838
20	6	16	5.720	5.480
30	8.9	14	7.360	7.160
40	11.9	12	9.212	9.32
50	14.9	9	10.788	10.619
60	17.9	7	13.238	13.293
70	20.8	6	13.955	14.797
80	23.8	4	15.17	15.394

Table A3. 9: 51.0 Wcm^{-2} acoustic power

Nutation Angle	Pulse Width/μs	Dummy Pulses	Intensity	
10	3	13	2.18	2.338
20	6	16	5.909	6.112
30	8.9	14	9.615	10.726
40	11.9	12	12.980	12.456
50	14.9	9	14.327	14.531
60	17.9	7	16.565	18.936
70	20.8	6	19.591	19.383
80	23.8	4	21.549	22.64

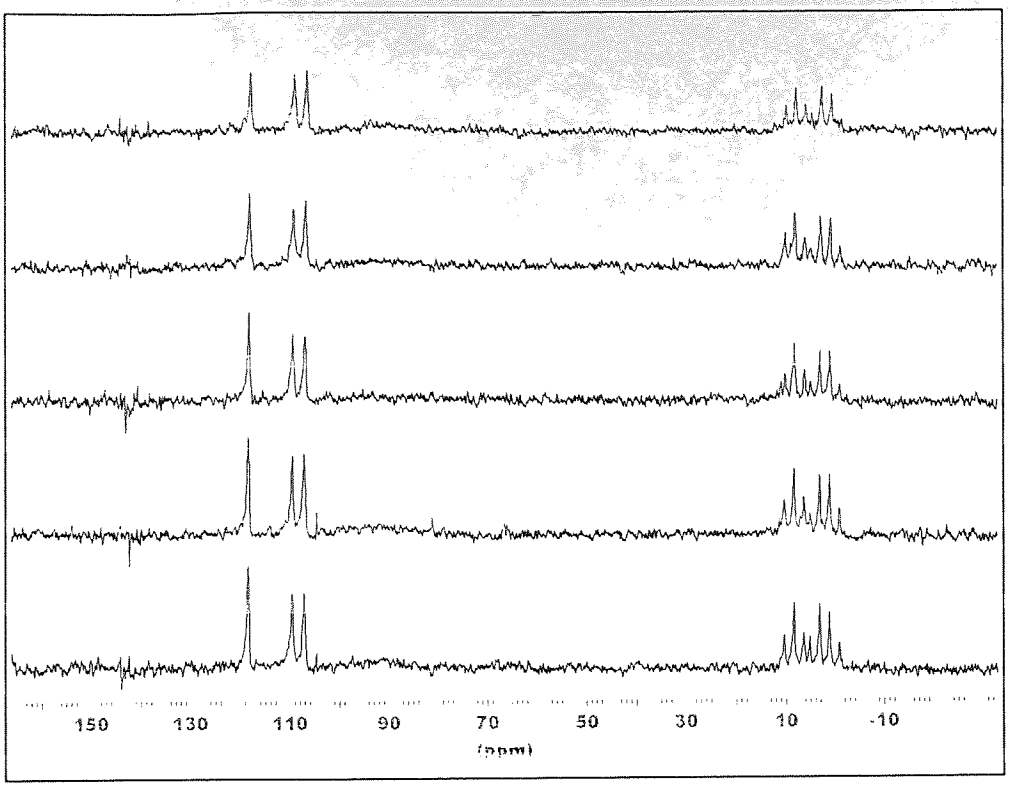

Figure A3.1: ^{13}C NMR spectra showing signal to noise enhancements with increasing ultrasound power for mesitylene/cyclohexane mixture: from top to bottom: 0, 12.7, 25.5, 38.3 and 51.0 Wcm^{-2}.